Thesis/
Reports
Fons,
W.L.

LIBRARY FILE COPY
Rocky Mountain Research Station

Blast effects on forest stands
by nuclear weapons

Interim Technical Report
AFSWP - 971

~~CONFIDENTIAL~~

KMO

TECHNICAL REPORT
AFSWP - 971
December 1957

BLAST EFFECTS ON FOREST STANDS BY NUCLEAR WEAPONS

still applies

~~FORMERLY RESTRICTED DATA~~
~~Handled as Restricted Data in Foreign Dissemination Sec. 144b. Atomic Energy Act, 1954~~

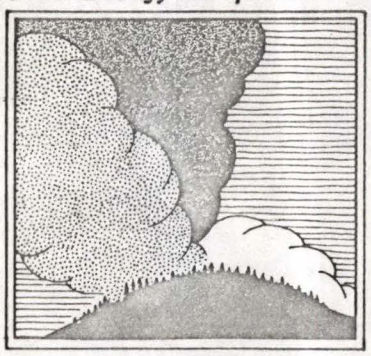

DIVISION OF FIRE RESEARCH
FOREST SERVICE
U. S. DEPARTMENT OF AGRICULTURE

UNCLASSIFIED

per DOE-DASA- Ltr. dated 9/20/62
(DASAAG-2 321)

~~CONFIDENTIAL~~

ACKNOWLEDGMENT

This report presents results of a group research project of the Division of Fire Research, Forest Service, Department of Agriculture, conducted at the California Forest & Range Experiment Station. The work reported here is largely the result of group effort. The authors wish to acknowledge the contribution of a large number of associates who carried out parts of the experimental work and made analyses. Thanks are accorded to Stanford Research Institute of Menlo Park, California for permitting the U. S. Forest Service to utilize the services of F. M. Sauer, formerly a member of the Station's Division of Fire Research, on part of this report.

BLAST EFFECTS ON FOREST STANDS BY NUCLEAR WEAPONS

by

W. L. Fons
F. M. Sauer
and
W. Y. Pong

Technical Report
AFSWP-971
December 1957

Handle as Restricted Data in
Foreign Dissemination Sec. 144b,
Atomic Energy Act, 1954

U. S. Department of Agriculture
Forest Service
Division of Fire Research
Washington, D. C.
A. A. Brown, Director

Project Leader: W. L. Fons
California Forest and Range Experiment Station
P. O. Box 245
Berkeley, California

CONFIDENTIAL - FORMERLY RESTRICTED DATA.

ABSTRACT

A method of estimating blast damage to trees and tree stands from nuclear explosions is developed and presented. Results of field studies on the natural period of tree stems, aerodynamic drag in tree crowns, bending and breakage characteristics of natural rooted trees, and crown characteristics of several tree species provide data which are integrated into the equation of motion for wind loading. A prediction system is developed by correlation of tree and shock wave parameters for estimating degree of damage by nuclear detonation in terms of weapon size, peak dynamic pressure, and wave form factor. Isodamage curves for light and severe damage are presented for five types of tree stands common in the northern hemisphere.

CONFIDENTIAL - FORMERLY RESTRICTED DATA

CONTENTS

Abstract 3

List of tables 6

List of illustrations 6

CHAPTER 1. Introduction 9
Background 9
Objective 11
Organization of report 14

CHAPTER 2. Tree characteristics 15
General 15
Tree structure 15
Crown characteristics 16
Stem form 18
Natural period 19
Internal damping 20

CHAPTER 3. Wind drag and stem breakage characteristics 24
General 24
Wind drag characteristics 24
Stem breakage characteristics 26

CHAPTER 4. Theoretical calculations of stem breakage--single stems 39
General 39
The equation of motion of the tree crown 39
Shock wave parameters 41
Integration of the equation of motion 44
Impulsive loading calculations 46
Maximum deflections for single ponderosa pine stems . . 48
Correlation of results 51
The variation of static work modulus with dynamic pressure wave form factor 56

CHAPTER 5. Construction of isodamage curves for tree stands . . . 65
General 65
Calculation procedure and illustrative example 65

CHAPTER 6. Isodamage curves for selected tree stands 76
General considerations 76
Type I stand, managed ponderosa pine 76
Type II stand, unmanaged ponderosa pine 78
Type III stand, unmanaged ponderosa pine 79
Type IV stand, unmanaged ponderosa pine 81
Type V stand, managed Douglas-fir 81
Isodamage curves 81

Appendix 94

Nomenclature 97

Literature cited 102

CONFIDENTIAL - FORMERLY RESTRICTED DATA

TABLES

Table 2.1--Values of constants a and b in equation $W_o H_c = a(d_c)^b$ 18

" 2.2--Values of constants a and b in stem form equation $Z = f/af + b$ 19

" 2.3--Constants a and b in natural period equation $\tau = a + b\,(H_{bh})^2/d_{bh}$ 20

" 3.1--Reference strain values for green wood of several species 35

" 4.1--Characteristics of ponderosa pine stems used in calculations 49

" 4.2--Input conditions and results corresponding to figure 4.4 51

" 6.1--Stand table for a managed 60-year-old ponderosa pine plantation on a good site 77

" 6.2--Stand table for a pure, even-aged, unmanaged, 80-year-old ponderosa pine stand of average stocking on a poor site 79

" 6.3--Stand table for a pure, even-aged, unmanaged, 80-year-old ponderosa pine stand of average stocking on a good site 80

" 6.4--Stand table for a pure, even-aged, unmanaged, 120-year-old ponderosa pine stand of average stocking on a good site 82

" 6.5--Stand table for a managed 60-year-old Douglas-fir plantation on a good site 83

ILLUSTRATIONS

Figure 1.1--Tree stand exposed on Operation UPSHOT-KNOTHOLE . . . 10

" 1.2--Natural broadleaf stand on Victor Island, Bikini Atoll (Operation CASTLE) 12

" 1.3--Blast damage from megaton weapon to broadleaf stand illustrated in figure 1.2 (Operation CASTLE) 12

" 1.4--Blast damage from kiloton weapon to tree stand on Uncle Island, Bikini Atoll (Operation CASTLE) 13

" 2.1--Good and poor site height-diameter relations for ponderosa pine, sugar pine, and white fir 17

" 2.2--Double-bark thickness-diameter relations for good and poor site ponderosa pine 17

" 2.3--Typical free vibration amplitude-time record for a tree stem with crown removed 21

" 2.4--A: Relative decay of free vibrations with successive cycles for a typical tree-stem 22

B: Relation between the damping factor per unit mass and the relative tree stem volume 22

CONFIDENTIAL - FORMERLY RESTRICTED DATA

Figure 3.1--Tree mounted on truck bed for drag tests 25
" 3.2--Dimensionless correlation of aerodynamic drag data for several conifer species 27
" 3.3--Dimensionless correlation of aerodynamic drag data for several broadleaf species 28
" 3.4--Location of center of pressure of wind drag for conifer trees 29
" 3.5--Location of center of pressure of wind drag for broadleaf trees 29
" 3.6--Schematic diagram showing tree stem and associated parameters 31
" 3.7--Dimensionless expression containing spring constant, k_r 33
" 3.8--Restoring force characteristics of idealized tree stem--single horizontal load 34
" 3.9--Actual frequency distribution of static work modulus, $\overline{E}_b$, for good and poor site ponderosa pine 37
" 3.10--Actual frequency distribution of static work modulus, $\overline{E}_b$, for all broadleaf trees tested 38
" 4.1--Tree stem and mass represented by spring-mass system 40
" 4.2--Theoretical particle velocity and density variation with time for free air 43
" 4.3--Drag coefficient variation with bending moment of tree stem (Stem 24-40 45
" 4.4--Typical deflection-time curves for ponderosa pine tree stem, 24-40-I 50
" 4.5--Analytical correlation of static work modulus for maximum deflection 53
" 4.6--Dynamic pressure modulus as a function of period modulus for various values of static work modulus. . 54
" 4.7--Energy modulus ratio for second to first maximum deflection as a function to period ratio 55
" 4.8--Illustration of method for estimating the effect of wave form factor, Q 57
" 4.9--Dynamic pressure modulus as a function of period modulus for various values of static work modulus (wave form factor, Q = 0.132) 59
" 4.10--Dynamic pressure modulus as a function of period modulus for various values of static work modulus (wave form factor, Q = 0.151) 60
" 4.11--Dynamic pressure modulus as a function of period modulus for various values of static work modulus (wave form factor, Q = 0.176) 61
" 4.12--Dynamic pressure modulus as a function of period modulus for various values of static work modulus (wave form factor, Q = 0.230) 62
" 4.13--Dynamic pressure modulus as a function of period modulus for various values of static work modulus (wave form factor, Q = 0.265) 63

CONFIDENTIAL--FOR[illegible]LY RESTRICTED DATA

Figure 4.14--Dynamic pressure modulus as a function of period modulus for various values of static work modulus (wave form factor, Q = 0.353) 64
" 5.1--Total probability (P_t) as a function of the first deflection energy modulus ($\overline{E}_1$) 66
" 5.2--Relationship of overpressure-duration-weapon yield . 68
" 5.3--Illustration of use of transparent overlay in computing static work modulus 69
" 5.4--Illustration of use of transparent overlay in computing static work moduli ratio 71
" 5.5--Stems broken per acre as a function of peak dynamic pressure and weapon yield 72
" 5.6--Light and heavy damage as a function of peak dynamic pressure and wave form factor 73
" 5.7--Composite dynamic pressure-wave form factor height of burst chart and illustration of isodamage curve construction 74
" 6.1--Light damage curves for Type I forest stand, by height of burst, ground distance and weapon size . . 84
" 6.2--Light damage curves for Type II forest stand, by height of burst, ground distance and weapon size . . 85
" 6.3--Light damage curves for Type III forest stand, by height of burst, ground distance and weapon size . . 86
" 6.4--Light damage curves for Type IV forest stand, by height of burst, ground distance and weapon size . . 87
" 6.5--Light damage curves for Type V forest stand, by height of burst, ground distance and weapon size . . 88
" 6.6--Severe damage curves for Type I forest stand, by height of burst, ground distance and weapon size . . 89
" 6.7--Severe damage curves for Type II forest stand, by height of burst, ground distance and weapon size . . 90
" 6.8--Severe damage curves for Type III forest stand, by height of burst, ground distance and weapon size . . 91
" 6.9--Severe damage curves for Type IV forest stand, by height of burst, ground distance and weapon size . . 92
" 6.10--Severe damage curves for Type V forest stand, by height of burst, ground distance and weapon size . . 93

CONFIDENTIAL - FORMERLY RESTRICTED DATA

CHAPTER 1

INTRODUCTION

Background

A study of blast and thermal effects of a nuclear explosion over a forested area was requested by the Department of the Army in 1950. This investigation was to determine, for a nominal atomic explosion over forest areas in the north temperate zone, the effects that would be of importance to offensive and defensive military operations. A preliminary analysis of blast damage to trees was made, principally to develop methods of analysis and delineate problem parameters. When sponsorship of this work was taken over by the Armed Forces Special Weapons Project in 1951, the preliminary analysis (1)[1/] provided the basis for a series of related field studies.

Field experiments determined the natural period of trees (2), the aerodynamic drag in tree crowns (3,4), and the bending and breakage characteristics of tree stems by static loading (5,6). Wind drag was correlated with the weight of foliage for broadleafs (3) and with the weight of crown for conifers (4). Measurements of conifer crown weights (7) and broadleaf foliage weights (8) were correlated with tree stem dimensions. Since the force-deflection relation of tree stems varies with stem form, data on stem form were also collected in the course of the tree crown and static bending studies. Other sources of similar data on stem form were used (9,10).

These studies of tree characteristics included 13 conifer and 6 broadleaf tree species. To cover a wide range of growing conditions, studies were made in several parts of the United States. Tests of broadleaf species were made on the Pisgah National Forest in North Carolina. Studies of conifers were carried out on the National Forests in California, Idaho, and Nevada.

The field studies provided specifications for all parameters for average trees of various dimensions. For these tree models the equation of motion was integrated numerically for various dynamic pressures and positive phase duration times to yield maximum deflection. Following the modeling experiments and theoretical analyses, a series of confirmatory experiments were conducted by exposing trees to nuclear blast at several field operations, first at the Nevada Proving Grounds and then at the Pacific Proving Grounds.

On Operation Tumbler-Snapper (11) 16 isolated conifer trees were placed in groups of four at four stations from ground zero so as to cover a range of peak overpressures and positive phase duration times. The results of the operation provided a field check on the computational

1/ Underlined numbers in parenthesis refer to Literature Cited, page 102.

CONFIDENTIAL - FORMERLY RESTRICTED DATA

systems being developed for predicting blast damage in terms of stem breakage, branch breakage, and defoliation in relation to peak overpressure and positive phase duration time. This operation also permitted the field testing of methods and techniques for measuring motion and strain on tree stems subjected to blast from atomic explosions. These techniques were used in instrumenting a forest stand planned for Operation Upshot-Knothole (12).

On Operation Upshot-Knothole, a stand of ponderosa pine covering approximately 1 1/4 acres and composed of 145 trees from 50 to 75 feet in height (figure 1.1) was exposed. The general purpose of exposing such a stand to an actual atomic explosion was to gather experimental data, of both fundamental and applied nature, to check methods being developed for predicting the effects of blast winds on a stand of trees. The test also provided information on whether pressure attenuation through a tree stand was significant.

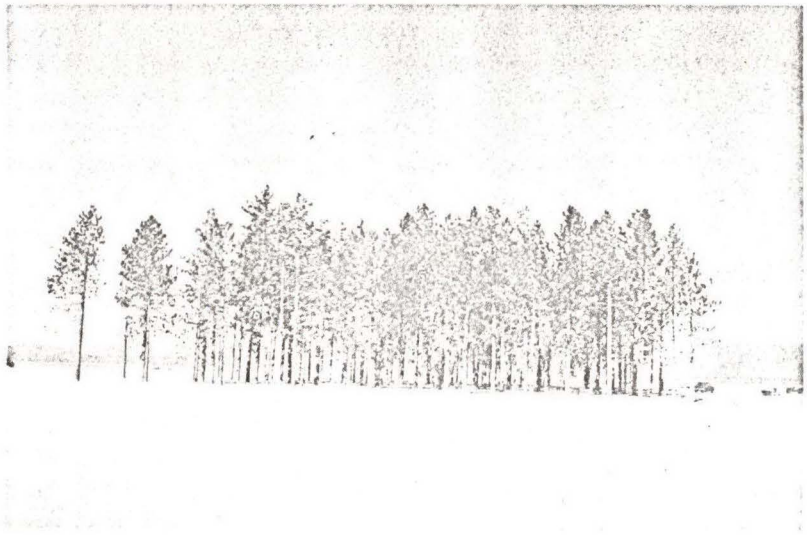

Figure 1.1--Tree stand exposed on Operation Upshot-Knothole

CONFIDENTIAL - FORMERLY RESTRICTED DATA

Within the limits of instrumentation no apparent attenuation of peak overpressure or dynamic pressure was observed for this size of stand. In fact, deflection and breakage of trees in the stand on Upshot-Knothole Shot 9 were approximately twice the values predicted on the basis of calculations of the first maximum deflection. The difference was due mainly to the fact that a substantial percentage of the trees were broken during the negative phase. By including the probability of breakage during the second maximum deflection, predictions were brought into agreement with experimental values.

It was also established that low burst height results in greater damage to drag type targets, such as trees, than is caused by the same peak dynamic pressure resulting from a weapon at a greater height of burst. This effect was attributed to an increase in dynamic pressure wave form factor, or an increase in the dynamic pressure impulse with decreasing height of burst. Therefore the wave form factor was included as a parameter in the damage-prediction system.

A criterion of damage related to ease of military operations in a forested area stemmed from observations of the damage to the stand in Operation Upshot-Knothole (12). It was agreed that damage was to be defined in terms of length of tree stems broken per acre of forest. Light damage was defined to include breakage up to 1,500 ft. per acre and severe damage to cover stem breakage greater than 9,000 ft. per acre.

Operation Castle (13) offered an opportunity to obtain experimental data on damage to natural tree stands (figure 1.2) from megaton weapons as well as to check whether peak overpressure and dynamic pressure were significantly attenuated by a large stand. Ground-level pressure measurements over a distance of 2,000 ft. into a natural tree stand definitely indicated no attenuation in peak overpressure by the presence of trees. Observed damage from two weapons of different yields compared favorably with that predicted. Damage to broadleaf stands is principally limb breakage and defoliation with occasional breakage of the main stem or uprooting (figure 1.3). Thus, the principal blast effect upon a broadleaf forest would not markedly hamper troop movement through such a forest. In fact, the shock wave may clear a dense forest stand sufficiently to permit easier transit, as illustrated in figure 1.4.

Objective

The purpose of this report is to bring together information required for offensive and defensive military operations relative to expected blast damage to forest stands by nuclear explosions. This information is compiled and correlated to provide a method of estimating blast damage to trees and to tree stands. The estimates of damage are determined on the premise that reasonable estimates of weapon size and height of burst are given. The damage estimates also presuppose that one out of the five typical stands analyzed will reasonably resemble the tree stand encountered in practice. For other types of stand, damage can be estimated from the basic data of tree characteristics and the method of calculations given in this report.

CONFIDENTIAL - FORMERLY RESTRICTED DATA

Figure 1.2--Natural broadleaf stand on Victor Island, Bikini Atoll (Operation Castle)

Figure 1.3--Blast damage from megaton weapon to broadleaf stand illustrated in figure 1.2, Operation Castle (ground range 62,500 ft., peak overpressure 2.4 psi)

CONFIDENTIAL - FORMERLY RESTRICTED DATA

Before

After

Figure 1.4--Blast damage from kiloton upon to tree stand on Uncle Island, Bikini Atoll Operation Castle (ground range 8,800 ft., overpressure 4.2 psi)

CONFIDENTIAL - FORMERLY RESTRICTED DATA

Organization of Report

Chapters 2 and 3 of the report present the basic information on tree crowns and tree stems of several of the more important conifer and broadleaf species. Chapter 2 presents results of studies correlating weight of branchwood and foliage, stem form, and natural period with total height of tree, percent of crown, and diameter of stem at a specified location. Chapter 3 presents results of studies concerned with wind drag, stem breakage, and energy required for breakage.

Chapters 4 and 5 bring the tree and the shock wave parameters together and formulate a breakage prediction system. Chapter 4 presents theoretical calculation of tree motion under shock loading and the probability of breakage for single tree stems. Chapter 5 describes the summation procedure for predicting the degree of damage sustained by tree stands following detonation of various nuclear weapons.

Chapter 6 presents isodamage curves for five tree stands selected to represent typical tree stands found in the Northern Hemisphere.

CONFIDENTIAL - FORMERLY RESTRICTED DATA

CHAPTER 2

TREE CHARACTERISTICS

General

The system for predicting breakage and uprooting of trees by strong winds requires information on weight of crown, branchwood and foliage, on stem form, on natural period, and on internal damping of stem. An experimental program, started in 1951, led to a number of generalized relations by which weight of crown components, stem forms, natural periods, and internal damping can be determined for a number of broadleaf and conifer species over a wide range of tree heights, diameters, and percent crowns. A summary of these relationships is given in this chapter.

Tree Structure

Forest trees are generally separated into generalized groups--broadleaves and conifers. Broadleaves, as the name implies, have leaves which are broad and flat and in most cases deciduous. In contrast, conifers have needle-like leaves which are persistent for 2-3 seasons of growth.

Branching habits of forest trees are quite variable, but in general two types are recognized--excurrent and deliquescent. Excurrent branching is typical of all conifers and some broadleaves. Trees with excurrent branching have a single well-defined main stem to which smaller diameter branches are attached at a wide angle. Crowns of these trees are usually cone-shaped and quite symmetrical. Trees with deliquescent branching have a poorly-defined main stem which terminates into a number of large branches attached to the stem at a sharp angle. This type of branching, typical of many species of broadleaves, forms crowns which are quite variable in shape usually without any definite geometrical form and lacking symmetry.

Conifers as well as broadleaves grow naturally in stands of varying species composition. They may be predominantly of one species (pure stand) or composed of 2 or more species (mixed stand). They are even-aged if most of the trees in the stand are approximately the same age, or all-aged if the trees in the stand cover a wide range of ages and sizes.

Trees in forest stands occur on a variety of sites. The capacity of these sites to produce a stand of trees is reflected by the average height of the taller trees. In general, five different site classes are recognized for forested areas--Site Class I - V, with Site Class I the most productive. For the purposes of this report, however, only two site classes are used--good and poor site. Good site includes the three highest Site Classes (I - III) and poor site the last two classes (IV - V).

CONFIDENTIAL - FORMERLY RESTRICTED DATA

Trees in forest stands on a good site are thrifty and fast growing, developing under conditions of adequate annual rainfall, deep rock-free soils with good drainage, a long growing season, and favorable topography. Middle elevations and latitudes provide longer growing seasons with warmer temperatures; and moderate, north-facing slopes or well-drained flats favor rapid growth.

In contrast, trees on a poor site are scrawny and slow-growing, developing under conditions of deficient annual rainfall, shallow rocky soils (often with poor drainage), a short growing season, and an unfavorable topography. These conditions are found on arid ridges, poorly drained flats, and steep south-facing slopes at high elevations and northerly latitudes.

Because of these site differences, trees growing on a good site will differ in their physical characteristics from those growing on a poor site. Figure 2.1 shows the height-diameter relations for good and poor site ponderosa pine, sugar pine, and white fir trees (14). It is apparent from these curves that good site trees are generally taller and larger than poor site trees.

Trees also differ in their bark characteristics. Broadleaves generally have a much thinner bark than conifers. Even within the same species bark thickness varies with diameter and site. Figure 2.2 presents the double-bark thickness-diameter relations for good and poor site ponderosa pine (14).

Crown Characteristics

Crowns and their components, branchwood and foliage, were analyzed for 211 conifer trees representing 13 species (7), and for 57 broadleaf trees representing 6 species (8). Weights of dry crown, dry branchwood, and dry foliage were found to be significantly related to the stem diameter at the base of live crown and the height of crown for each of the species studied. The relation for crown weight was found to vary with species and site, but not with crown geometry, position of the crown in the canopy or age of trees. Both branchwood and foliage relations appeared to behave similarly. Geometrical similarity of tree crowns was found to exist for each species for trees of all sizes and crown lengths. This means that the same relation holds for the diameter of stem at base of crown, length of crown, and the weight of dry crown regardless of tree size. In general, the ratio of branchwood to foliage exceeds 1.0 for trees with stem diameter at base of crown larger than 5 inches for the conifer species and larger than 1 inch for broadleaf species.

The relationship established between the weight of crown and crown components and the stem diameter and length of crown, which resulted in the highest correlation for all species is

$$W_o H_c = a(d_c)^b \qquad (2.1)$$

CONFIDENTIAL - FORMERLY RESTRICTED DATA

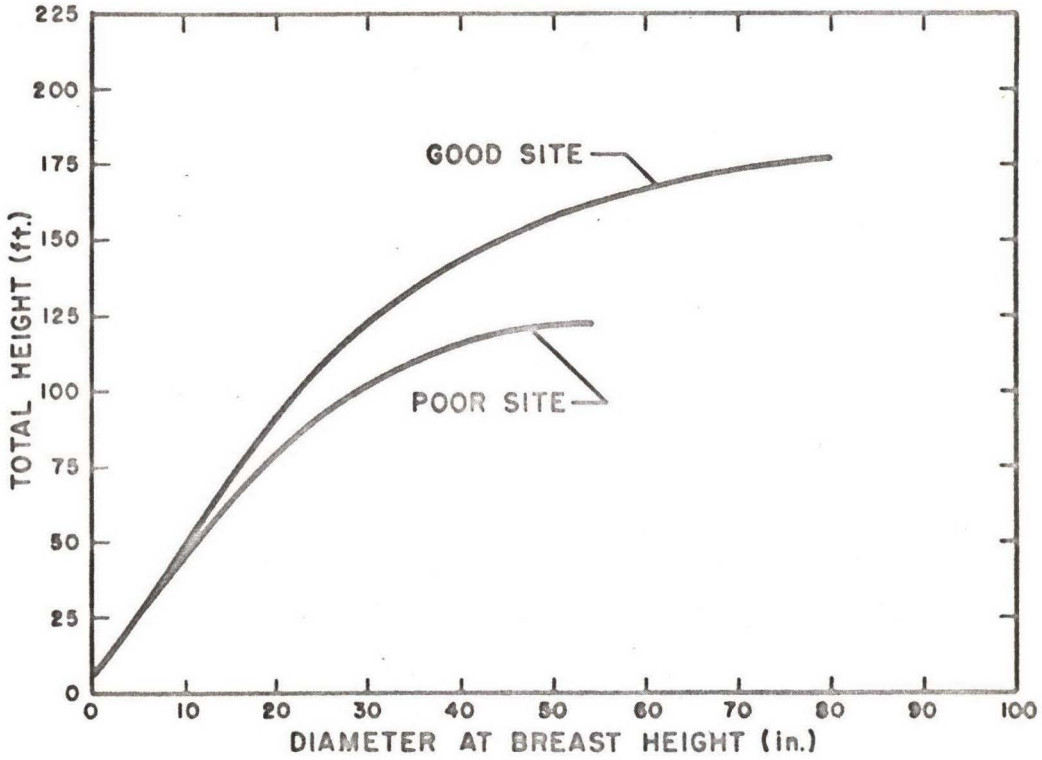

Figure 2.1--Good and poor site height-diameter relations for ponderosa pine, sugar pine, and white fir

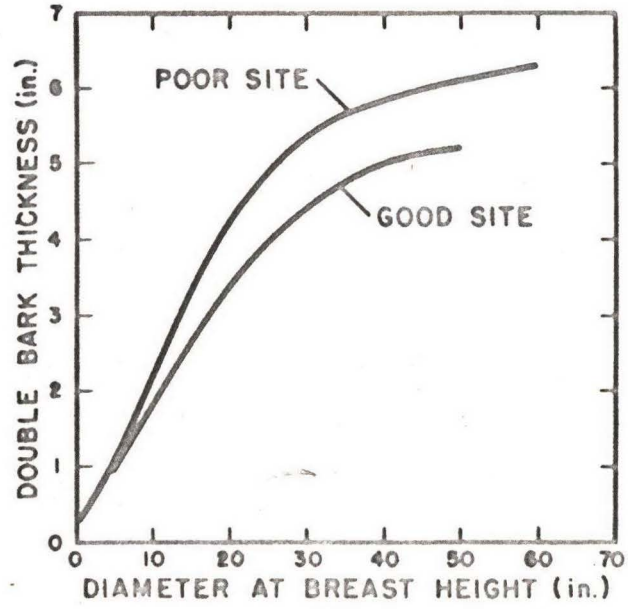

Figure 2.2--Double bark thickness-diameter relations for good and poor site ponderosa pine

CONFIDENTIAL - FORMERLY RESTRICTED DATA

where, W_o = weight of dry crown, dry foliage, or dry branchwood, lbs.[2/]

H_c = length of crown, ft.

d_c = diameter of stem at base of crown, inches

a and b = constants determined statistically.

Table 2.1 presents values of constants a and b for several of the more important conifer and broadleaf species.

Table 2.1--Values of constants a and b in equation $W_o H_c = a(d_c)^b$ for determination of dry weight of crown, branchwood or foliage[1/]

Tree species and location	Number of trees	For weight of dry crown when $W_o = W_c$		For weight of dry branchwood when $W_o = W_b$		For weight of dry foliage when $W_o = W_f$	
		a	b	a	b	a	b
Ponderosa pine (Calif.)	13	1.14	3.92	0.39	4.22	1.01	3.42
Sugar pine (Calif.)	4	1.81	3.46	0.54	3.86	1.30	3.09
Lodgepole pine (Calif.)	4	1.21	3.83	0.44	4.11	1.07	3.36
Loblolly pine (S. Car.)	9	9.11	3.11	3.10	3.45	6.28	2.74
White fir (Calif.)	9	2.77	3.51	0.81	3.78	2.23	3.23
Douglas-fir (Calif.)	6	3.34	3.52	1.00	3.88	2.52	3.10
Engelmann spruce (Idaho)	14	7.33	3.19	3.52	3.39	6.31	2.92
Incense cedar (Calif.)	6	2.58	3.53	0.80	3.76	2.51	3.19
Western larch (Idaho)	11	8.84	2.91	4.96	3.21	6.75	2.65
Silver maple	8	4.09	2.70	24.75	2.63	29.37	2.64
Sweet birch	10	3.58	2.90	13.15	3.19	16.76	3.14
Pignut hickory	10	6.41	2.75	24.31	2.98	30.21	2.96
American beech	8	9.28	2.38	27.71	2.89	35.99	2.82
Yellow-poplar	12	4.97	2.46	15.85	2.60	21.24	2.56
Scarlet oak	9	6.56	2.66	11.12	3.30	15.92	3.20

1/ From References (7) and (8).

Stem Form

Tree stem dimensions, expressed as stem form, characterize the force and deflection phenomena. Measurements of cross-sections of tree stems of many species (5,6,9) have shown that tree stems are generally hyperboloid in shape. The stem form is then represented by an equation

2/ See Nomenclature, page 97.

CONFIDENTIAL - FORMERLY RESTRICTED DATA

of a hyperbola, namely

$$Z = \frac{f}{af + b} \qquad (2.2)$$

where, a and b are constants, f is the length of stem (H) measured from top downward to any point divided by length of stem (H_{bh}) above breast height[3/], and Z is the ratio of diameter of stem inside bark (d) at any point along the stem to diameter outside bark at breast height, (d_{bh}) (figure 3.6).

Table 2.2 presents values of the constants a and b in the stem form equation for dominant trees of several species.

Table 2.2--Values of constants a and b in stem form equation $Z = f/af + b$

Tree species	Constants	
	a	b
Ponderosa pine[1/]	0.69	0.52
Ponderosa pine[2/]	0.81	0.47
Douglas fir	0.69	0.53
Broadleaf[3/]	0.60	0.54

1/ Good site.
2/ Poor site.
3/ Average of the 6 species listed in Table 2.1.

Natural Period

Analysis of damage to trees by the blast winds associated with nuclear weapons (1,12) demonstrated that trees are a drag type target by virtue of their long natural periods and the relatively short time required for shock to equalize around crown components. A survey of literature yielded no information on period characteristics of trees.

Two hundred and eighty-four trees with natural crowns, including 217 conifers, 37 broadleafs, and 30 palms were tested for natural period. Crowns were removed from most of these trees, and periods of the bare stem were measured.

For several ponderosa pine trees, tests were made of the effect of crown lengths on natural period. Using total height, the tree was divided into five sections and the base of the crown trimmed to the nearest 20 percent. After measuring the period for the full crown, the lower 20 percent section of the crown was removed and the period again measured. Similarly, period measurements were made after each succeeding crown section was removed.

3/ Breast height is 4 1/2 feet above ground level.

CONFIDENTIAL - FORMERLY RESTRICTED DATA

To determine the relation between the period of a tree and its geometrical and physical parameters, it was assumed that a tree stem was analogous to a conical rod with its tip free and the base fixed. It was further assumed that the effects of stem form, density, and modulus of elasticity were small compared with the effects of tree height, stem diameter, and weight of crown.

The relationship between period, τ, and height of tree and diameter of stem was established by plotting the measured period, τ, against values of $(H_{bh})^2/d_{bh}$ for various groups of tree species. For each group, regression equations were determined of the form

$$\tau = a + b\,(H_{bh})^2/d_{bh} \qquad (2.3)$$

Constants a and b in equation (2.3) for the more important species and groups are presented in Table 2.3.

Table 2.3--Constants a and b in natural period equation $\tau = a + b\,(H_{bh})^2/d_{bh}$ for several important tree species[1/]

Tree species or group	Crown	Constants	
		a	b
	(percent)		
Ponderosa pine[2/]	0	0.62	0.048
" "	20	0.90	0.053
" "	40	1.03	0.067
" "	60	0.99	0.074
" "	80	1.02	0.074
Conifers	40 to 80	0.94	0.067
Broadleaf	" " "	1.68	0.070
Bare stem, average for all species	0	0.63	0.028

1/ From reference (2).
2/ Good site.

Internal Damping

Internal damping in terms of certain tree stem characteristics was obtained from records on free oscillations of several natural tree stems with crown removed. A typical displacement-time record for an actual tree stem following the removal of the external force is shown in figure 2.3. The record indicates that amplitude gradually diminishes with each successive oscillation which is typical of a damped spring-mass system (15). If the damping is viscous the decay of the amplitude

CONFIDENTIAL - FORMERLY RESTRICTED DATA

is exponential. The rate of decay, called the logarithmic decrement, depends on the internal damping factor, α, the natural period of the stem, τ_s, and the effective mass of the stem, m_s. The amplitude, for each successive half cycle, n, as the oscillations diminish is (15)

$$y_n = y_o \, e^{-\frac{\alpha \tau_s}{2m_s} n} \tag{2.4}$$

or

$$\ln \frac{y_n}{y_o} = -\frac{\alpha \tau_s}{2m_s} n \tag{2.5}$$

Values of $\ln y_n/y_o$ were determined for several tree stems and plotted against corresponding values of n as shown in figure 2.4A. The slope of the straight line is $-\alpha\tau_s/2m_s$ which is the logarithmic decrement of the amplitude for the decaying free oscillations of a tree stem. Values of the logarithmic decrement were determined for 12 conifer tree stems comprising several species. Since the effective mass for the stem is not known, a ratio of the internal damping factor to the effective mass, α/m_s, was determined by multiplying the value $-\alpha\tau_s/2m_s$ by the measured value of $2/\tau_s$ for the tree stem.

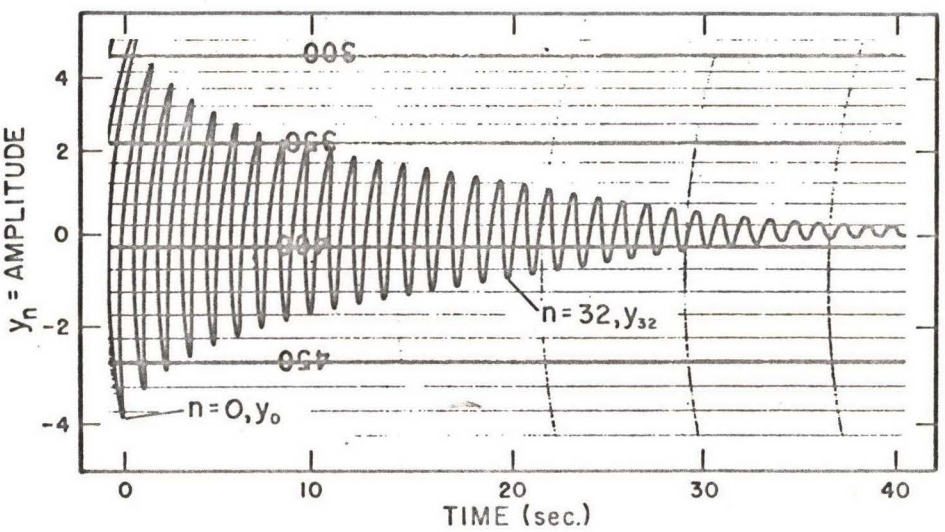

Figure 2.3--Typical free vibration amplitude-time record for a tree stem with crown removed

CONFIDENTIAL - FORMERLY RESTRICTED DATA

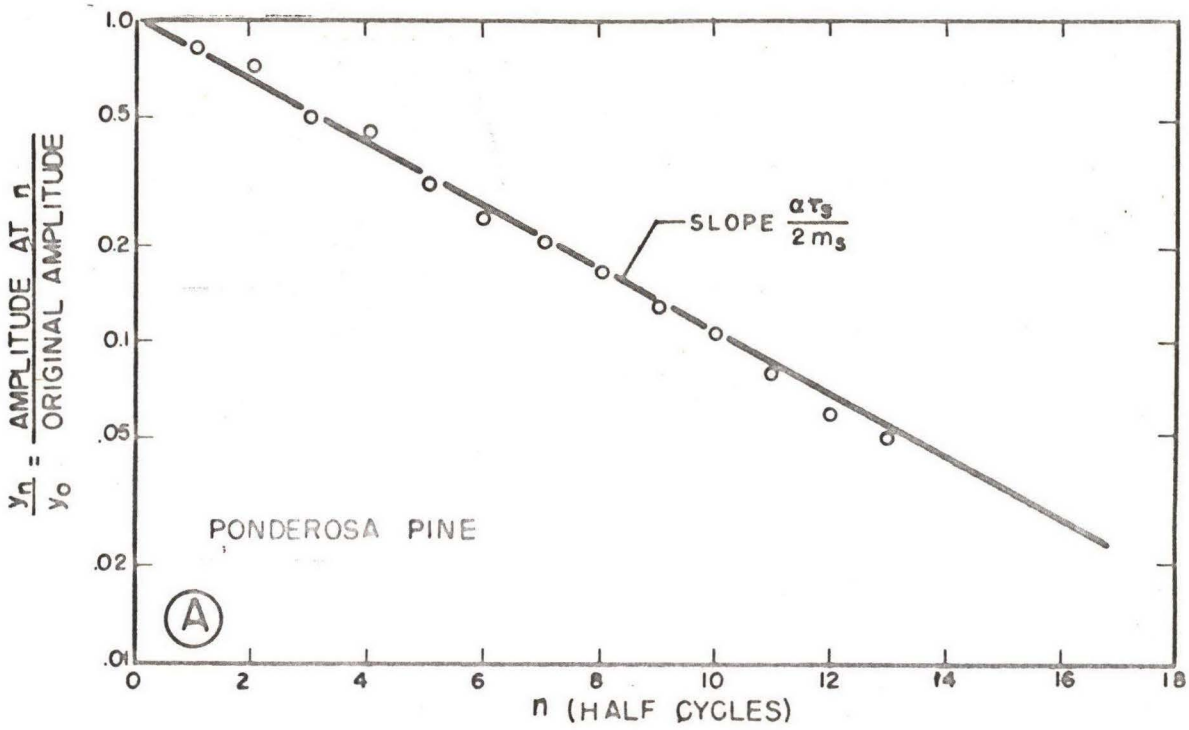

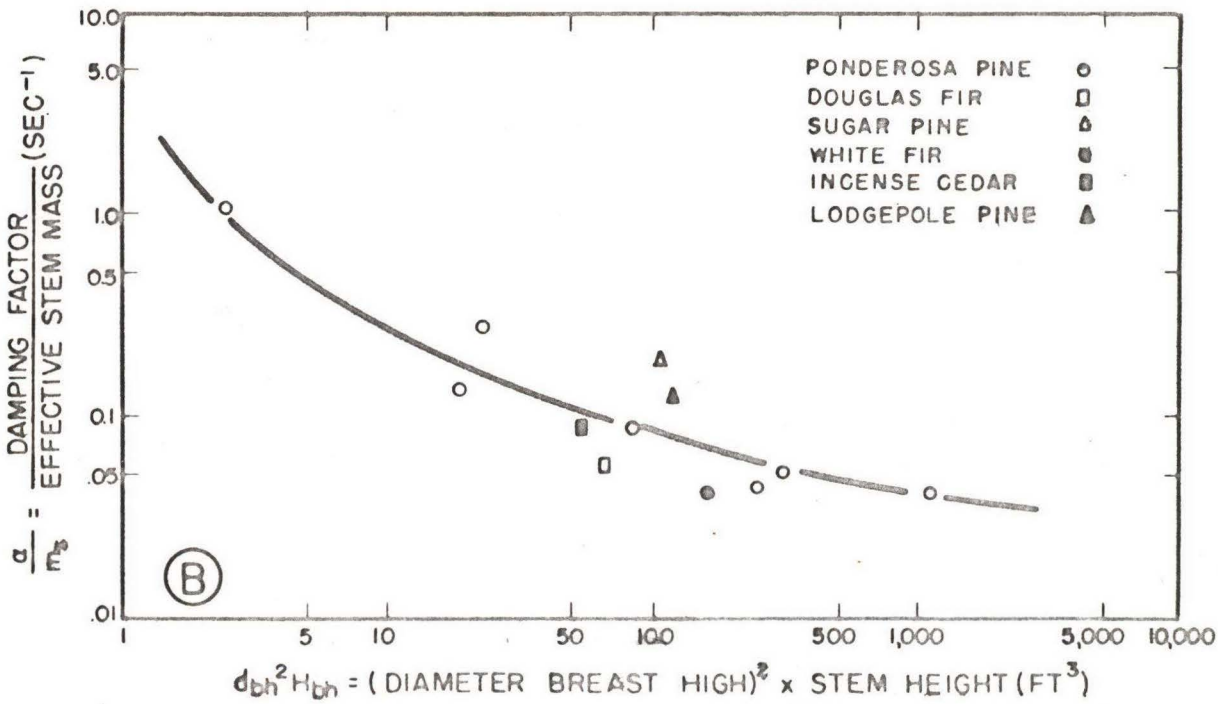

Figure 2.4A: Relative decay of free vibrations with successive cycles for a typical tree-stem

B: Relation between the damping factor per unit mass and the relative tree stem volume

CONFIDENTIAL - FORMERLY RESTRICTED DATA.

Correlation was established between α/m_s and the relative tree stem volume or $d_{bh}^2 H_{bh}$ and is shown in figure 2.4B

$$\frac{\alpha}{m_s} = \phi \left(d_{bh}^2 H_{bh}\right) \tag{2.6}$$

The internal damping factor-mass ratio for the tree stem with crown may be determined since the spring constant is the same for the stem with or without crown

$$\frac{\alpha}{m} = \frac{\alpha}{m_s}\left(\frac{\tau_s}{\tau}\right)^2 \tag{2.7}$$

CONFIDENTIAL - FORMERLY RESTRICTED DATA

CHAPTER 3

WIND DRAG AND STEM BREAKAGE CHARACTERISTICS

General

In the equation of motion (Chapter 4) for a tree stem acted upon by an external force, the inertial force is primarily a function of the drag force of the wind acting on the tree crown and of the restoring force of the deflected tree stem. Studies started in 1951 determined the nature of the drag of natural tree crowns under steady wind and the restoring force variation with deflection of naturally rooted tree stems under static loading.

Wind Drag Characteristics

Wind drag tests were made on 13 conifer trees representing 6 species (4) and 18 broadleaf trees representing 8 species (3).

For these tests freshly cut trees with length of crown up to 20 feet and with stems 7 feet in length below the crown were placed vertically in a special cage mounted on a flat bed 1 1/2-ton truck (figure 3.1). The tree stem inside the cage was connected to two ring dynamometers for measuring the drag of the crown and one ring dynamometer for measuring the moment force about the base of the crown. The base of the tree stem rested on a plate which was mounted on rollers. Each tree, after being instrumented, was transported at various steady speeds, 10 to 55 mph at 5 mph intervals, over a predetermined distance on a level road. Moment and drag measurements were automatically recorded for each run. Upon completion of the tests for a tree, weight of stem, branchwood and foliage; total height of tree, length of crown, and diameters of stem at specified locations were recorded.

As is characteristic with all bodies in submerged flow, the drag force of tree crowns is proportional to dynamic pressure and area upon which it acts. The proportionality factor, or drag coefficient, is not always constant, but depends on the mechanism which brings about drag. For rigid bodies the drag mechanism is usually characterized by a Reynolds modulus based on some geometrical dimensions of the body. However, non-rigid bodies such as tree crowns tend to deform under drag loading. The drag coefficient then is dependent on the method and amount of deformation. The total drag of a tree crown is further complicated by the fact that the area on which the drag forces act is not known independently and furthermore it changes with tree crown deformation.

Wind tunnel tests on conifer saplings indicated that drag was linear with velocity in the range of interest. This linearity is a characteristic of pure laminar skin friction drag. Since the linear portion of the curve does not extrapolate to zero drag at zero velocity,

CONFIDENTIAL - FORMERLY RESTRICTED DATA

Figure 3.1--Tree mounted on a truck bed for drag test (Douglas fir)

the laminar drag region must be preceded by a region of non-linear variation or turbulent drag. Such a turbulent drag region had previously been indicated by qualitative results obtained by Tirén (16) from wind tunnel measurements made on a single branch. This transition from a turbulent to a laminar type drag as the velocity increases is contrary to other known patterns of drag variations. It was concluded, then, that the variation of drag was principally due to the bending of the tree crown. On the basis of results of wind tunnel tests with saplings (4) and Tirén's findings (16), data from the vehicle drag tests were correlated with dimensionless parameters that depend upon the wind force and the tree crown and stem characteristics. The correlation of drag on the basis of dimensionless parameters presumes linearity of the various important geometric relationships of the tree crown regardless of size. This was found to be true for several species from analysis of weights of crown (7) and (8).

CONFIDENTIAL - FORMERLY RESTRICTED DATA

The correlation of drag data resulted in functional relationships. For the conifers the relation is

$$D/W_c = \phi\left(\frac{M}{d_c^3}\right)\left(\frac{W_b}{W_f}\right) \div \left(\rho \frac{U^2}{2}\right) \tag{3.1}$$

For the broadleaf the relation is

$$D/W_f = \phi\left(\frac{M}{d_c^3}\right) \div \left(\rho \frac{U^2}{2}\right) \tag{3.2}$$

Experimental curves for estimating drag for conifer and broadleaf tree crowns are presented in figures 3.2 and 3.3.

The moment, M , about the base of crown for each tree tested was determined directly with a ring dynamometer measuring the moment force. Theoretically the moment, M , is the product of the drag force, D , and the position of the center of pressure with respect to the distance from the base of the crown, h . For estimating the position of center of pressure it was necessary to establish a relationship between the center of pressure of the drag force and the geometrical characteristics of the tree crown. Correlation of test data established such relationships. For conifer trees the relation is

$$\frac{\overline{H}_{cp}}{d_c} = \phi\left(\frac{H_c}{d_c}\right)\left(\frac{W_b}{W_f}\right) \tag{3.3}$$

For broadleaf trees the relation is

$$\frac{\overline{H}_{cp}}{H_c} = \phi\left(\frac{H_{bh}\, d_c}{d_{bh}}\right) \tag{3.4}$$

Experimental curves for estimating the position of center of pressure for conifer and broadleaf tree crowns are presented in figures 3.4 and 3.5.

Stem Breakage Characteristics

Ponderosa pine trees (poor and good site)[4/] and several broadleaf species (good site) were used for static bending tests with crowns removed. These tests determined restoring force variations with deflection of naturally rooted trees. The tree stems varied from 6 to 32 inches in diameter and from 33 to 124 feet in height. The test was performed by

4/ Tree Structure, Chapter 2.

CONFIDENTIAL - FORMERLY RESTRICTED DATA

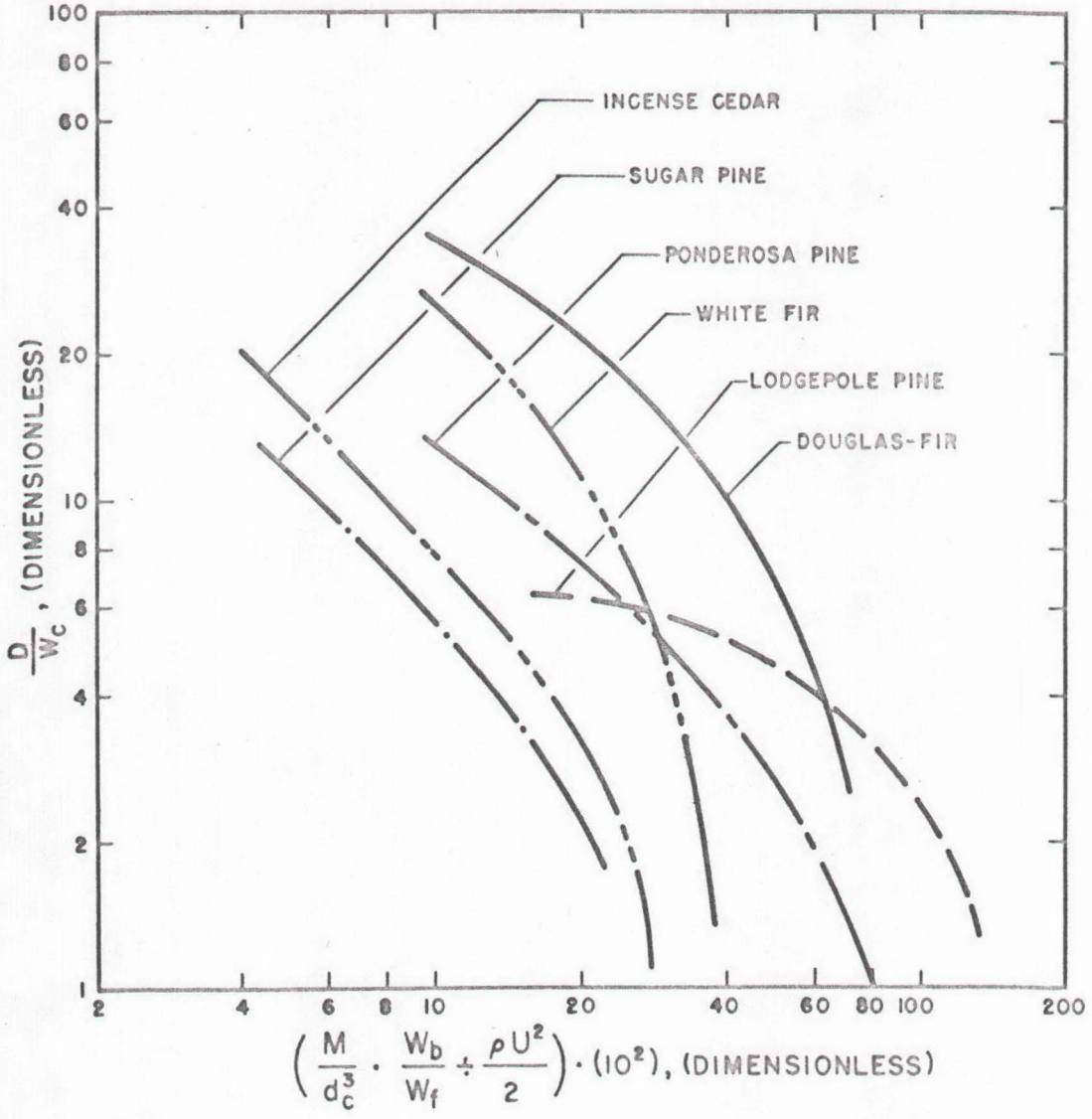

Figure 3.2--Dimensionless correlation of aerodynamic drag data for several conifer species

attaching a cable between a winch and a preselected loading point on the stem and increasing the load until the stem failed. A recorder connected to a ring dynamometer attached to the cable measured the force of the applied load. Transit measurements of the horizontal and vertical angle to the point of loading provided data for calculating the displacement of the loading point. After failure, by either breakage or uprooting, tree stem dimensions were recorded for use in calculating stem form factor and loading characteristics.

CONFIDENTIAL - FORMERLY RESTRICTED DATA

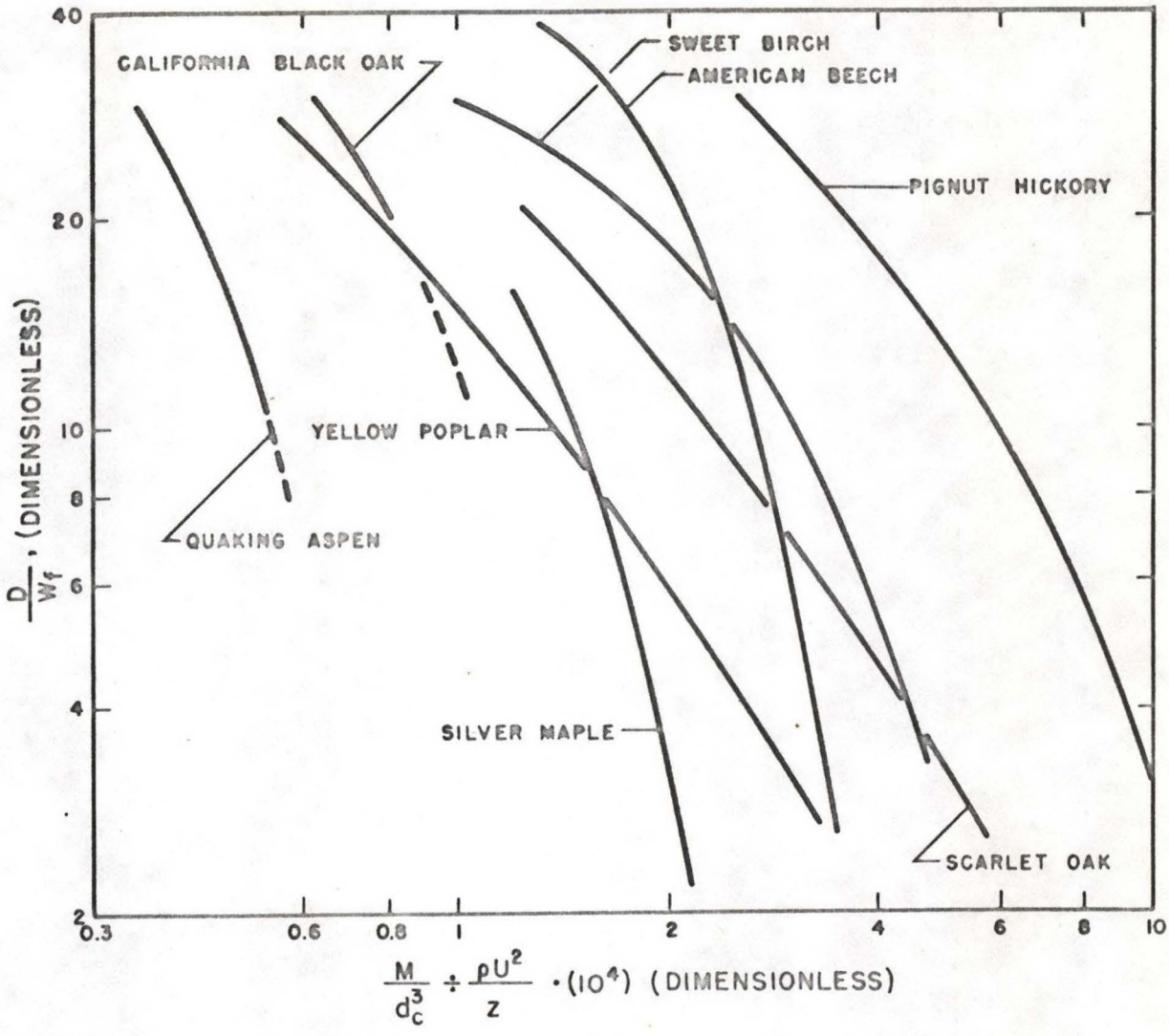

Figure 3.3--Dimensionless correlation of aerodynamic drag data for several broadleaf species

Theoretical specification of the forces required and the large relative deflections associated with tree-stem breakage under static loading involves solution of a nonlinear second order differential equation. The problem is further complicated by elastic plastic deformation at high stress, by inherent stress concentrations, nonuniformity of the tree stem, and variations in the mechanical properties of the wood itself.

CONFIDENTIAL - FORMERLY RESTRICTED DATA

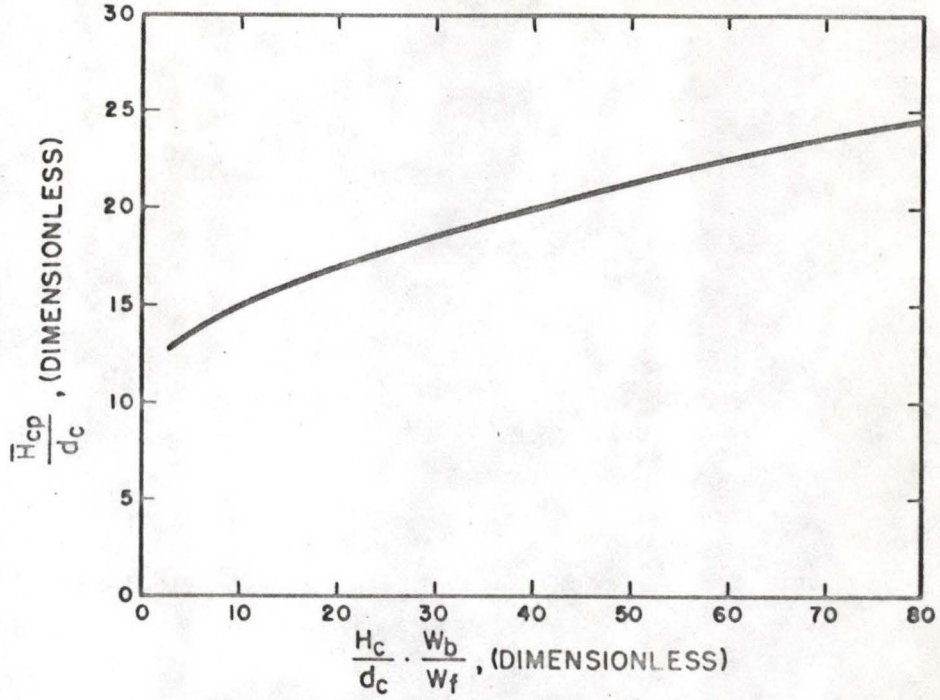

Figure 3.4--Location of center of pressure of wind drag for conifer trees

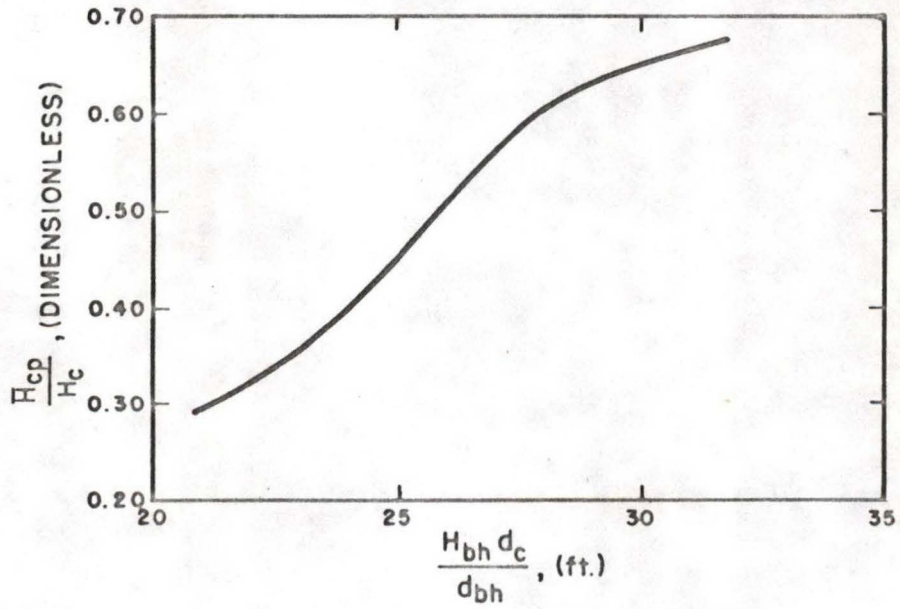

Figure 3.5- Location of center of pressure of wind drag for broadleaf trees

CONFIDENTIAL - FORMERLY RESTRICTED DATA

Previous analysis (6), based on small deflection theory, delineated essential parameters concerned with tree stem breakage by a single load. Equations derived presented the basis for the correlation of experimental data for tree stem breakage by static bending of conifers (6) and broadleaf species (5). The tree stem was considered to be a homogeneous cantilever beam of circular cross section fixed at breast height. Since root swell is usually pronounced up to breast height this assumption of no bending below that point should not seriously affect prediction of deflection in the upper part of the tree stem. Figure 3.6 shows a schematic diagram of a tree stem and gives the essential stem parameters used in the analysis.

Compressive or tensile unit stress due to loading was determined by the flexure formula

$$S = \frac{MC}{I} \tag{3.5}$$

where,

$$M = R\, H_{bh}(1-f_1)$$

Bark thickness is not considered to contribute to stem strength, consequently moment of inertia is determined for stem diameter inside bark. Stress at breast height ($f = 1$) due to a horizontally applied force is (figure 3.6)

$$S_{bh} = \frac{32RH_{bh}}{\pi d_i^3}\,(1-f_1) \tag{3.6}$$

and along the stem the stress is

$$S = \frac{f-f_1}{1-f_1}\left[\frac{f+c}{f(1+c)}\right]^3 S_{bh} \tag{3.7}$$

where $c = \frac{b}{a}$, a and b are the stem form constants, equation (2.2).

The maximum stress occurs at

$$f_m = c \pm (c^2-3cf_1)^{1/2} \tag{3.8}$$

with the sign (-) for $c > o$ and (+) for $c < o$.

Hence maximum stress is

$$S_m = \frac{f_m-f_1}{1-f_1}\left[\frac{f_m+c}{f_m(1+c)}\right]^3 S_{bh} \tag{3.9}$$

CONFIDENTIAL - FORMERLY, RESTRICTED DATA

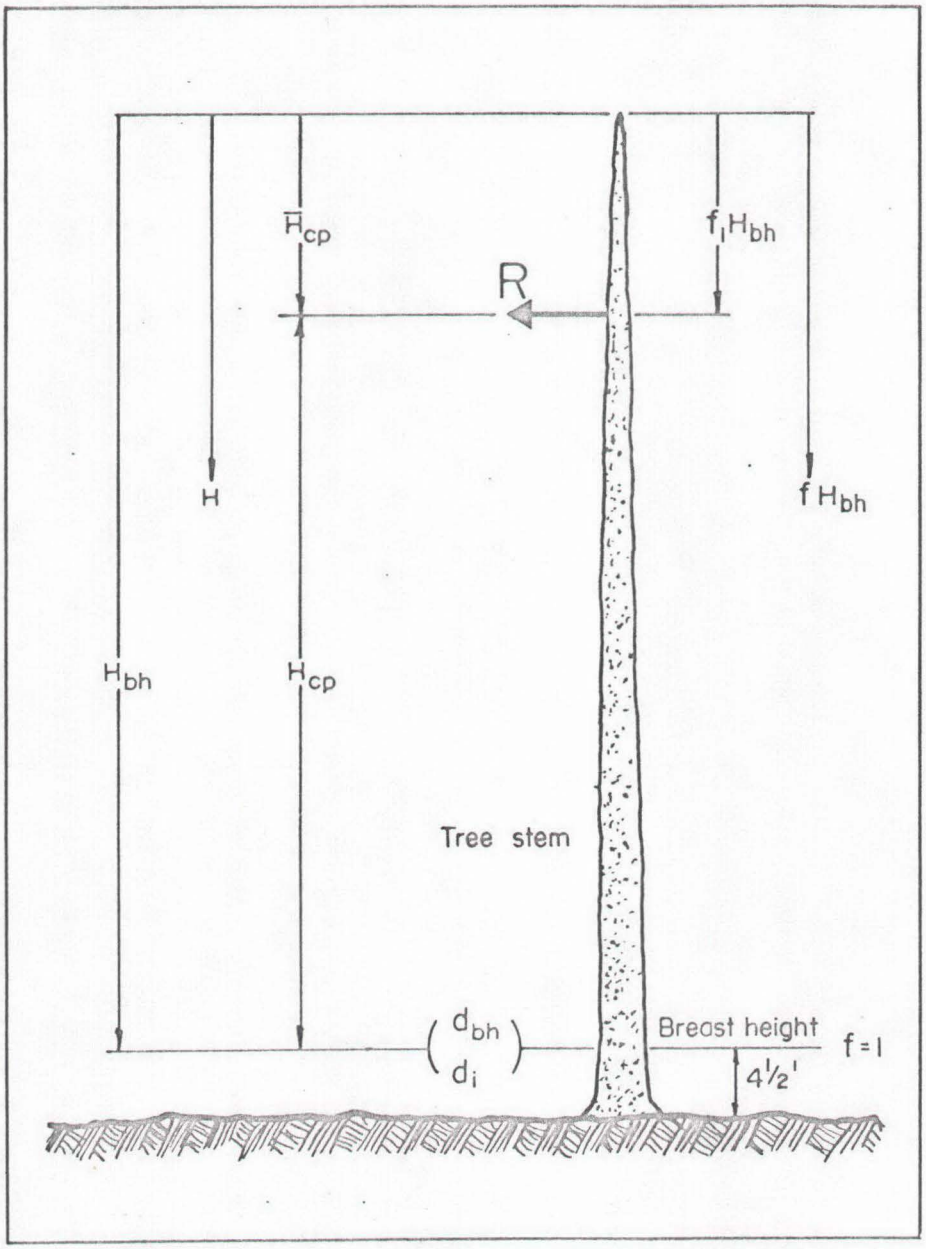

Figure 3.6--Schematic diagram showing tree stem and associated parameters

CONFIDENTIAL - FORMERLY RESTRICTED DATA

In the region where deflection is proportional to applied force, the theoretical spring constant is

$$k_r = \frac{R}{y(f_1)} \tag{3.10}$$

where $y(f_1)$ is the horizontal deflection at the point of load application.

By considering small deflections the following expression for stem deflection was derived from the elastic curve equation of a beam (17)

$$y = \frac{RH_{bh}^3}{3EI_i} \phi\,(c,f_1,f) \tag{3.11}$$

Letting $y = y(f_1)$ in equation (3.11) and combining with equation (3.10) yielded a dimensionless expression containing the spring constant

$$\frac{k_r H_{bh}^3}{3EI_i} = \phi^{-1}\,(c,f_1) = \psi\,(c,f_1) \tag{3.12}$$

Equation (3.12) is shown graphically in figure 3.7 for applicable ranges of c and f_1.

In the elastic region the unit-stress in the wood equals the modulus of elasticity times the unit-strain in the direction of the stress, hence the maximum strain is

$$\delta_m = \frac{S_m}{E} \tag{3.13}$$

and by combining equation (3.13) with equations (3.11) and (3.6)

$$\frac{\delta_m}{y(f_1)} = \left[\frac{3d_i(1-f_1)}{2H_{bh}^2}\,\psi\,(c,f_1)\right]\frac{S_m}{S_{bh}} \tag{3.14}$$

For the analysis, the restoring force characteristics of the stem were idealized as shown in figure 3.8. A measured spring constant k_a for the elastic region was determined for each tree stem from the horizontal component R of the measured force and from the horizontal deflection y by use of equation (3.10). Values of k_r, y_r, and R_r, corresponding to the point of load application, were computed in order using first, equation (3.12), and then equation (3.14) with $\delta_m = \delta_r$, finally equation (3.10). The reference strain δ_r is a measure of the

CONFIDENTIAL - FORMERLY RESTRICTED DATA

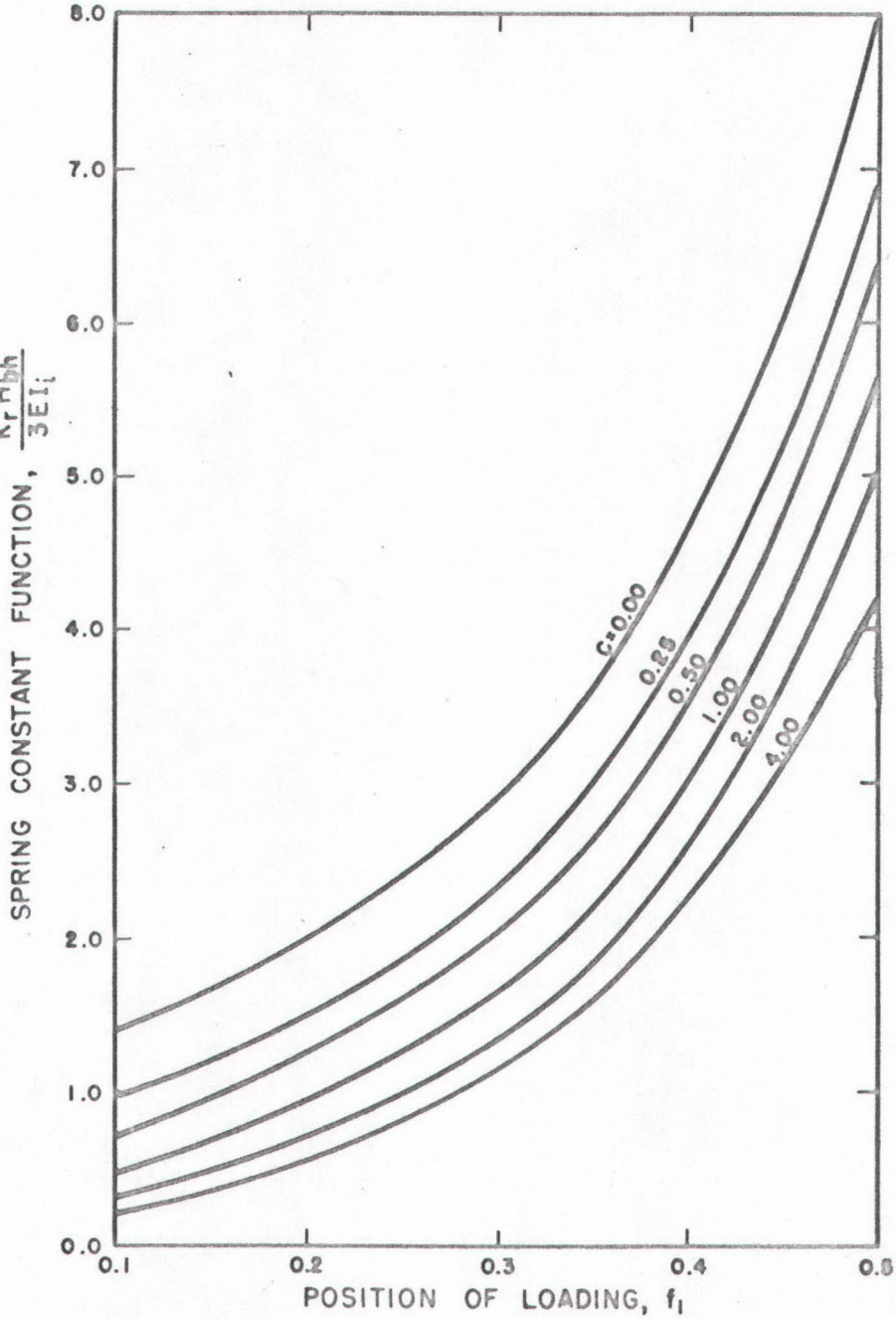

Figure 3.7--Dimensionless expression containing spring constant, k_r, as a function of position of loading, f_1, and stem form factor, c

CONFIDENTIAL - FORMERLY RESTRICTED DATA

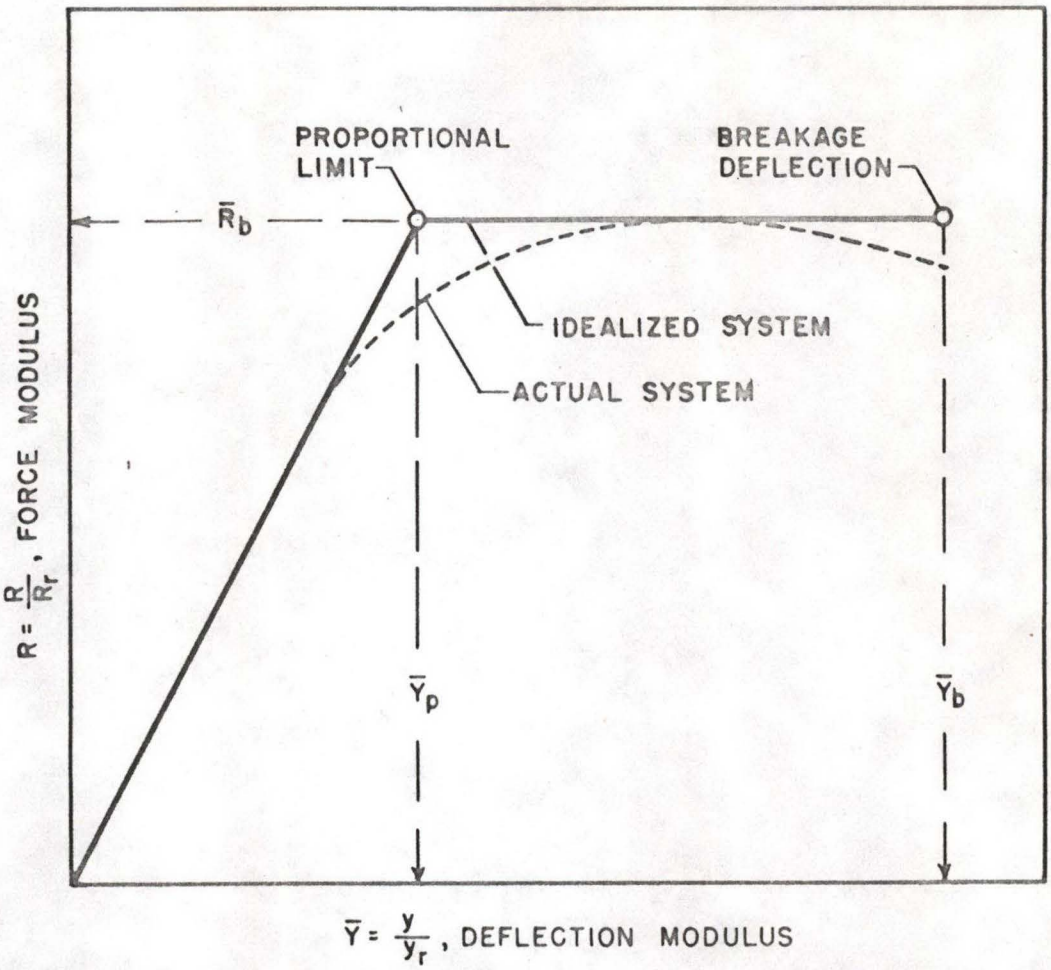

Figure 3.8--Restoring force characteristics of idealized tree stem--single horizontal load

inherent strength of the wood fiber and varies between species. It is defined as

$$\delta_r = \frac{S_r}{E}, \frac{\text{modulus of rupture (green wood)}}{\text{modulus of elasticity (green wood)}} \qquad (3.15)$$

In Table 3.1 are reference strain values for several species determined from the mechanical properties of green wood (18). The variations of the restoring force characteristics due to species, form, stem dimensions, and position of loading are eliminated by forming the following breakage moduli

CONFIDENTIAL - FORMERLY RESTRICTED DATA

$$\overline{R}_b = \frac{R_b}{R_r} \text{ , breakage force modulus} \qquad (3.16)$$

$$\overline{Y}_b = \frac{y_b}{y_r} \text{ , breakage deflection modulus} \qquad (3.17)$$

$$\overline{K} = \frac{k_a}{k_r} = \overline{R}_b / \overline{Y}_p \text{ , spring constant modulus} \qquad (3.18)$$

Table 3.1--Reference strain values for green wood of several species[1/]

Species	Modulus of elasticity, E	Modulus of rupture, S_r	Reference strain, $\delta_r = \frac{S_r}{E}$
	lbs/sq in.	lbs/sq in.	in./in.
Ponderosa pine	0.97×10^6	5,000	0.0051
Douglas fir	1.55×10^6	7,600	0.0049
Loblolly pine	1.41×10^6	7,300	0.0052
Cedar	0.84×10^6	6,200	0.0074
White fir	1.03×10^6	5,700	0.0055
Yellow-poplar	1.09×10^6	5,400	0.0049
Silver maple	0.94×10^6	5,800	0.0062
Scarlet oak	1.48×10^6	10,400	0.0071

1/ Values for E and S_r from reference (18).

Static breakage measurements indicated a wide variation in breakage moduli. This is not unexpected since wood is not a homogeneous material. Variations in these moduli are due to inherent variations in the strength properties of the wood, and knots and other defects; hence, it was necessary to develop a method for presenting the results on a statistical basis.

Breakage data for the statistical analysis were expressed in terms of the static work required to break a given stem. This amount of work is the integral under the curve in Figure 3.8, or

$$E_b = \int_o^{y_b} R \, dy \qquad (3.19)$$

CONFIDENTIAL - FORMERLY RESTRICTED DATA

Work required to bend the stem to the reference deflection is $R_r y_r/2$. In order to present the breakage results in a nondimensional form, a static work modulus was defined to include the reference work, $R_r y_r/2$,

$$\bar{E}_b = \frac{1}{R_r y_r} \int_o^{y_b} R \, dy = \int_o^{\bar{Y}_b} \bar{R} \, d\bar{Y} \tag{3.20}$$

or, for the idealized system of figure 3.8

$$\bar{E}_b = \bar{R}_b \left[\bar{Y}_b - \frac{\bar{Y}_p}{2} \right] \tag{3.21}$$

Values of $\bar{E}_b$ (using equation (3.21)) were determined for all the trees tested and cumulative normal frequency distributions were then calculated. Probability of occurrence of static work modulus for the three tree populations studied are presented in figures 3.9 and 3.10.

CONFIDENTIAL - FORMERLY RESTRICTED DATA.

CONFIDENTIAL--FORMERLY RESTRICTED DATA

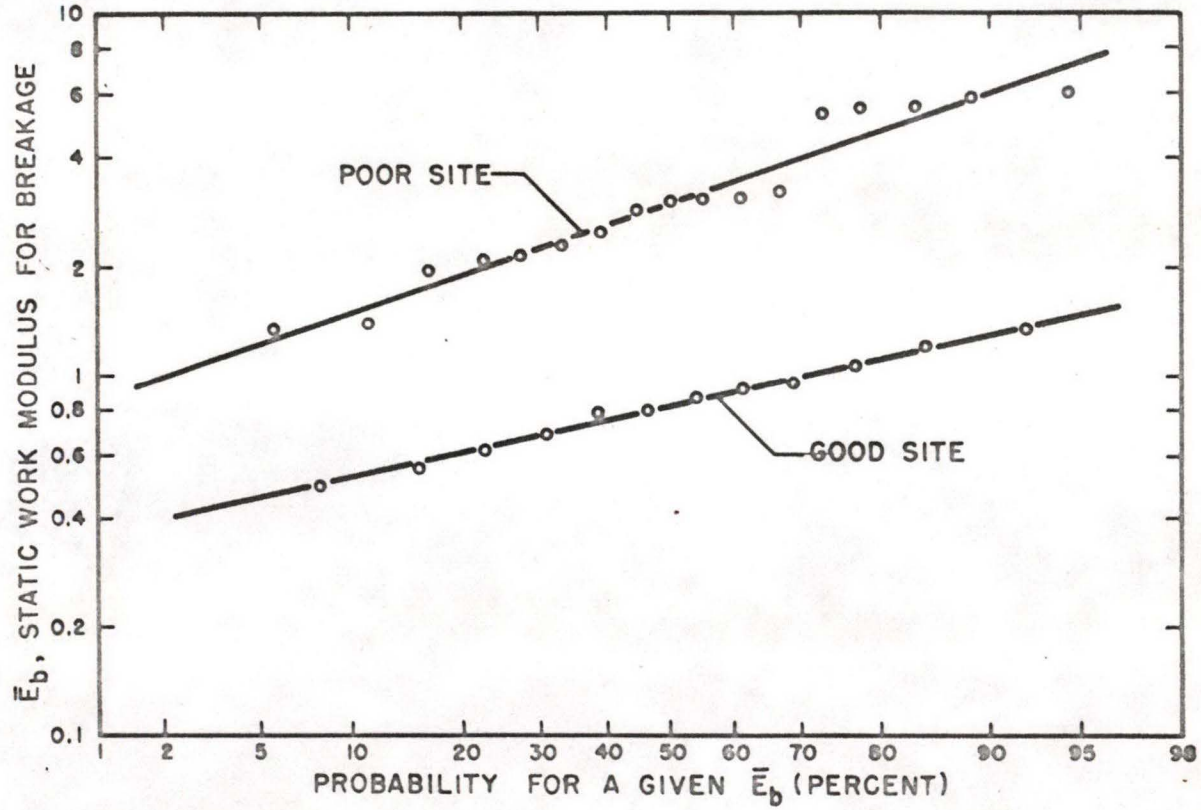

Figure 3.9--Actual frequency distribution of static work modulus, $\bar{E}_b$, for good and poor site ponderosa pine

CONFIDENTIAL - FORMERLY RESTRICTED DATA

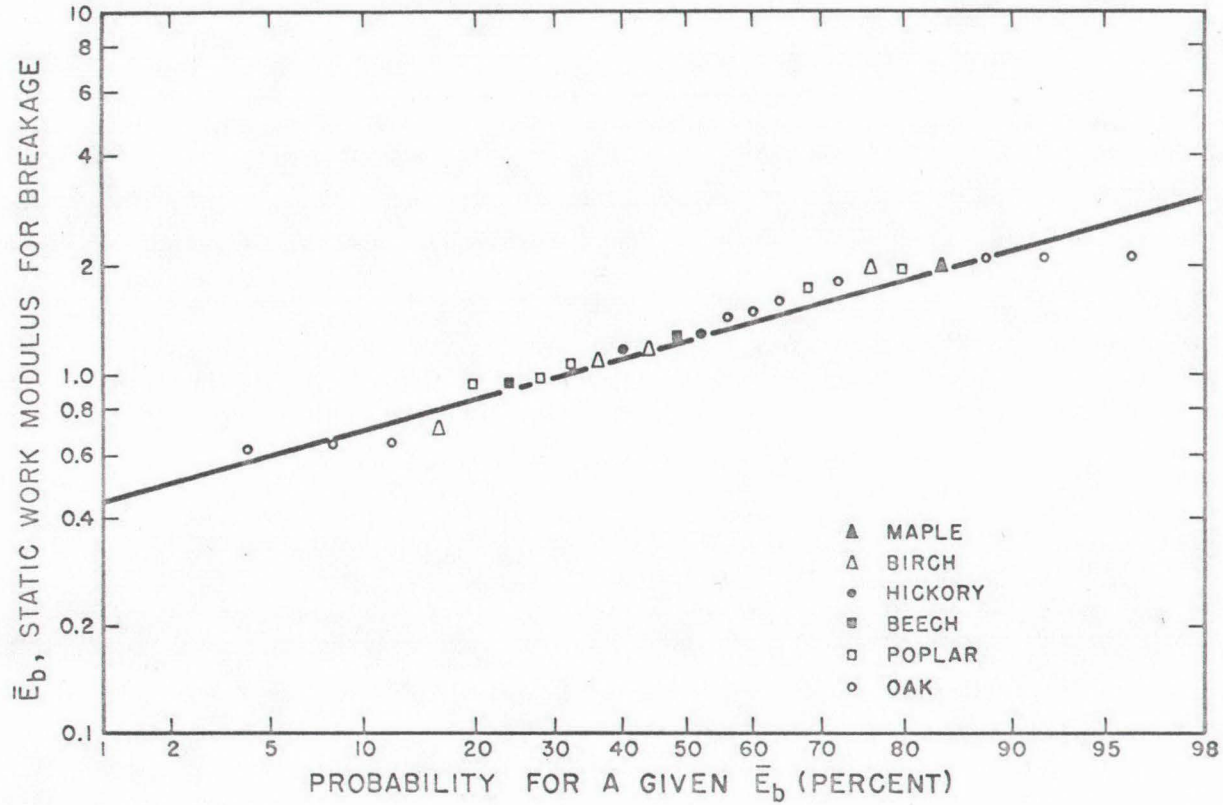

Figure 3.10--Actual frequency distribution of static work modulus, $\bar{E}_b$, for all broadleaf trees tested grouped into one sample population

CHAPTER 4

THEORETICAL CALCULATIONS OF STEM BREAKAGE--SINGLE STEMS

General

This chapter deals with the theoretical calculation of tree motion under shock wave loading and prediction of the probability of breakage for single tree stems.

This calculation procedure was developed over a period of time during which a number of changes were made, consistent with new data on tree characteristics and increased experimental knowledge of stem breakage. No attempt has been made to recount these historical events, and calculating procedures are given in their final form.

A substantial number of assumptions have been made throughout the calculations. Many of these are of an a priori nature and can only be justified on the basis of overall experimental checks. Most assumptions arise through a need to simplify the very complex nature of tree stem motion and to generalize the results.

Calculations apply to trees consisting of a clearly defined stem associated with a single crown. This type of structure is characteristic of most conifers and some broadleaf species, e.g., yellow poplar. Stem breakage was assumed to constitute the major type of breakage and this has been shown experimentally to be the case for ponderosa pine.

The Equation of Motion of the Tree Crown

The tree crown and associated stem were assumed to constitute a single degree of freedom spring-mass system having a lumped mass, m, located at the crown center of pressure and an internal viscous damping factor, α, (figure 2.4A). Figure 4.1 displays the velocity and force notation used in the analysis.

The particle velocity, u, associated with the blast wave, was assumed horizontal and its magnitude was independent of elevation above the ground. These assumptions restrict calculated results to pressure levels where Mach stem height is larger than tree height. In the range of pressure levels causing stem breakage, this condition is generally met. It is not believed, however, that serious error is introduced in the region of regular shock reflection or if the Mach stem height does not exceed tree height.

For the system of figure 4.1 the force equation becomes

$$m\ddot{s} + \alpha\dot{s} + R_s(y) = D_s(M,t) \qquad (4.1)$$

CONFIDENTIAL - FORMERLY RESTRICTED DATA

CONFIDENTIAL - FORMERLY RESTRICTED DATA

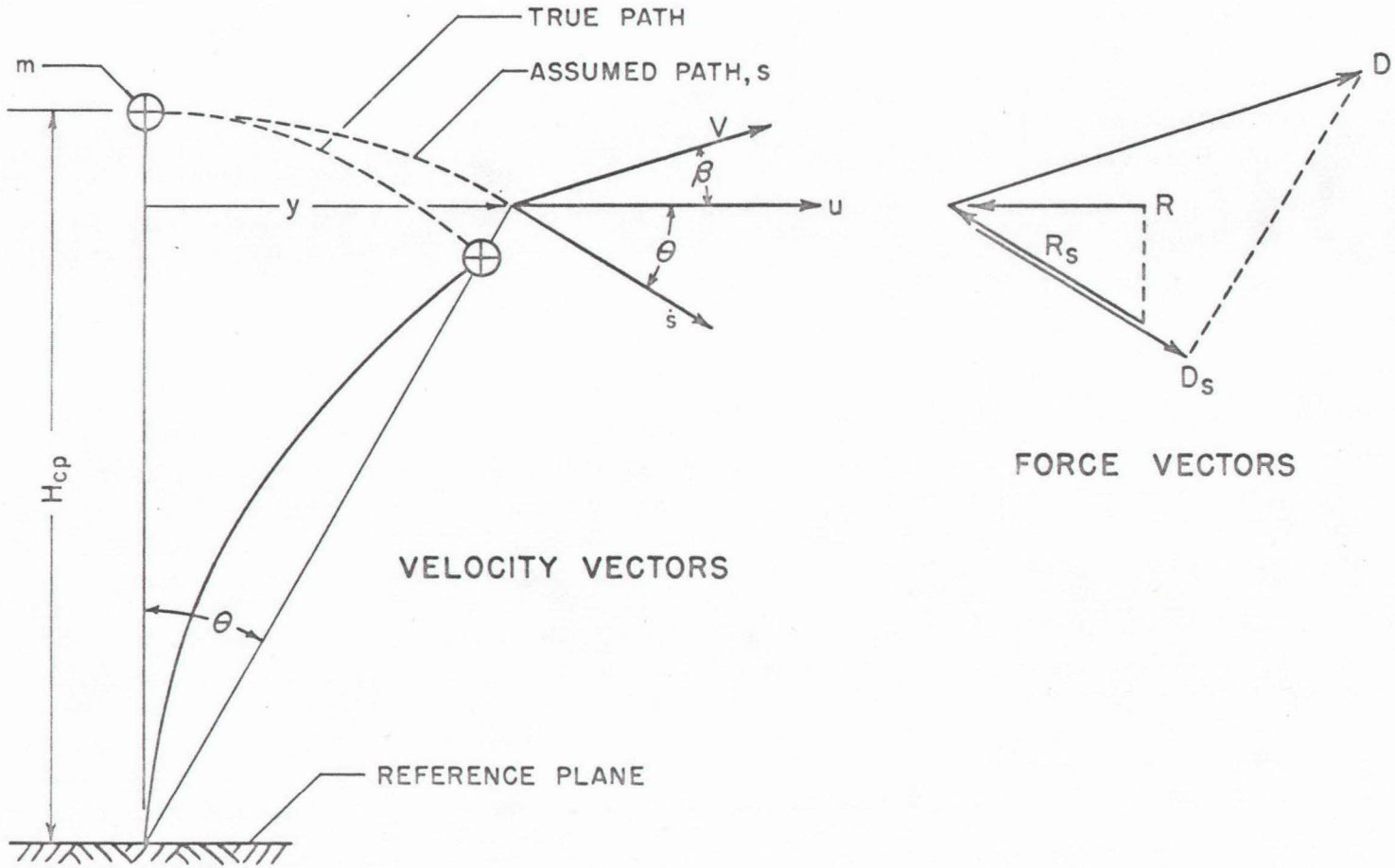

Figure 4.1--Tree stem and mass represented by a spring-mass system

where the restoring force in the direction of motion, R_S, is a function of the horizontal displacement, y, (figure 4.1). The aerodynamic drag of the tree crown in the direction of motion, D_S, is a function of the bending moment, M, about the base of crown (figure 3.2) and its time dependency comes about through the temporal variation of density and particle velocity in the afterflow of the shock wave.

The path traveled by the mass center depends, in an extremely complex manner, on the stem form, and temporal and spatial variation of the drag loading vector. For the purpose of defining the vector velocity, $\dot{s}$, and the horizontal displacement, y, of the center of mass the mass center was assumed to travel along an arc having a radius equal to H_{cp}.

The restoring force, R, was defined as the horizontal component of a force at an angle θ necessary to produce a deflection equal to y. Hence

$$R_s = R(y) \sec \theta \tag{4.2}$$

In view of the irregular nature of the tree crown, aerodynamic drag forces were assumed independent of the angle of attack. The drag force in the direction of motion is then

$$D_s = \left[\frac{D}{\rho U^2}(M)\right] \rho(t)\, V^2(t) \cos(\beta + \theta) \tag{4.3}$$

where V is the particle velocity relative to the velocity of the center of mass expressed as

$$V^2 = u^2 + \dot{s}^2 - 2u\dot{s} \cos \theta \tag{4.4}$$

and

$$\tan \beta = \frac{\dot{s} \sin \theta}{u - \dot{s} \cos \theta} \tag{4.5}$$

The drag coefficient, $D/\rho U^2$, is a function of the bending moment about the base of the crown, i.e., $M = Rh$.

Shock Wave Parameters

A generalized description of the air density and particle velocity field in the shock afterflow, as influenced by the ground plane, does not exist. An approximation of the temporal variation of these quantities was made using a normalized form of the free air results from the LASL Problem M calculations (11). Peak values of ground level overpressure and positive phase duration were then used to resolve the shock wave into an approximation of the shock afterflow in the Mach region.

CONFIDENTIAL - FORMERLY RESTRICTED DATA

The normalized particle velocity and air density are shown in figure 4.2 for a range of peak overpressures between 2.2 to 8.4 psi (at sea level). Within this pressure range the normalized results, computed from LASL Problem M calculations, are fitted quite satisfactorily by the emperical equations

$$\frac{u}{u_1} = \left(1 - \frac{t}{1\text{-}4t_+}\right) e^{-\frac{t}{1.4t_+}} = \psi_1(t/t_+) \tag{4.6}$$

and

$$\frac{\rho - \rho_o}{\rho_1 - \rho_o} = (1 - \frac{t}{t_+})e^{-\frac{t}{t_+}} = \psi_2(t/t_+) \tag{4.7}$$

For Mach reflection the particle velocity and density at the shock front are, in terms of the overpressure, with $\gamma = 7/5$ (11)

$$\left(\frac{u_1}{a_o}\right)^2 = \frac{\frac{25}{7}\left(\frac{\Delta p_1}{p_o}\right)^2}{7 + 6\frac{\Delta p_1}{p_o}} \tag{4.8}$$

$$\frac{\rho_1}{\rho_o} = \frac{7 + 6\frac{\Delta p_1}{p_o}}{7 + \frac{\Delta p_1}{p_o}} \tag{4.9}$$

and the associated dynamic pressure is

$$\frac{\rho_1 u_1^2}{2p_o} = \frac{5/2\left(\frac{\Delta p_1}{p_o}\right)^2}{7 + \frac{\Delta p_1}{p_o}} \tag{4.10}$$

Combining equations (4.6) with (4.8) and (4.7) with (4.10) the particle velocity and density become

$$u = \frac{1.89 a_o \Delta p_1}{\sqrt{p_o}\sqrt{7p_o + 6\Delta p_1}} \cdot \psi_1(t/t_+) \tag{4.11}$$

CONFIDENTIAL - FORMERLY RESTRICTED DATA

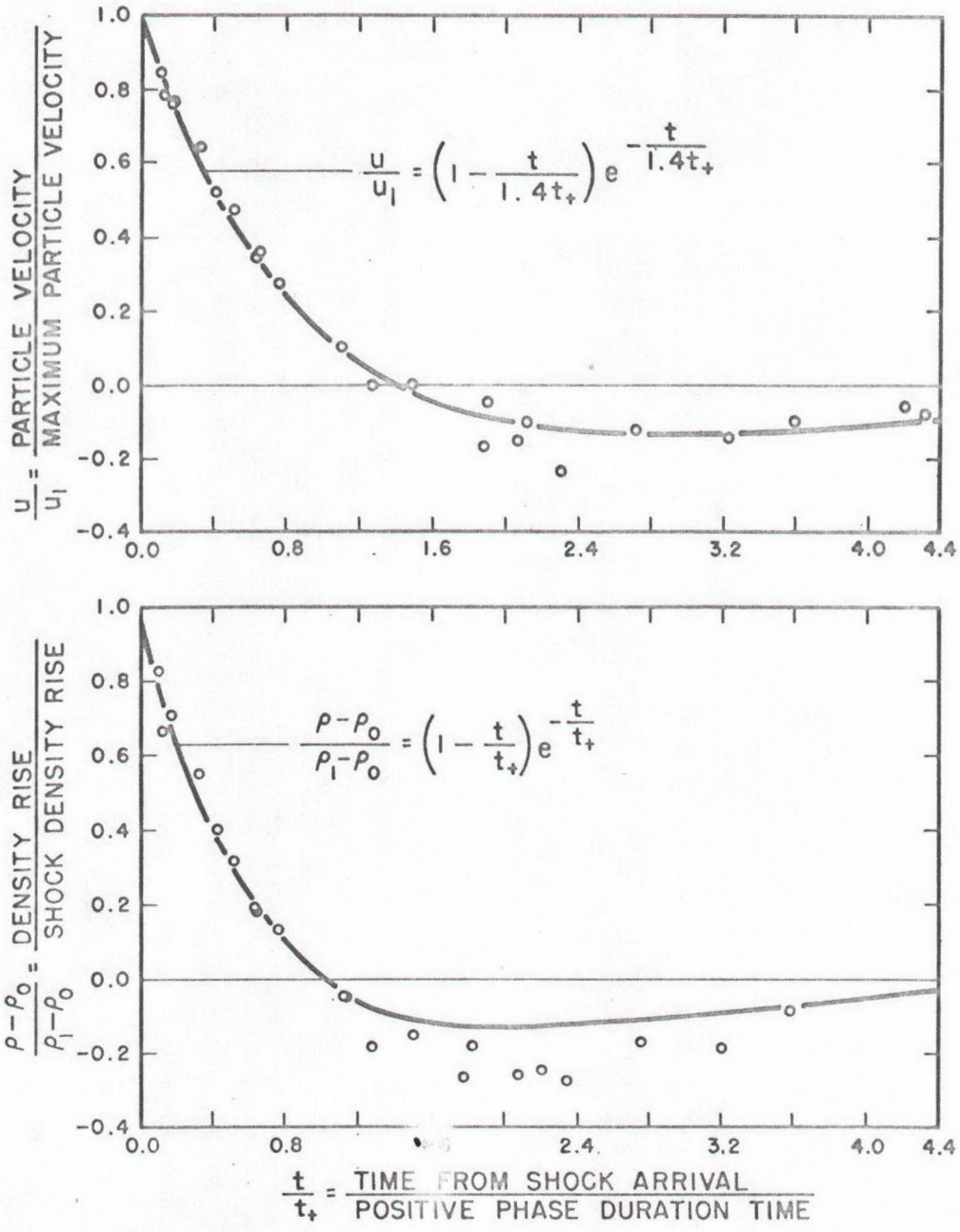

Figure 4.2--Theoretical particle velocity and density variation with time for free air, $2.2 < (\Delta p_1) < 8.4$ psi. Subscript o refers to preshock values, subscript 1 to peak values.

CONFIDENTIAL - FORMERLY RESTRICTED DATA

$$p = p_o \left[1 + \frac{5\Delta p_1}{7p_o + \Delta p_1} \cdot \psi_2(t/t_+) \right] \tag{4.12}$$

Integration of the Equation of Motion

Equation 4.1, the equation of motion of the center of mass, is non-linear and must be integrated for specific input conditions and tree characteristics by a stepwise procedure. For a tree of a particular species, diameter, height, and percent-crown, the necessary tree stem and crown characteristics were determined from Chapters 2 and 3 (see Appendix, page 94). For example, the equivalent mass was determined from the natural period of the tree with crown (Table 2.3) and the spring constant for a force located at the center of pressure (Chapter 3).

$$m = \frac{\tau^2}{4\pi^2} \bar{k}_a \tag{4.13}$$

where $\bar{k}_a$ was determined from the average spring constant modulus $\bar{K}$ for the particular species.[5/] Shock wave input functions were determined from equations (4.11) and (4.12) once the overpressure and its positive phase duration were chosen.

The time scale was divided into incremental divisions so that

$$t_n = n\Delta t, \quad (n = 0, 1, 2 \ldots n) \tag{4.14}$$

The time interval, Δt, was chosen uniformly as 0.04 sec. Within the interval Δt, as a first approximation, the system was considered linear, hence the velocity and displacement of the center of mass were given by

$$\dot{s}_{n+1} = \dot{s}_n + \ddot{s}_n \Delta t \tag{4.15}$$

$$s_{n+1} = s_n + \frac{\dot{s}_n + \dot{s}_{n+1}}{2} \Delta t \tag{4.16}$$

and from equation (4.1)

$$\dot{s}_{n+1} = \frac{D_{s_{n+1}}}{m} - \frac{R_{s_{n+1}}}{m} - \frac{\alpha}{m} \dot{s}_{n+1} \tag{4.1a}$$

where D_s and R_s were determined using the angles, velocities, and deflection evaluated at time equal to t_{n+1}, and $\frac{\alpha}{m}$ was determined from equation (2.7).

A second approximation was made using the average acceleration to compute the center of mass velocity ·

5/ Average $\bar{K}$ value from Table 5, reference (6).

CONFIDENTIAL - FORMERLY RESTRICTED DATA

$$\dot{s}'_{n+1} = \dot{s}_n + \frac{\ddot{s}_n + \ddot{s}_{n+1}}{2} \Delta t \qquad (4.15a)$$

and the iteration continued using the new velocity. In general, the first computed acceleration, $\ddot{s}_{n+1}$ and the second, $\ddot{s}'_{n+1}$ were sufficiently close that further iteration was unnecessary. This procedure also served as a preliminary calculation check.

Drag coefficient-bending moment curves were prepared for each tree using the stem and crown characteristics determined as in Chapters 2 and 3 and the drag correlation for ponderosa pine (figure 3.2). A typical curve is shown in figure 4.3. Note that the drag coefficient at zero bending moment corresponds to the vertical asymptote in figure 3.2.

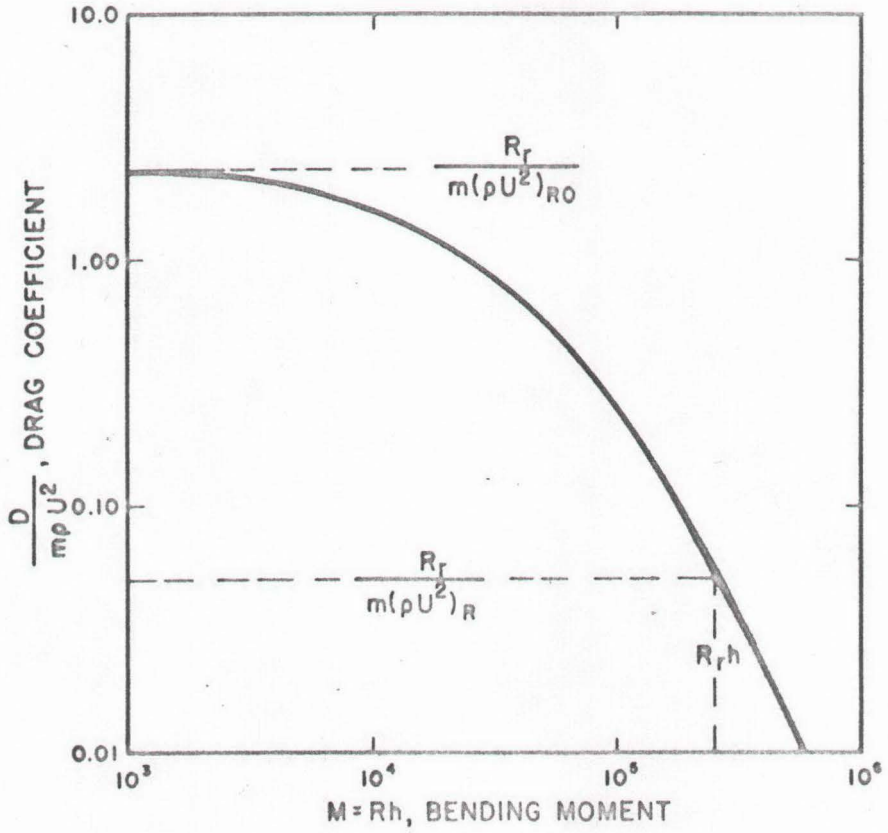

Figure 4.3--Drag coefficient variation with bending moment of tree stem (Stem 24-40-I).

CONFIDENTIAL - FORMERLY RESTRICTED DATA

Calculations were started with the initial (n = 0) conditions

$$s_o = 0$$

$$\dot{s}_o = 0$$

$$\ddot{s}_o = \frac{1}{m}\left(\frac{D}{\rho U^2}\right)_o \rho_1 u_1^2$$

where $\left(\frac{D}{\rho U^2}\right)_o$ is the drag coefficient at zero bending moment (figure 4.3).

Calculations were carried out as far as the first (positive) maximum deflection, y_1, in all cases and as far as the second (negative) maximum deflection, y_2, for those conditions where the second appeared to be significant. Static work moduli for maximum deflection, corresponding in form to the static work modulus for breakage, were then calculated using equation (3.21), Chapter 3, i.e.,

$$\bar{E}_1 = \bar{R}_b\left(\bar{Y}_1 - \frac{\bar{Y}_p}{2}\right) \qquad \bar{Y}_p < \bar{Y} \qquad (4.17)$$

$$\bar{E}_2 = \bar{R}_b\left(\bar{Y}_2 - \frac{\bar{Y}_p}{2}\right)$$

or

$$\bar{E}_1 = \frac{\bar{K}\,\bar{Y}_1^2}{2} \qquad 0 < \bar{Y} < \bar{Y}_p \qquad (4.17a)$$

$$\bar{E}_2 = \frac{\bar{K}\,\bar{Y}_2^2}{2}$$

where

$\bar{Y}_1$ and y_1/y_r and $\bar{Y}_2 = y_2/y_r$

Impulsive Loading Calculations

If the positive phase duration is very short compared with the natural period of the tree, then the blast wave will have completely passed before significant movement of the center of mass occurs. In this case, the loading may be considered impulsive and the initial conditions for integration of equation (4.1) become

CONFIDENTIAL - FORMERLY RESTRICTED DATA.

$$s_o = 0$$

$$\dot{s}_o = \frac{2}{m}\left(\frac{D}{\rho U^2}\right)_o I_+$$

where I_+ is the dynamic pressure impulse associated with the positive velocity phase, and $u = o$ for $n > o$.

The dynamic pressure impulse was evaluated using equations (4.6) and (4.7)

$$I_+ = \int_o^{1.4t_+} \frac{\rho u^2}{2}\, dt \qquad (4.18)$$

$$\frac{2I_+}{\rho_1 u_1^2 t_+} = \int_o^{1.4} \left\{1-\lambda\left[1-(1-z)e^{-z}\right]\right\}\left[(1-\frac{z}{1.4})e^{-\frac{z}{1.4}}\right]^2 dz \qquad (4.19)$$

where

$$z = t/t_+ \quad \text{and} \quad \lambda = \frac{\rho_1-\rho_o}{\rho_1} = \frac{5\Delta p}{7p_o+6\Delta p} \qquad (4.19a)$$

Letting $\zeta = z/1.4$, equation (4.19) becomes

$$\frac{2I_+}{1.4\rho_1 u_1^2 t_+} = (1-\lambda)\int_o^1 (1-\zeta)^2 e^{-2\zeta} d\zeta$$

$$+ \lambda\int_o^1 (1-1.4\zeta)(1-\zeta)^2 e^{-3.4\zeta} d\zeta \qquad (4.20)$$

$$= \frac{(1-\lambda)}{4}(1-e^{-2}) + 0.133\lambda$$

or

$$Q = \frac{2I_+}{\rho_1 u_1^2 t_+} = 0.302 - 0.116\lambda \qquad (4.21)$$

where Q has been designated as the dynamic pressure wave form factor.

CONFIDENTIAL - FORMERLY RESTRICTED DATA

Maximum Deflections for Single Ponderosa Pine Stems

Integration of the equation of motion and determination of maximum deflection moduli were carried out for a series of ponderosa pine stems of varying diameter and percent crown. Three values of spring constant modulus were used, representative of the mean and the extreme values. Stem form for all trees were taken as $a = 0.69$ and $b = 0.52$. Tree characteristics and derived quantities are shown in table 4.1.

Calculations for a number of pressure levels were carried out for values of positive phase duration equal to 0.20, 0.40, 0.80, 2.0, 4.0, 8.0 seconds and infinite (ρ and u constant), and for impulse loading.

After a few calculations it was found that the internal damping term, $\alpha\dot{s}$, of equation (4.1) was a negligible quantity when compared with the restoring force and/or drag terms. In subsequent calculations internal damping was neglected.

Figure 4.4 illustrates some typical results of these calculations for the stem identified as 24-40-I in table 4.1. Input conditions and results for these calculations are given in table 4.2.

Static work moduli for the first and second maximum deflections were calculated from equations (4.17) and (4.17a), whichever applied.

The probability of breakage for each maximum deflection was found by equating the static work modulus for maximum deflection to the static work modulus for breakage in each case. Assuming these trees to be part of a poor site stand, then, the probability of breakage for each deflection may be found from figure 3.9. The total probability of breakage, P_t , on n deflections is

$$(1-P_t) = (1-P_1)(1-P_2)(1-P_3) \ldots . (1-P_n) \qquad (4.22)$$

The total probability of breakage was found using only the first two deflections, hence

$$P_t \simeq 1 - (1-P_1)(1-P_2) \qquad (4.23)$$

CONFIDENTIAL - FORMERLY RESTRICTED DATA

Table 4.1--Characteristics of ponderosa pine stems used in calculations[1/]

Code No.	Diameter d_{bh}	Height H_{bh}	Crown	τ	k_r	y_r	k_a	R_r	R_b	$(\rho U^2)_{RO}$	$(\rho U^2)_R$
	in.	ft	percent	sec	lbs/ft	ft	lbs/ft	lbs	lbs	psf	psf
			$\bar{R} = 1.15$ $\bar{K} = 0.943$								
9-40-I	9	44.5	40	2.55	35	11.6	33	406	471	12.2	156
12-40-I	12	54.5	40	2.73	63	12.8	59	806	935	15.3	136
24-40-I	24	101.5	40	3.83	197	20.2	186	3,979	4,616	29.7	168
24-60-I	24	101.5	60	4.15	288	15.2	272	4,379	5,080	36.9	137
			$\bar{R} = 0.42$ $\bar{K} = 0.482$								
9-40-II	9	44.5	40	2.55	35	11.6	16.9	406	171	12.2	156
12-40-II	12	54.5	40	2.73	63	12.8	30	806	339	15.3	136
24-40-II	24	101.5	40	3.83	197	20.2	95	3,979	1,671	29.7	168
24-60-II	24	101.5	60	4.15	288	15.2	139	4,379	1,839	36.9	137
			$\bar{R} = 0.79$ $\bar{K} = 0.712$								
24-40-III	24	101.5	40	3.83	197	20.2	140	3,979	3,143	29.7	168

1/ For values of other parameters for tree 24-40-I, see Appendix.

CONFIDENTIAL--FORMERLY RESTRICTED DATA

CONFIDENTIAL - FORMERLY RESTRICTED DATA

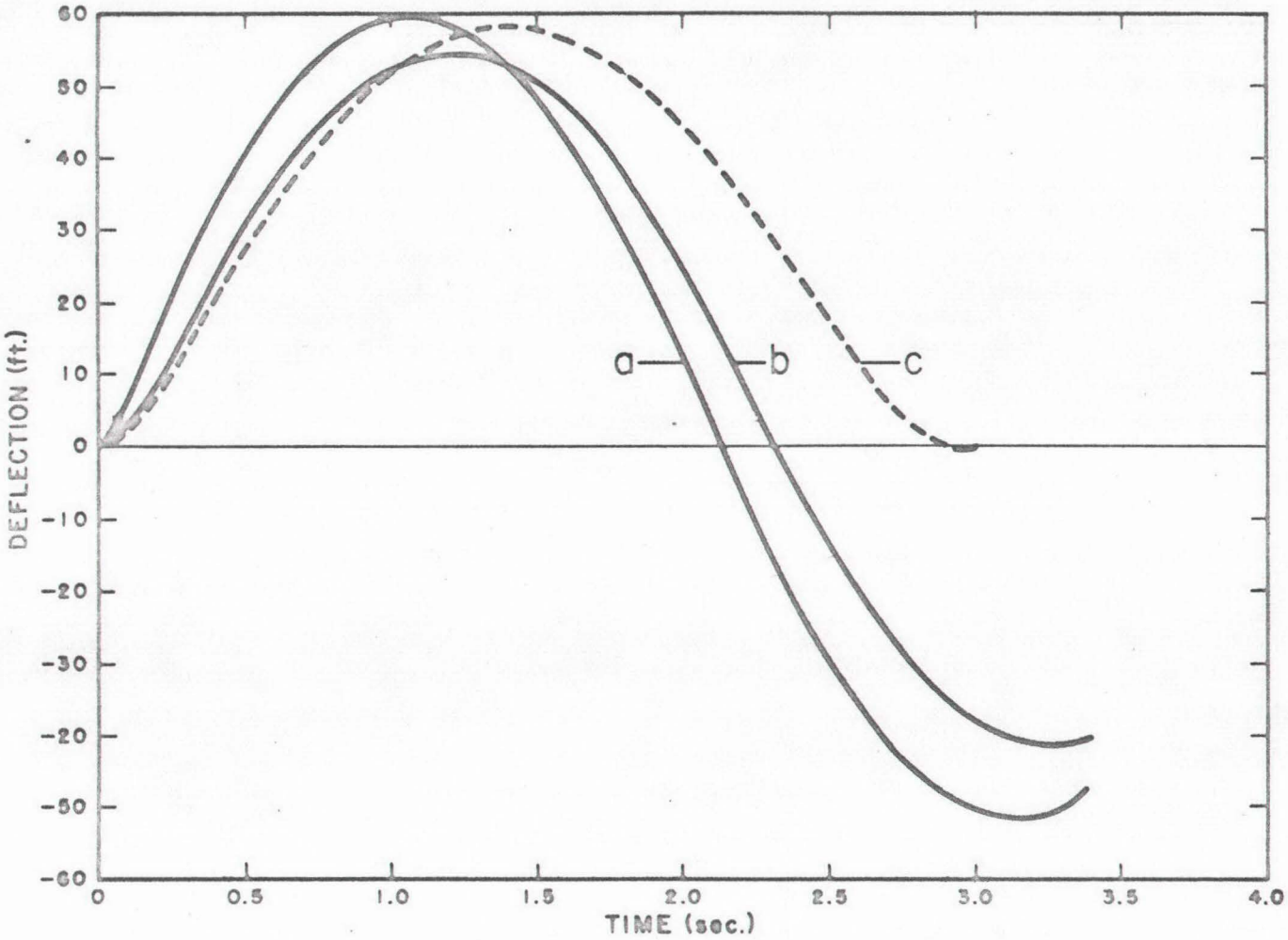

Figure 4.4--Typical deflection-time curves for ponderosa pine tree stem, 24-40-I. (Input condition: see Table 4.2.)

Table 4.2--Input conditions and results corresponding to figure 4.4

Curve	q_1	t_+	y_1	y_2	$\bar{E}_1$	$\bar{E}_2$	P_1	P_2	P_t
	psi	sec	ft	ft			pct	pct	pct
a	4.48	0.2	59.7	51.4	2.72	2.24	42.0	28.0	58.2
b	1.11	2.0	54.7	41.3	2.43	1.66	34.0	12.8	42.4
c	0.825	8.0	58.3	0.40	2.63	0.12	40.0	.000	40.0

Correlation of Results

The very great number of possible combinations of tree stem characteristics and shock wave input parameters prohibited individual computations for each case. For the purpose of generalizing computed results, correlation of these results was undertaken in the following manner:

Integration of the equation of motion resulted in a system of many degrees of freedom, hence the form of the generalized correlation was not readily apparent. A much simpler system was first investigated. Consider a linear system, whose motion is initiated by an impulse due to aerodynamic drag. Assuming that the center of mass moves thereafter in simple harmonic motion, it is easily derived that

$$\frac{s_m}{\dot{s}_o} = \frac{\tau}{2\pi} = \sqrt{\frac{m}{k}} \tag{4.24}$$

where s_m is the maximum deflection (amplitude).

For impulsive loading

$$s_o = \frac{2I_+}{m}\left(\frac{D}{\rho U^2}\right)_o = \frac{Q}{m}\left(\frac{D}{\rho U^2}\right)_o \rho_1 u_1^2 t_+ \simeq \frac{0.350}{m}\left(\frac{D}{\rho U^2}\right)_o \rho_1 u_1^2 t_+ \tag{4.25}$$

and for a linear system the potential energy adsorbed at a particular deflection, s , is equal to $\frac{ks^2}{2}$. The static work modulus, for this system, is then

$$\bar{E} = \left(\frac{s_m}{y_r}\right)^2 = \left[0.70\pi \frac{(\rho_1 u_1^2)}{(\rho U^2)_{RO}} \frac{t_+}{\tau}\right]^2 \tag{4.26}$$

CONFIDENTIAL - FORMERLY RESTRICTED DATA

where $(\rho U^2)_{RO}$ is twice the dynamic pressure required to produce the reference force at the initial drag coefficient, i.e.,

$$(\rho U^2)_{RO} = \frac{R_r}{\left(\frac{D}{\rho U^2}\right)_{M=0}} \tag{4.27}$$

Hence

$$\rho_1 u_1^2 = 0.455\ (\rho U^2)_{RO}\ \frac{\tau}{t_+}\ \sqrt{\bar{E}} \tag{4.28}$$

From this point on, the analysis was purely emperical. A second reference dynamic pressure was defined, based on the drag coefficient when the bending moment about the base of crown is equal to $R_r h$, i.e.,

$$(\rho U^2)_R = \frac{R_r}{\left(\frac{D}{\rho U^2}\right)_{M=R_r h}} \tag{4.29}$$

This quantity was a measure of the degree to which the drag coefficient decreases as the tree crown changes its shape or frontal area. Dividing both sides of equation (4.28) by this quantity, the final form of the proposed correlation was obtained.

$$\frac{\rho_1 u_1^2}{(\rho U^2)_R} = 0.455\ \frac{(\rho U^2)_{RO}}{(\rho U^2)_R}\ \frac{\tau}{t_+}\ \sqrt{\bar{E}} \tag{4.30}$$

Generalizing this relationship in terms of a nonlinear system, the following relationship was proposed

$$\frac{\rho_1 u_1^2}{(\rho U^2)_R} = \psi_1 \left[\frac{(\rho U^2)_{RO}}{(\rho U^2)_R}\ \frac{\tau}{t_+}\right] \cdot \psi_2\ (\bar{E}) \tag{4.31}$$

Static work moduli of the previous section were tested for correlation, based on equation (4.31). These results, for the first deflection, are plotted in figure 4.5. Figure 4.6 displays a cross plotting for even values of $\bar{E}$. Results for the second maximum energy modulus, $\bar{E}_2$, are shown in figure 4.7 and were correlated against τ/t_+ rather than $(\rho U^2)_{RO}/(\rho U^2)_R\ \frac{\tau}{t_+}$.

CONFIDENTIAL - FORMERLY RESTRICTED DATA

CONFIDENTIAL - FORMERLY RESTRICTED DATA

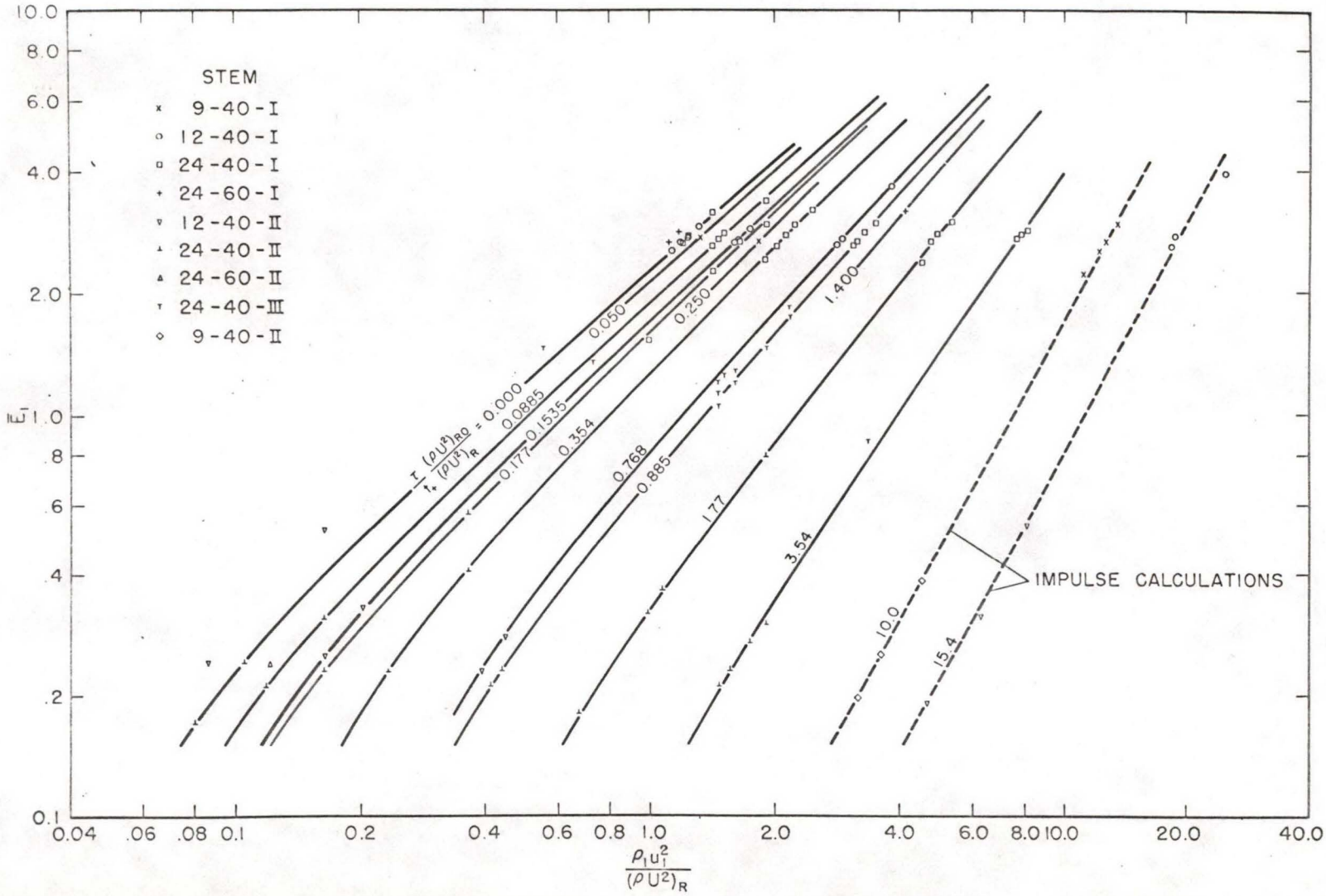

Figure 4.5--Analytical correlation of static work modulus for maximum deflection as a function of period modulus and dynamic pressure modulus.

CONFIDENTIAL - FORMERLY RESTRICTED DATA

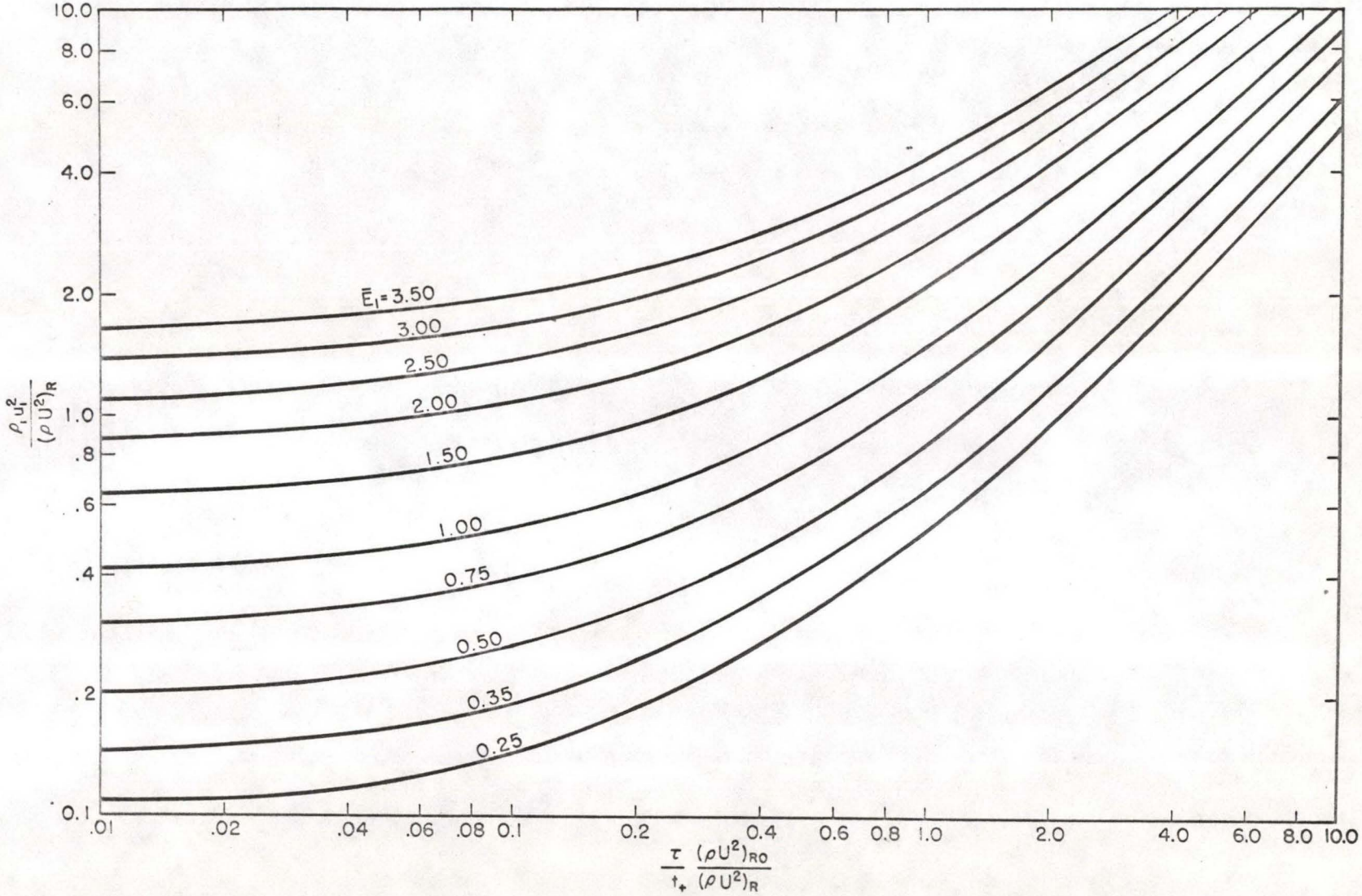

Figure 4.6--Dynamic pressure modulus as a function of period modulus for various values of static work modulus (crossplot of Figure 4.5).

- CONFIDENTIAL - FORMERLY RESTRICTED DATA -

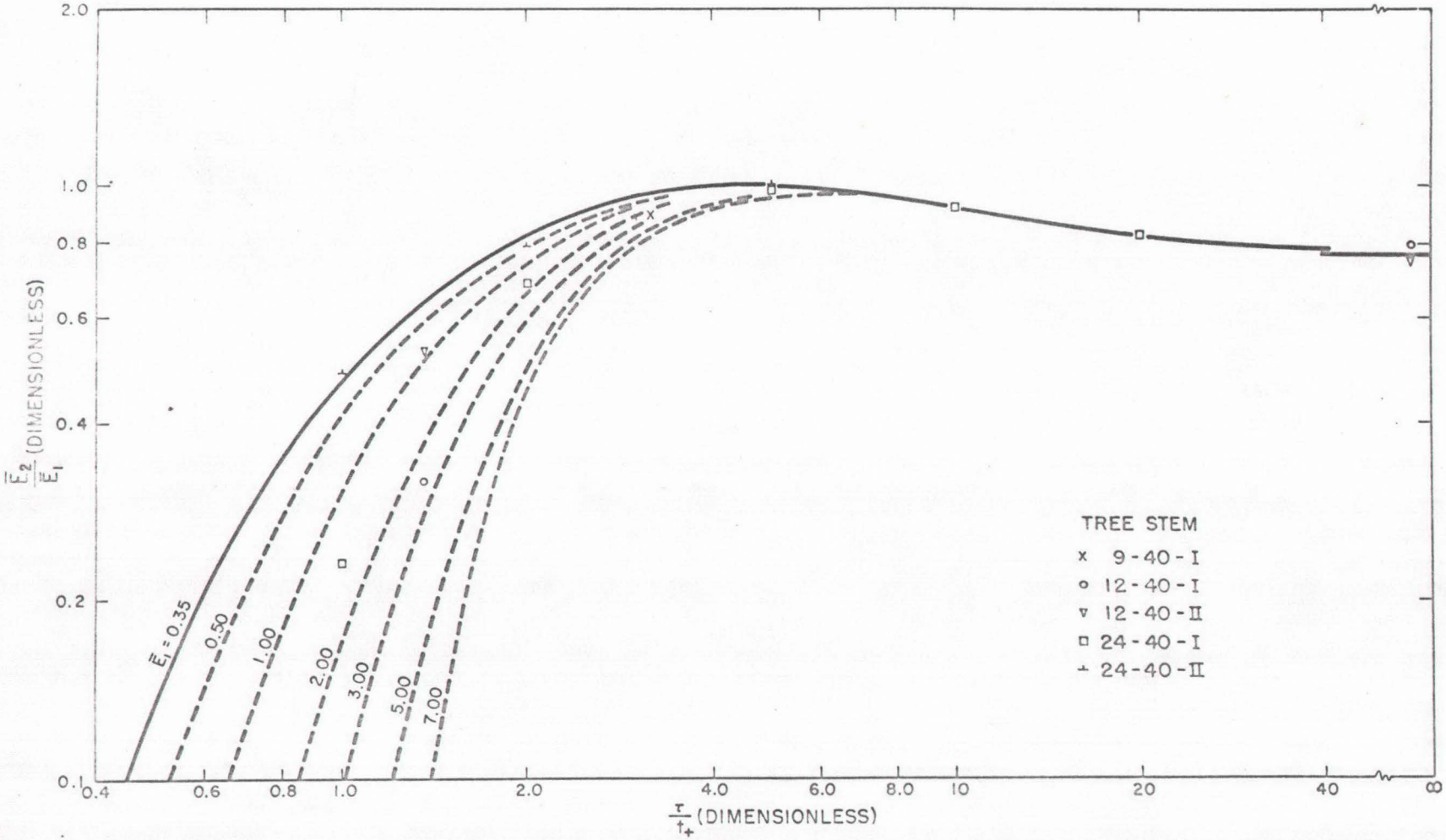

Figure 4.7--Energy modulus ratio for second to first maximum deflection as a function to period ratio.

In order to plot the results of impulse loading calculations on a peak dynamic pressure basis in figure 4.5, a standard positive phase duration of 0.02 sec was assumed. The corresponding peak dynamic pressure in figure 4.5 was given by equation (4.21) rearranged as

$$\frac{\rho_1 u_1^2}{2} = \frac{I_+}{Qt_+} \tag{4.32}$$

The dynamic pressure wave form factor, Q, was evaluated for a mean overpressure of 4.4 psi ($\frac{\Delta p_1}{p_o} = 0.30$). From equation (4.19a), $\lambda = 0.17$ and from equation (4.21), $Q = 0.283$. Hence, in figure 4.5

$$\frac{\rho_1 u_1^2}{2} = .177 I_+ \tag{4.33}$$

The Variation of Static Work Modulus with Dynamic Pressure Wave Form Factor

The calculations of static work modulus described in the preceding sections were carried out using a standardized wave form for both particle velocity and density behind the shock wave. The average positive phase dynamic pressure wave form factor was 0.28. Extensive experimental checks of both static work moduli for maximum deflection and stem breakage predictions using these calculations were made on UPSHOT-KNOTHOLE Shot 9 (12). Experimental data verified the calculation method, but the experimentally determined positive phase dynamic pressure wave form factor for this shot was 0.23. Experimental static work moduli for maximum deflection on UPSHOT-KNOTHOLE Shot 10 significantly exceeded those calculated. This result was attributed to the observed increase of positive phase dynamic pressure wave form factor.

Subsequently, an analysis was made of the variation of dynamic pressure wave form factor with height of burst and ground range in the Mach reflection region (19). Significant variations in form factor were found, and it became apparent that it would be necessary to estimate the effect of wave form on the calculated static work moduli.

The procedure used in estimating this effect may be followed in figure 4.8. At small values of τ/t_+, with $\bar{E}$ constant, the tree responds to peak dynamic pressure, and its response is independent of the form factor, Q. At large values of τ/t_+, the tree responds to the dynamic pressure impulse and hence from equation (4.32) the peak dynamic pressure is inversely proportional to Q; and I_+ and t_+ remaining constant. Consequently, point "a" (figure 4.8) will assume a new value "b", on the impulse (dotted) curve as Q increases. However, where the $\bar{E}$ curve becomes tangent to the impulse curve the values of τ/t_+ increase (e.g., consider the case $Q = 1$) as shown in figure 4.8.

CONFIDENTIAL - FORMERLY RESTRICTED DATA

-CONFIDENTIAL- FORMERLY -RESTRICTED DATA-

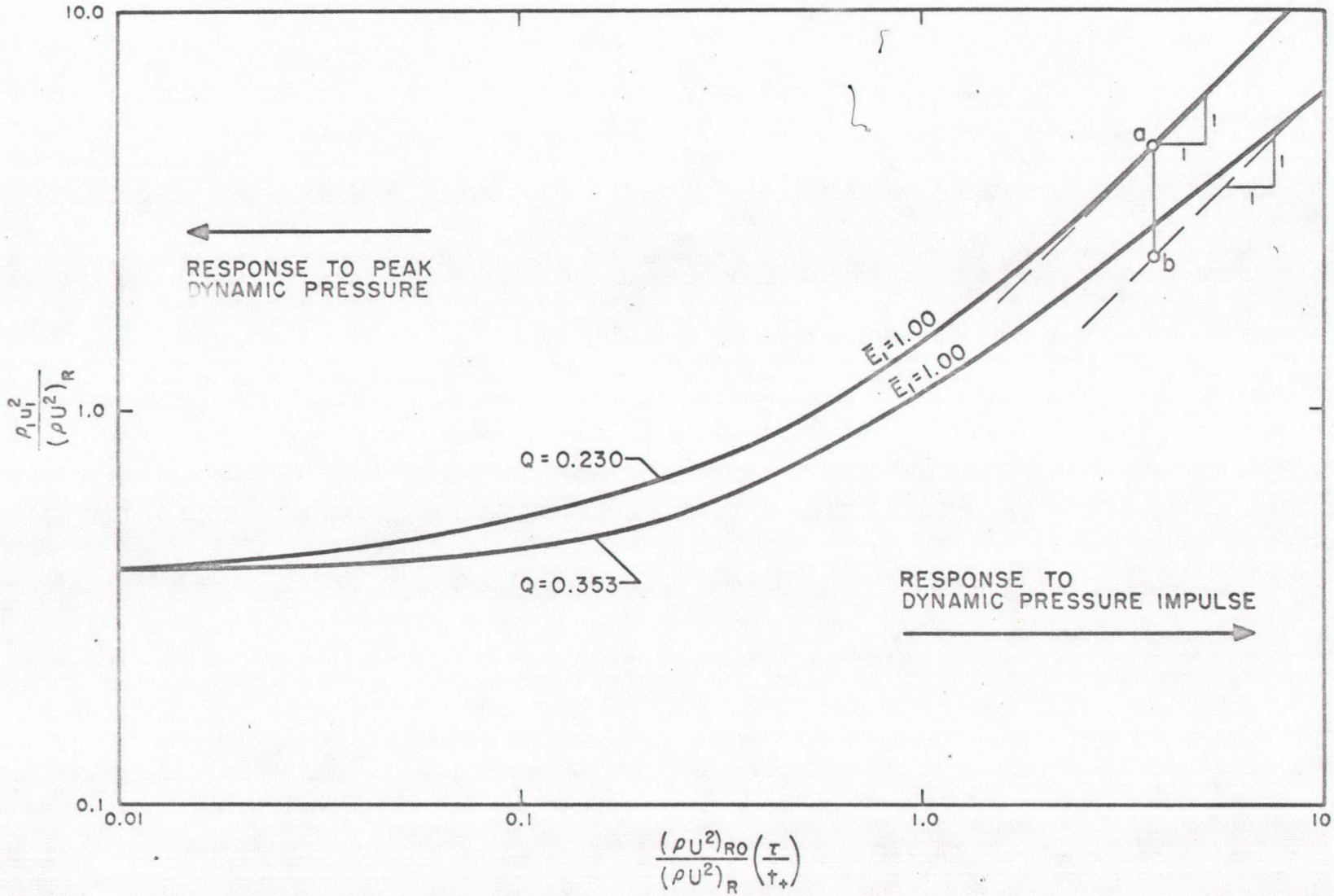

Figure 4.8--Illustration of method for estimating the effect of wave form factor, Q.

In estimating tree response for values of Q, other than that used in the calculations, it was assumed that the calculations held for $Q = 0.23$, the experimentally determined value on UPSHOT-KNOTHOLE Shot 9 (12). All curves were adjusted from this value by first drawing the corrected impulse curve and then fairing in the intermediate portions, using a shape similar to the original curve and remembering that the point of tangency moves to the right as Q increases.

In this manner new sets of $\overline{E}$ curves were constructed for six values of Q from 0.132 to 0.353 inclusive (figures 4.9 to 4.14 inclusive). To be sure, the method used is a rather crude substitute for actual calculations, however, an expedient compromise was necessary in order to provide damage predictions for Operation CASTLE and TM-23-200(22). The resulting curves are believed to be within the overall accuracy of the assumptions contained in the original computations, coupled with those involved in the correlation technique.

CONFIDENTIAL - FORMERLY RESTRICTED DATA

CONFIDENTIAL - FORMERLY RESTRICTED DATA

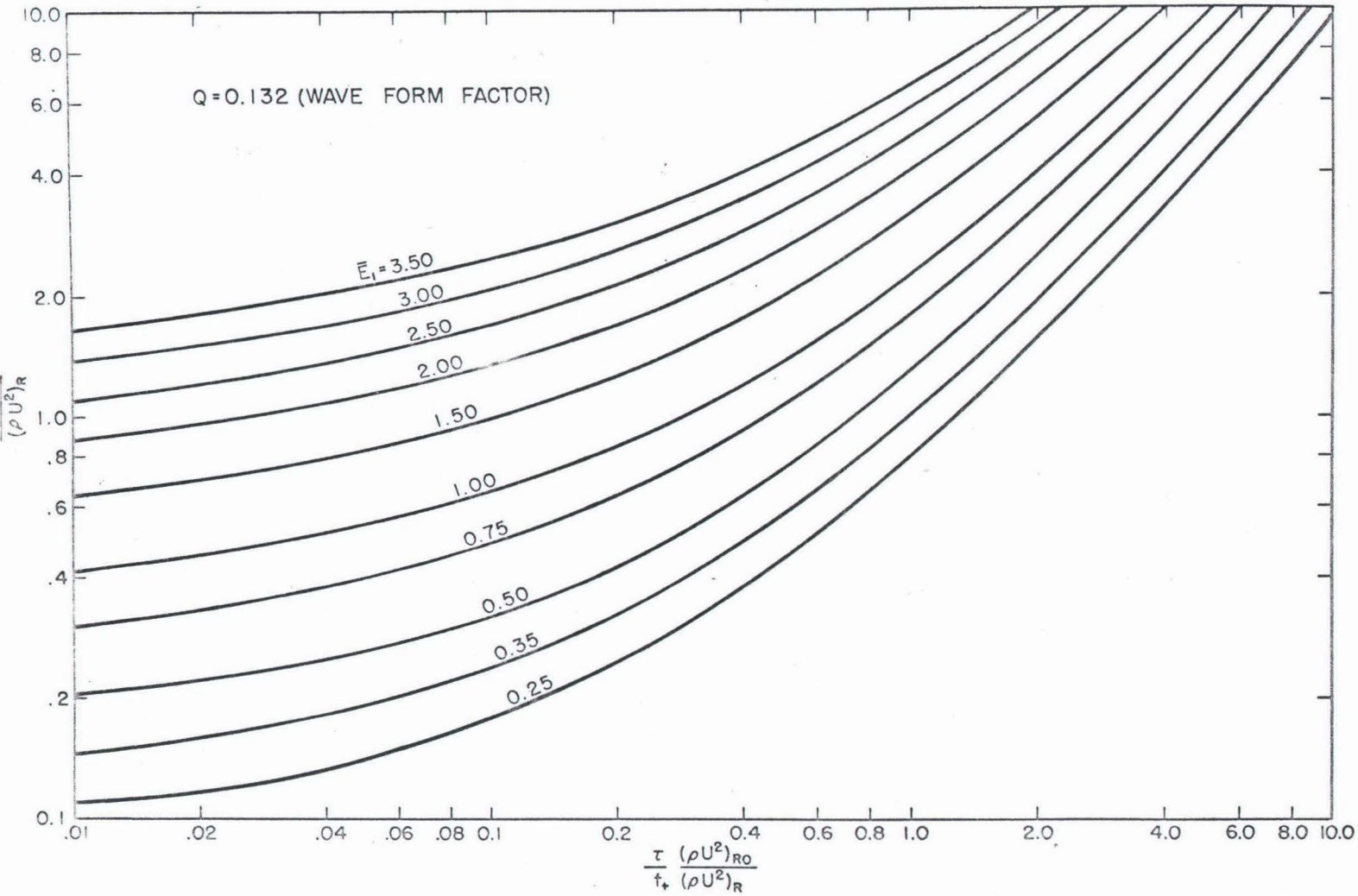

Figure 4.9--Dynamic pressure modulus as a function of period modulus for various values of static work modulus (wave form factor, Q = 0.132).

CONFIDENTIAL - FORMERLY RESTRICTED DATA

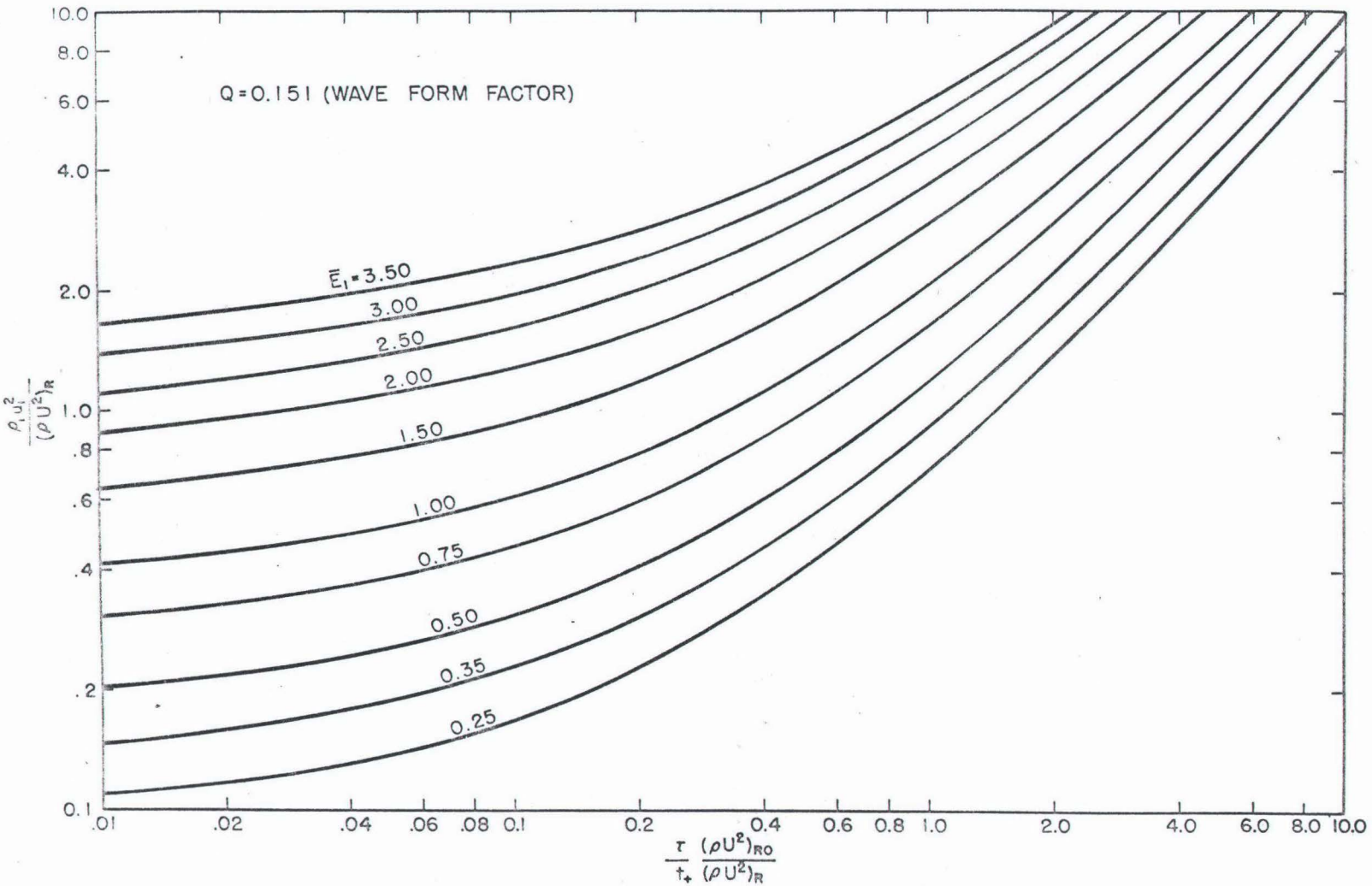

Figure 4.10--Dynamic pressure modulus as a function of period modulus for various values of static work modulus (wave form factor, Q = 0.151).

CONFIDENTIAL - FORMERLY RESTRICTED DATA

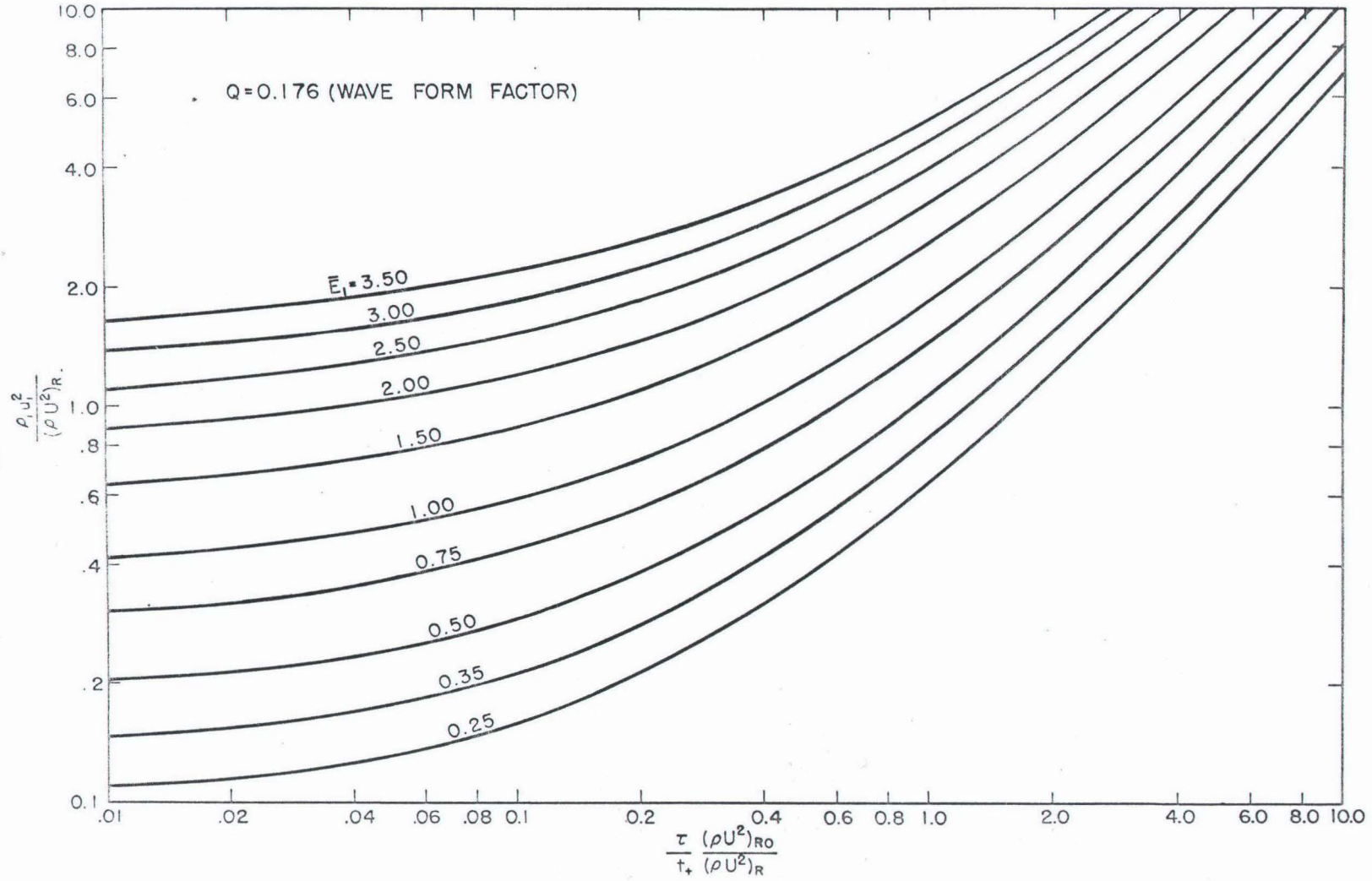

Figure 4.11--Dynamic pressure modulus as a function of period modulus for various values of static work modulus (wave form factor, Q = 0.176).

CONFIDENTIAL - FORMERLY RESTRICTED DATA

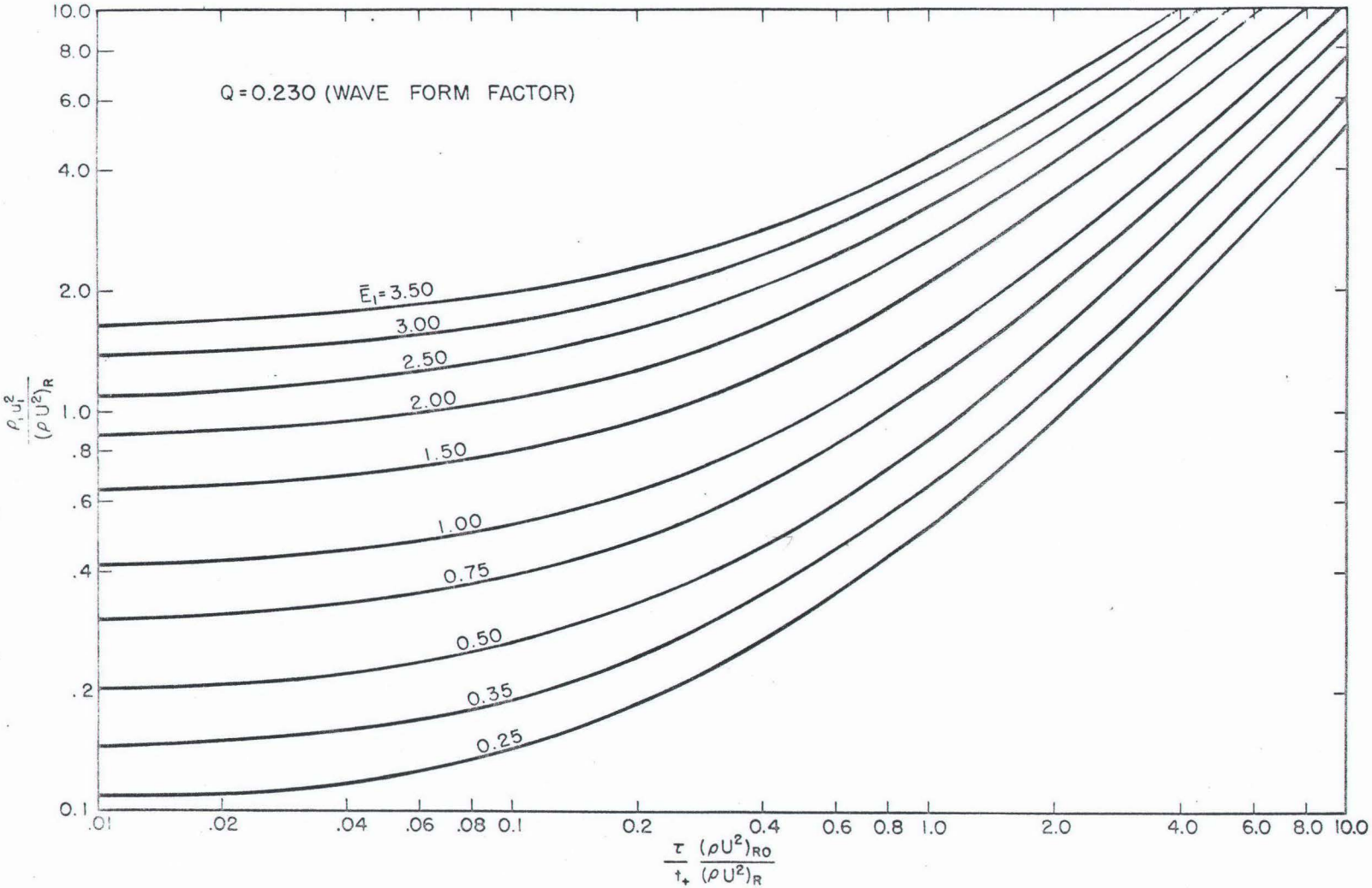

Figure 4.12--Dynamic pressure modulus as a function of period modulus for various values of static work modulus (wave form factor, Q = 0.230).

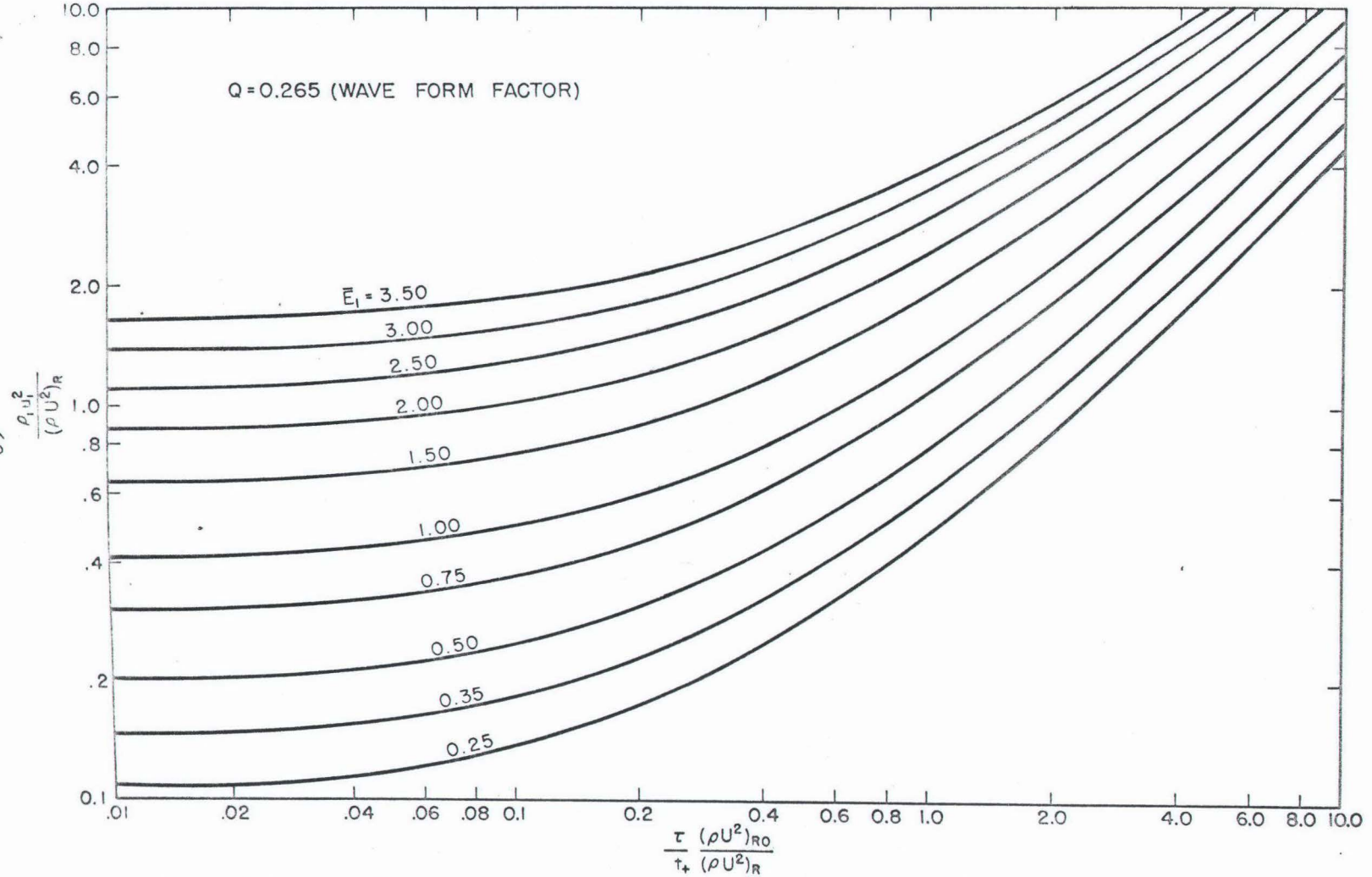

Figure 4.13--Dynamic pressure modulus as a function of period modulus for various values of static work modulus (wave form factor, Q = 0.265).

CONFIDENTIAL - FORMERLY RESTRICTED DATA

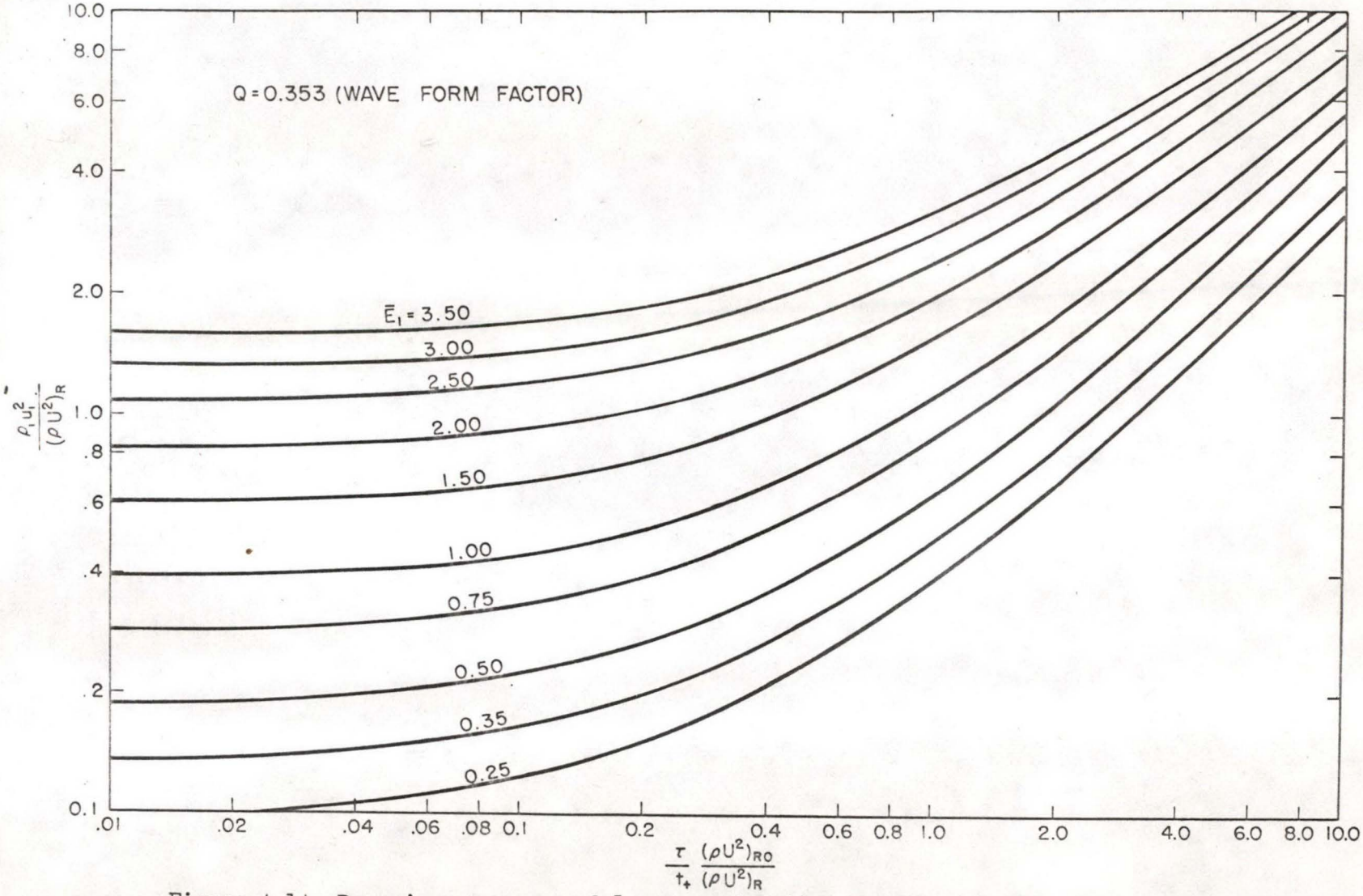

Figure 4.14--Dynamic pressure modulus as a function of period modulus for various values of static work modulus (wave form factor, Q = 0.353).

CHAPTER 5

CONSTRUCTION OF ISODAMAGE CURVES FOR TREE STANDS

General

Calculations of stem breakage in tree stands was based on two major assumptions:

(a) The work modulus-peak dynamic pressure, positive phase relationships developed for ponderosa pine (figures 4.7 and 4.9 through 4.14) may be used for other species.

(b) The peak dynamic pressure and positive phase are unaffected by the presence of the stand and are those of the free field.

The free field peak overpressure and positive phase duration are not independent variables. This relationship is presented by Vortman and Merritt (20). Using equation (4.10), for Mach reflection, a relationship was derived between peak dynamic pressure and overpressure positive phase duration. The dynamic pressure field was taken as that described in UPSHOT-KNOTHOLE "Summary Report of Technical Director," (21) and the dynamic pressure wave form factor field as that described by Sauer and Lai (19).

Calculation Procedure and Illustrative Example

The criterion adopted as a measure of damage was length of stems broken per acre, L_t (chapter 1). This quantity is the sum of the stems broken per acre times their length, i.e.,

$$L_t = \sum_{1}^{n} (P_t)_n \, N_n (H_{bh})_n \tag{5.1}$$

where N_n is the number of trees per acre of diameter class n and having a height of $(H_{bh})_n$, and $(P_t)_n$ is the total probability of breakage for this class.

$(P_t)_n$ may be expressed as a function of $\bar{E}_1$ and $\bar{E}_2$ or of $\bar{E}_1$ and $\bar{E}_2/\bar{E}_1$, and for a particular site (chapter 3) a curve may be constructed (such as figure 5.1) using equation (4.23) and figure 3.9. $\bar{E}_1$ and $\bar{E}_2/\bar{E}_1$ are functions of peak dynamic pressure, positive phase duration, and wave form factor. Determination of $\bar{E}_1$ and $\bar{E}_2/\bar{E}_1$ were carried out graphically as follows:

CONFIDENTIAL - FORMERLY RESTRICTED DATA

CONFIDENTIAL - FORMERLY RESTRICTED DATA

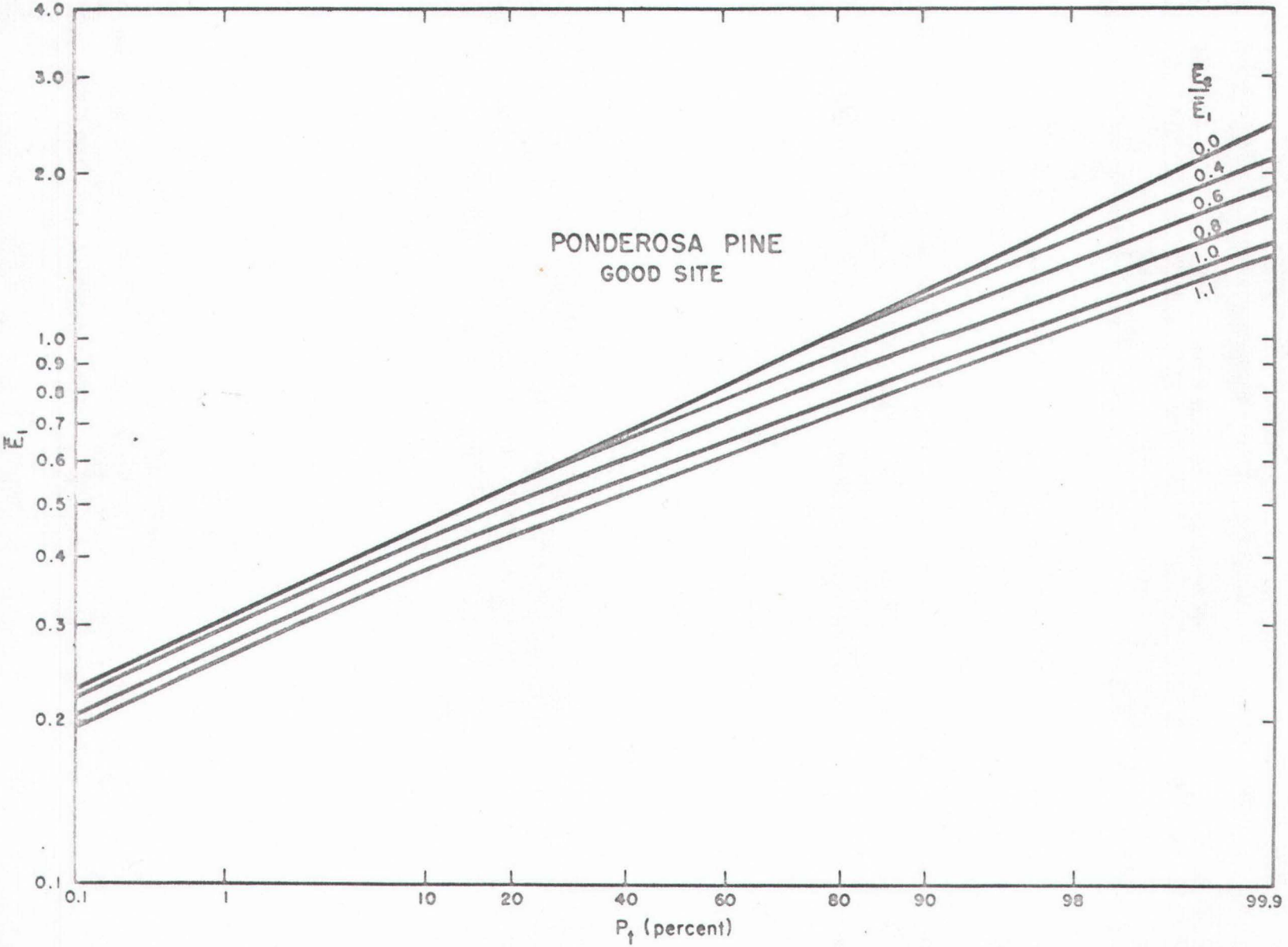

Figure 5.1--Total probability (P_t) as a function of the first deflection energy modulus $(\overline{E}_1)$.

The $\bar{E}_1$ and $\bar{E}_2/\bar{E}_1$ curves (figures 4.6 and 4.7) were prepared to the same scale on log-log coordinate paper. To an identical scale the relationship between peak dynamic pressure and reciprocal of positive phase duration as a function of overpressure and weapon yield (20) was plotted on a transparent overlay (figure 5.2). The point corresponding to 5 psi and 27 KT (chosen as the reference conditions) was marked by a circle.

The procedure from this point on is best illustrated by a numerical example. The first step is to compute τ, $(\rho U^2)_R$ and $(\rho U^2)_{RO}$. From table 4.1 for stem 24-40-I we have:

$$\tau = 3.83 \text{ sec}$$

$$(\rho U^2)_R = 1.17 \text{ psi}$$

$$(\rho U^2)_{RO} = 0.206 \text{ psi}$$

Next, the independent variables of figures 4.6 and 4.7 for an overpressure of 5 psi[6/] and a yield of 27 KT are computed

$$\frac{\rho_1 u_1^2}{2} = 0.587 \text{ psi}$$

$$t_+ = 0.96 \text{ sec}$$

hence,

$$\frac{\rho_1 u_1^2}{(\rho U^2)_R} = 1.00$$

and

$$\frac{\tau}{t_+} \frac{(\rho U^2)_{RO}}{(\rho U^2)_R} = 0.705.$$

This point is then plotted on each of the $\bar{E}_1$ charts (for the various values of Q). The transparent overlay (figure 5.2) is then placed over the particular $\bar{E}_1$ chart so that the circled point on the overlay corresponded to the calculated point (i.e., 27 KT at 5 psi in each case) as illustrated in figure 5.3.

Since both plots are of the same logarithmetic scale the correct multiplication is provided by reading $\bar{E}_1$ values corresponding to other values of overpressure and weapon yield. Values of $\bar{E}_1$ are then read

---

6/ Overpressure is used as an independent variable for convenience only.

CONFIDENTIAL - FORMERLY RESTRICTED DATA

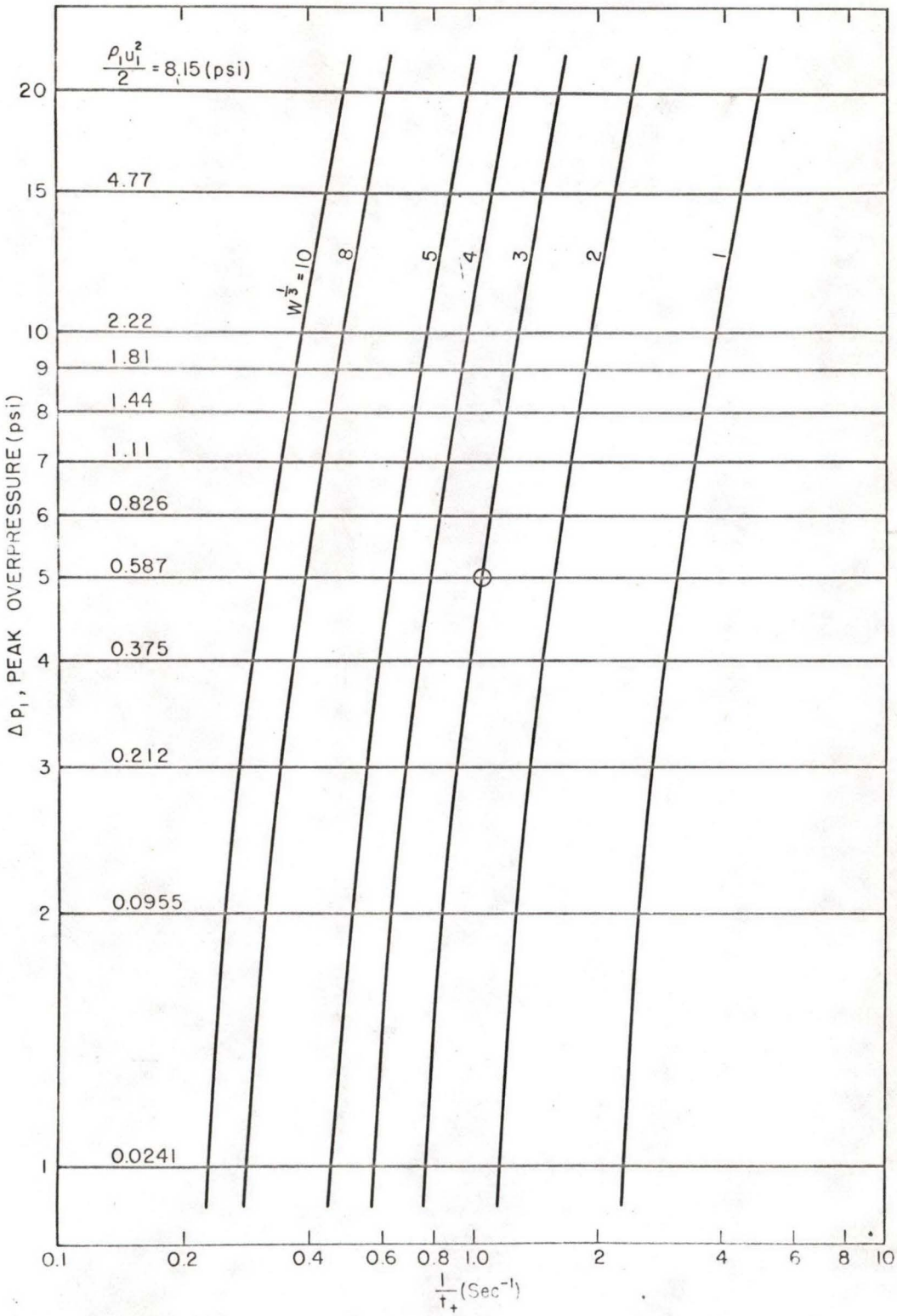

Figure 5.2--Relationship of overpressure-duration-weapon yield.

CONFIDENTIAL - FORMERLY RESTRICTED DATA

CONFIDENTIAL FORMERLY RESTRICTED DATA

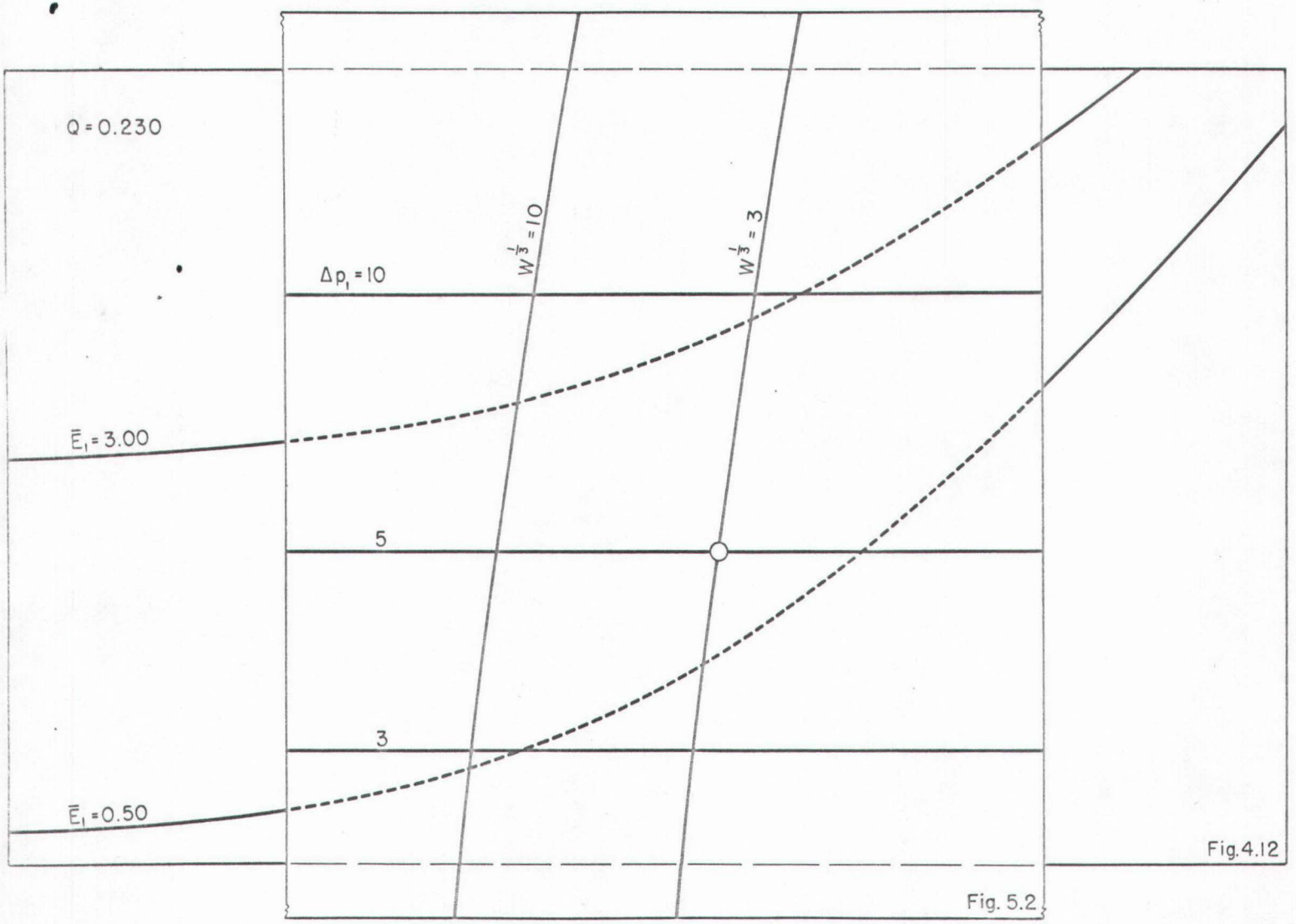

Figure 5.3--Illustration of use of transparent overlay in computing static work modulus.

off the superimposed graphs for the various overpressures for $W^{1/3} = 3$. These values are tabulated and the procedure repeated for other values of weapon yield.

Next the value of τ/t is plotted on figure 4.7 at a convenient position (not necessarily on the $\bar{E}_2/\bar{E}_1$ curve), and the circled point of figure 5.2 overlayed at this position (figure 5.4). The value of $\bar{E}_2/\bar{E}_1$ is then determined by reading vertically from the Δp_1, $W^{1/3}$ position to the proper $\bar{E}_1$ curve determined previously. For example: from the 5 psi, 27 KT intersection, path a; from 10 psi, 27 KT, path b; and from 3 psi, 10^3 KT, path c. These values are tabulated with the previous results.

By using $\bar{E}_1$ and $\bar{E}_2/\bar{E}_1$, determined by figures 5.3 and 5.4, the total probability of breakage is then read from figure 5.1. Continuing the example: for 5 psi, 27 KT and Q = 0.23

$$\bar{E}_1 = 0.770 \qquad \frac{\bar{E}_2}{\bar{E}_1} = 0.028^{7/}$$

Assuming this stem to be part of a forest stand on a good site and that there are, on the average, 12 trees of this diameter class per acre and that $H_{bh} = 101.5$ ft., then the length of stems broken in this diameter class will be

$$L_n = (P_t)_n \cdot N_n (H_{bh})_n$$

$$= (0.50)\ (12)\ (101.5) = 609 \text{ ft/acre}$$

This procedure is repeated for each diameter class in the stand and the results summed for each combination of input conditions (Δp_1, $W^{1/3}$, and Q). The total lengths of stems down per acre are then plotted versus the peak dynamic pressure with yield as a parameter for each wave form factor value (figure 5.5).

Finally, the input conditions for light (1500 ft/acre) and severe (9000 ft/acre) damage are then found by interpolation, and curves are drawn of peak dynamic pressure versus wave form factor for each weapon yield (figure 5.6).

A master height of burst chart which superimposes the wave form factor yield on the dynamic pressure field is shown in figure 5.7. By referring to figure 5.6, curves corresponding to light and severe damage are transferred on to figure 5.7 for each weapon yield. This procedure requires visual interpolation between dynamic pressure lines in figure 5.7. Isodamage curves are then faired in as illustrated in figure 5.7.

7/ Extrapolation of figure 4.7 necessary for this particular condition.

CONFIDENTIAL - FORMERLY RESTRICTED DATA

CONFIDENTIAL--FORMERLY RESTRICTED DATA

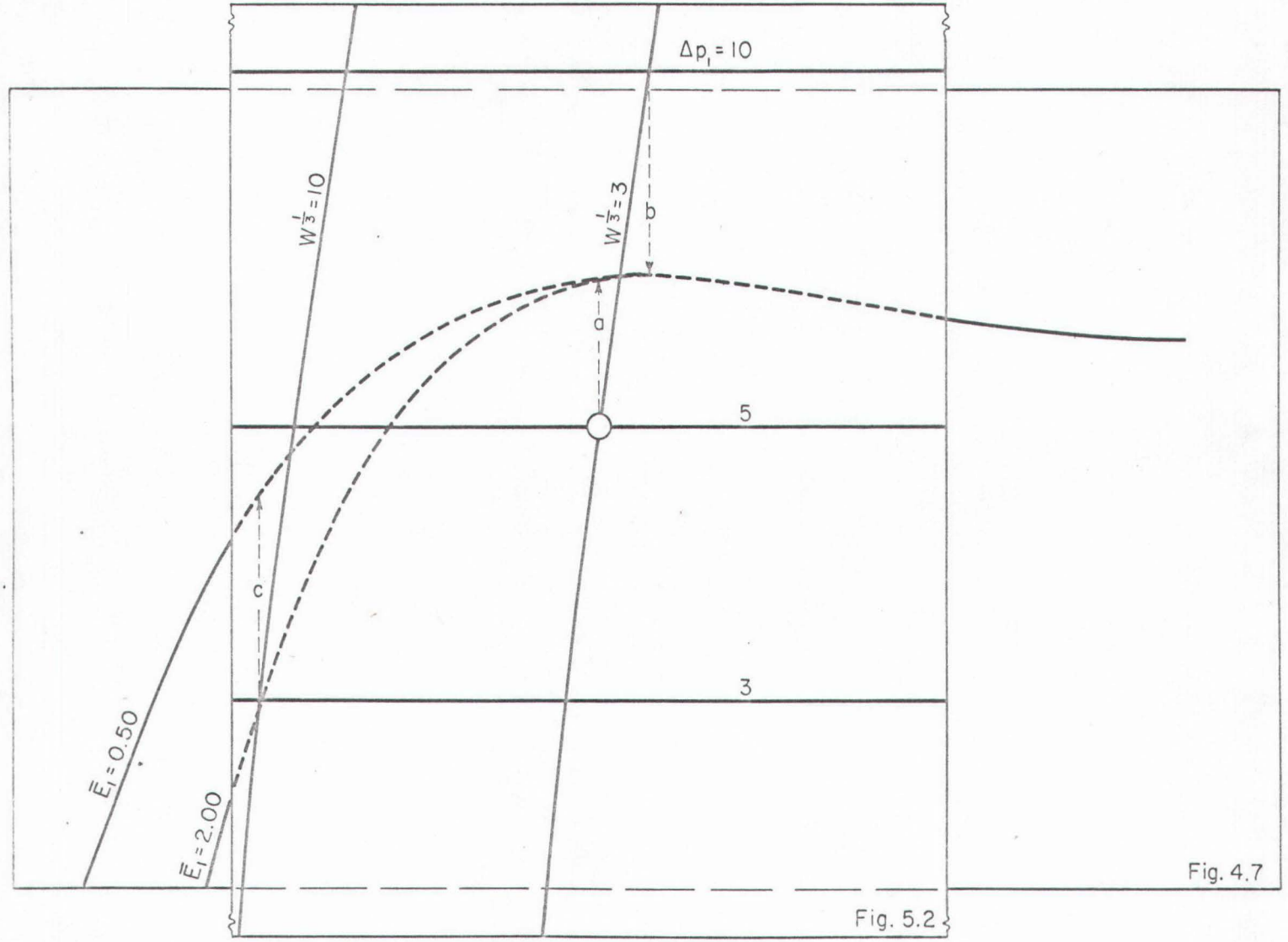

Figure 5.4--Illustration of use of transparent overlay in computing static work moduli ratio.

CONFIDENTIAL - FORMERLY RESTRICTED DATA

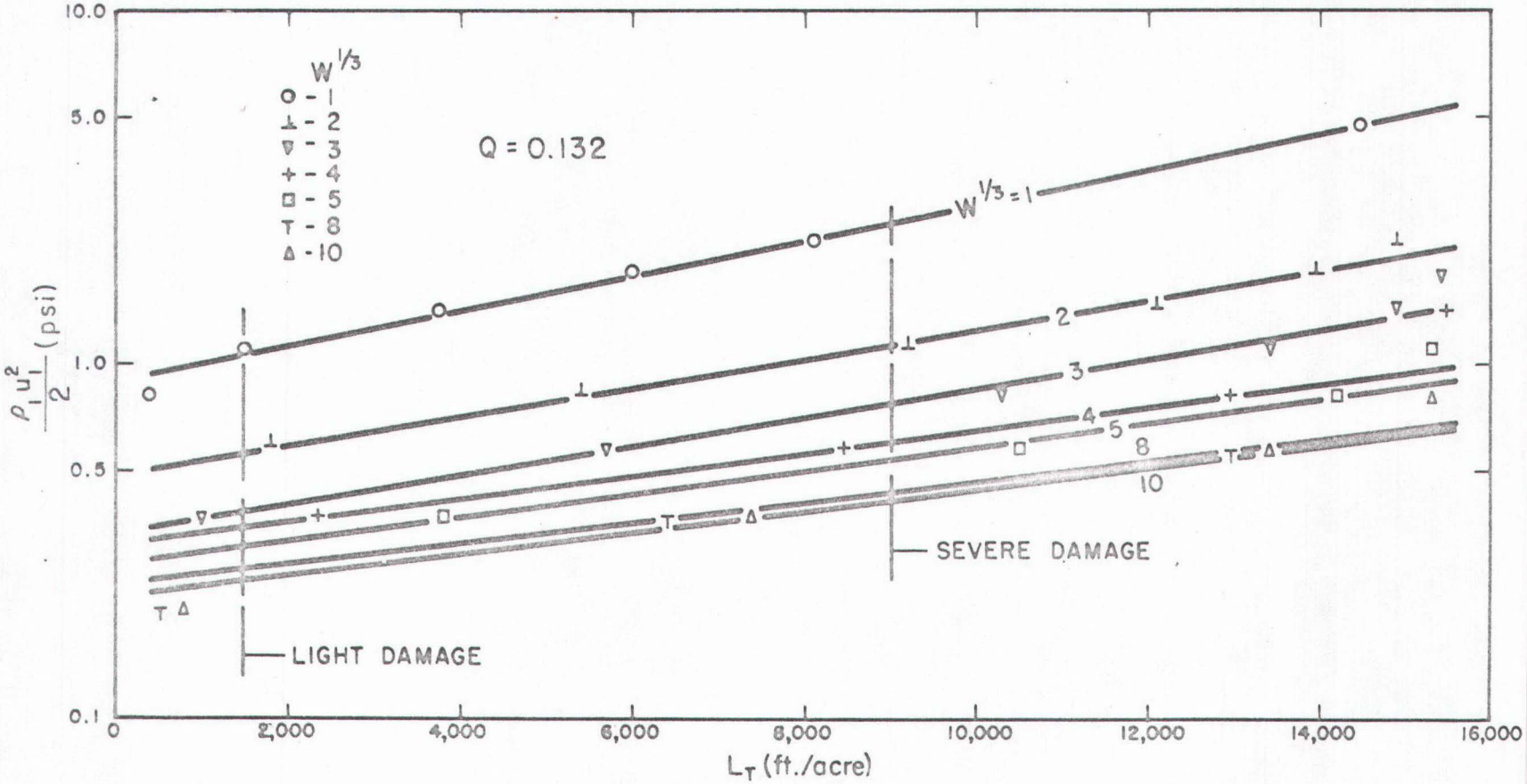

Figure 5.5--Stems broken per acre as a function of peak dynamic pressure and weapon yield (Type III stand, Chapter 6).

CONFIDENTIAL - FORMERLY RESTRICTED DATA

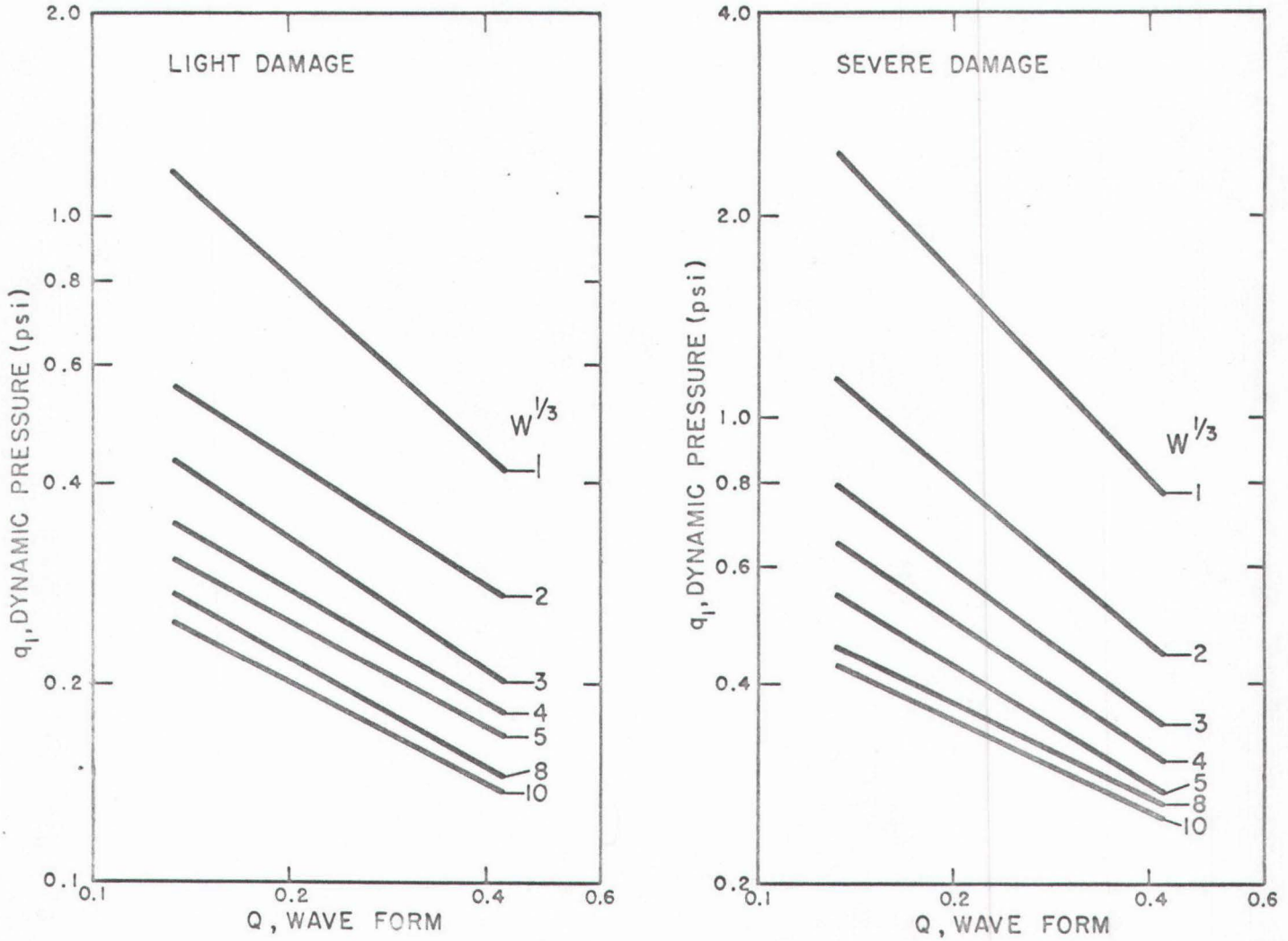

Figure 5.6--Light and heavy damage as a function of peak dynamic pressure and wave form factor. (Type III stand, Chapter 6).

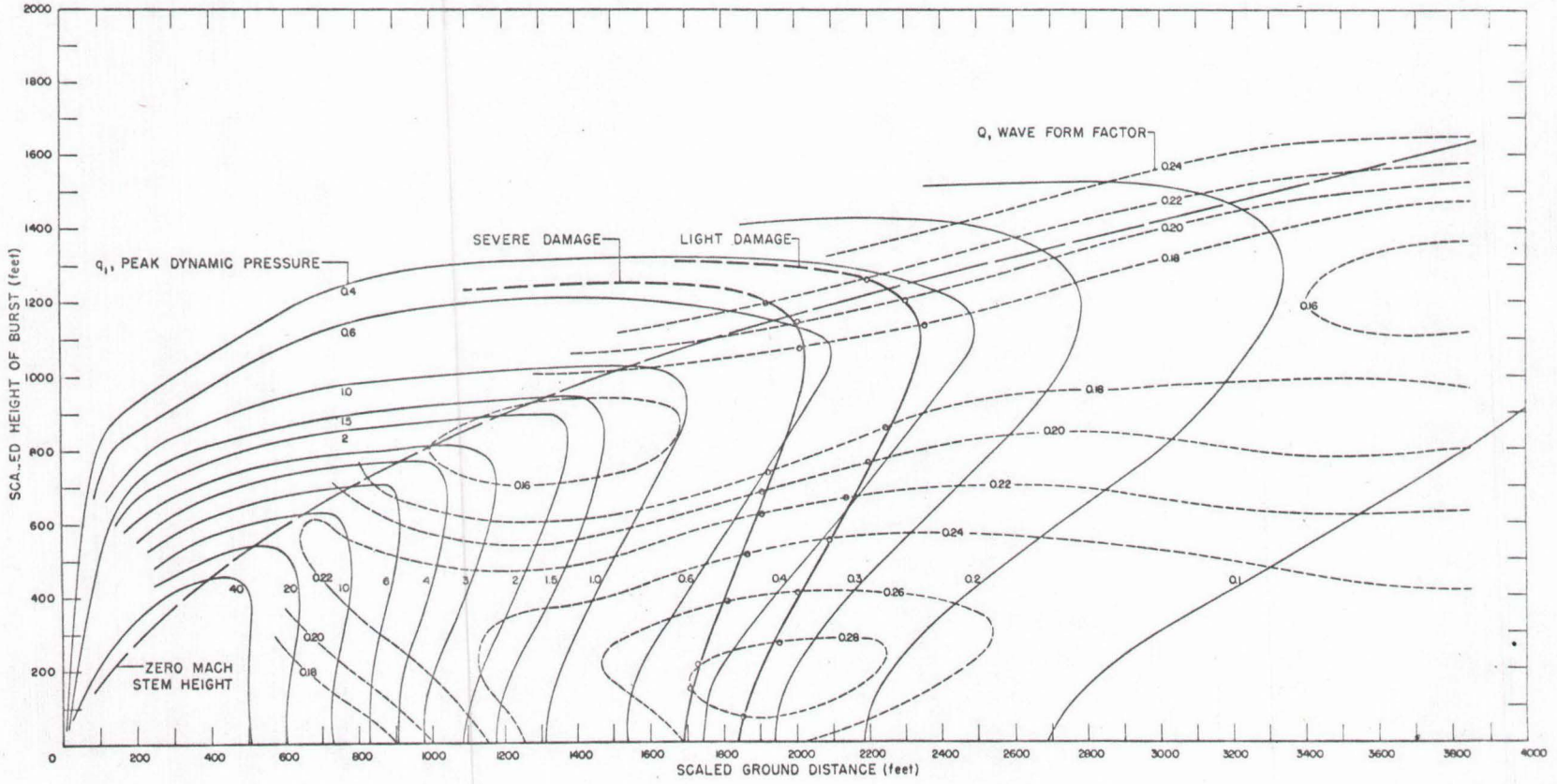

Figure 5.7--Composite dynamic pressure-wave form factor height of burst chart and illustration of isodamage curve construction (Type III stand, 27 KT).

CONFIDENTIAL - FORMERLY RESTRICTED DATA

The entire procedure outlined in the preceding sections is based on the assumption of Mach reflection. Computation of damage by this general procedure in the region of regular reflection is further hampered by lack of information on dynamic pressure-positive phase relationships and wave form factors. Hence, in the regular reflection region, isodamage curves are determined by extrapolation assuming them to parallel the dynamic pressure isobars.

•CONFIDENTIAL - FORMERLY RESTRICTED DATA

CHAPTER 6

ISODAMAGE CURVES FOR SELECTED TREE STANDS

General Considerations

A limited number of tree stands were selected to represent stand conditions encountered in practice.

As a guide in selecting such representative stands for analysis of species common to northern hemisphere the following parameters were considered:

1. Extreme variations in stem form and percent crown in stand types.
2. Variation in strength properties of common species.
3. Characteristics of managed and unmanaged stands.
4. Diameter-height relationship for good and poor site stands.
5. Age of stands commonly found in the northern hemisphere.

Five representative tree stands, found on both the European and the American continents, were selected. Description of these five stands and isodamage curves calculated for such stands are presented in the following sections. Calculations for trees less than 6 inches diameter were not made because trees of such small size offer little impedement to military operations.

Type I Stand, Managed Ponderosa Pine

The stand chosen as representative of a Type I stand is an intensively managed 60-year-old good site ponderosa pine (Pinus ponderosa) plantation. Stands of this type are common throughout Central Europe where good management is feasible, but as yet they are rare in North America. Isolated examples may be found on lands of some of the larger pulp and timber companies located in the southern United States where long leaf and loblolly pine stands are under management. Details of a Type I stand are given in table 6.1.

Managed timber stands are characteristically grown in regular blocks of 20 to 100 acres, usually with definite borders. Trees planted at uniform spacing are periodically thinned at intervals of 2 to 5 years after approximately 17 years of initial growth. The principle followed in thinning the stand favors the most promising dominant and codominant trees for future growth, and removes trees in the lower crown classes which are not likely to survive.

CONFIDENTIAL - FORMERLY RESTRICTED DATA

Table 6.1--Stand table for a managed 60-year-old ponderosa pine plantation on a good site[1/]

Diameter Class (in.)	Diameter Midpoint (in.)	Average height[2/] (ft)	No. trees per acre
2	2.0		
4	4.0		
6	6.0		
8	8.0		
10	10.0		
12	12.0		
14	14.0	104	6
16	16.0	111	10
18	18.0	115	18
20	20.0	120	23
22	22.0	125	12
24	24.0	129	7

Total all trees	76
Total 6.0 in. or larger	76
Weighted average height	118.0 ft.
Average d_{bh}	19.4 in.
Spacing	25 ft x 25 ft

1/ Adapted from Management of Forests for Timber Production, Barr, P.M., Univ. of Calif., 1952.

2/ Based on average diameter for "Normal" stands from Yield of Douglas-fir in the Pacific Northwest, McArdle, R.E., and W. H. Myer, Tech. Bull. 201, U.S.D.A., 1930, Rev. Oct. 1949.

When a managed stand is viewed from the air, crown canopies appear quite uniform and smooth with only occasional small patches of ground showing through. Within the stand, trees are fairly uniform in height and nearly the same in diameter. They are generally vigorous in appearance and fast growing. Needles are long; foliage is luxuriant and deep green in color. Internodes (the distance between successive whorls of branches along the stem) in the live crown are 3 to 4 feet or more.

CONFIDENTIAL - FORMERLY RESTRICTED DATA

Usually there are evidences of the application of management practice in the stand, such as low stumps resulting from periodic thinning and clear lower tree trunks as a result of pruning. Periodic entry for stand improvement work plus heavy shading keep underbrush down, and this, combined with the few clean, large stems, gives the interior of the stand a clean park-like appearance and affords good visibility and easy entry.

The most productive forest soils are usually selected for forest plantations. In these areas the soil is well-drained, deep, and rock-free; yearly precipitation is adequate, and temperatures are favorable for a long growing season. Thus, sites located in the middle elevations and latitudes are generally selected for forest plantations. Topography is also an important factor with north-facing slopes and valley bottoms the most favorable choices.

Type II Stand, Unmanaged Ponderosa Pine

The stand chosen as representative of a Type II stand is an unmanaged, naturally occurring, pure 80-year-old ponderosa pine (Pinus ponderosa) stand, of average stocking, growing on a poor site. It is typical of the poorer low vigor type of wild, thrifty-mature European or North American coniferous stands. Details of a Type II stand are given in table 6.2.

Stands of this type are characterized by a random distribution of diameters from small to large, a large total number of trees per acre, a small average stand diameter, and a short average stand height. Growth is often patchy with dense clumps of trees all of one size alternating with irregular bare areas, giving the crown canopy a ragged, uneven appearance when viewed from above. Stands such as these may cover large areas with only irregular natural boundaries such as ridge tops and rock outcrops. They may also be found in small natural patches with uneven borders. These stands appear low in vigor, needles are short, light green in color, and sparse. Trunks have rapid taper and develop platy bark at an early age. Crowns are quite long with branch whorls spaced 1 foot or less apart.

The forest floor within the stand is generally cluttered with dead, fallen trees which, when combined with the persistent dead limbs on the dense growing live stems, impede entrance into the stand and decrease visibility. Underbrush is usually heavy in the numerous stand openings, and young reproduction is scanty; individual seedlings have close branch whorls.

Poor, slow-growing Type II stands develop under conditions of deficient annual rainfall, shallow rocky soils (often with poor drainage), and a short growing season such as is found at higher altitudes and in the more northerly latitudes. Topography may contribute to slow growth with arid ridges, poorly drained falts, and steep south-facing slopes most unfavorable.

CONFIDENTIAL - FORMERLY RESTRICTED DATA

Table 6.2--Stand table for a pure, even-aged, unmanaged, 80-year-old ponderosa pine stand of average stocking on a poor site[1/]

Diameter Class (in.)	Diameter Midpoint (in.)	Average height (ft)	No. trees per acre[2/]
1	0.6	12	17
2-3	2.6	28	82
4-5	4.6	38	119
6-7	6.6	46	112
8-9	8.6	54	74
10-11	10.6	59	42
12-13	12.6	63	19
14-15	14.6	68	8
16-17	16.6	73	3

Total all trees	476
Total 6.6 in. or larger	258
Weighted average height (6.6 in. or larger)	55.2 ft.
Average d_{bh} (6.6 in. or larger)	9.1 in.
Spacing	13 ft x 13 ft

1/ From: The Yield of Even-aged Stands of Ponderosa Pine, Meyer, W.H., U.S.D.A. Tech. Bull. No. 630, 1938.

2/ The number of trees per acre is 75% of normal and is considered to be an average stocking.

Type III Stand, Unmanaged Ponderosa Pine

Representative of a Type III stand is an unmanaged, naturally occurring, pure 80-year-old ponderosa pine (Pinus ponderosa) stand of average stocking, growing on a good site. It is typical of the better high vigor type of wild, thrifty-mature European or North American coniferous stands and is in contrast to the poorer type described under Type II. Details of a Type III stand are given in Table 6.3.

CONFIDENTIAL - FORMERLY RESTRICTED DATA

Table 6.3--Stand table for a pure, even-aged, unmanaged, 80-year-old ponderosa pine stand of average stocking on a good site[1/]

Diameter Class (in.)	Diameter Midpoint (in.)	Average height (ft)	No. trees per acre[2/]
1	0.6		
2-3	2.6	30	5
4-5	4.6	47	14
6-7	6.6	56	26
8-9	8.6	67	37
10-11	10.6	75	38
12-13	12.6	83	33
14-15	14.6	92	27
16-17	16.6	97	17
18-19	18.6	104	10
20-21	20.6	110	5
22-23	22.6	115	2
24-25	24.6	120	1

Total all trees	215
Total 6.6 in. or larger	196
Weighted average height (6.6 in. or larger)	85.3 ft.
Average d_{bh} (6.6 in. or larger)	12.8 in.
Spacing	15 ft x 15 ft

1/ From: The Yield of Even-aged Stands of Ponderosa Pine, Meyer, W.H., U.S.D.A. Tech. Bull. No. 630, 1938.

2/ The number of trees per acre is 75% of normal and is considered to be average stocking.

Type III stands are characterized by a random distribution of diameters from small to large with a good proportion of the trees in the larger diameter classes. Stands of this type have a smaller total number of trees per acre, and a larger average stand height and diameter than a Type II stand. As on poorer sites, growth is often patchy, with

CONFIDENTIAL - FORMERLY RESTRICTED DATA

dense clumps of trees all of one size alternating with irregular bare areas imparting to the crown canopy a ragged, uneven appearance when viewed from above. These stands may cover large areas, especially in North America, but they are seldom continuous, being broken by meadows, rock outcrops, and bodies of water. They may also be found in small natural patches with uneven borders. Type III stands appear high in vigor. Needles are long, deep-green in color, and luxuriant. Trunks have slow taper and do not develop a platy bark at an early age. Crowns are short with branch whorls spaced 2 feet to 4 feet apart.

The forest floor within the stand may be cluttered with fallen, dead trees which impede entrance into the stand. By the age of 80 years, the thrifty trees have pruned themselves sufficiently and visibility is fairly good. Underbrush is generally light while young reproduction is heavy. Individual seedlings are vigorous in appearance.

Thrifty, fast-growing Type III stands develop under conditions of adequate annual rainfall, deep rock-free soils with good drainage, a long growing season, and favorable topography. Middle elevations and latitudes provide longer growing seasons with warmer temperatures, and moderate, north-facing slopes or well-drained flats favor rapid growth.

Type IV Stand, Unmanaged Ponderosa Pine

Type IV stand represents unmanaged, naturally occurring, pure 120-year-old ponderosa pine (Pinus ponderosa) stand of average stocking, growing on a good site. It is typical of the better high vigor type of wild, thrifty-mature European or North American coniferous stands developing from a Type III stand. Conditions under which these stands develop are similar to those described for a Type III stand. Details of a Type IV stand are given in Table 6.4.

Type V Stand, Managed Douglas-fir

Type V stand represents an intensively managed 60-year-old good site Douglas-fir (Pseudotsuga taxifolia) plantation. A stand of this type is similar to the one described under Type I for ponderosa pine. Conditions under which these stands develop are similar to those described for a Type I stand. Details of a Type V stand are given in table 6.5.

Isodamage Curves

Calculations were made of stem breakage as outlined in Chapter 5 for the five selected stands described above. Figures 6.1 to 6.5, inclusive give isodamage curves for light damage by weapon yields from $W^{1/3} = 1$ to $W^{1/3} = 20$. Figures 6.6 to 6.10 inclusive give isodamage curves for severe damage by weapon yields from $W^{1/3} = 1$ to $W^{1/3} = 20$.

CONFIDENTIAL - FORMERLY RESTRICTED DATA

Table 6.4--Stand table for a pure, even-aged, unmanaged, 120-year-old ponderosa pine stand of average stocking on a good site[1/]

Diameter Class (in.)	Diameter Midpoint (in.)	Average height (ft)	No. trees per acre[2/]
1	0.6		
2-3	2.6		
4-5	4.6	47	2
6-7	6.6	56	4
8-9	8.6	70	7
10-11	10.6	82	11
12-13	12.6	92	15
14-15	14.6	100	17
16-17	16.6	107	16
18-19	18.6	114	15
20-21	20.6	119	12
22-23	22.6	123	8
24-25	24.6	127	4
26-27	26.6	130	2
28-29	28.6	135	1

Total all trees	114
Total 6.6 in. or larger	112
Weighted average height (6.6 in. or larger)	102.1 ft
Average d_{bh}	16.8 in.
Spacing	20 ft x 20 ft

1/ From: The Yield of Even-aged Stands of Ponderosa Pine, Meyer, W. H., U.S.D.A. Tech. Bull. No. 630, 1938.

2/ The number of trees per acre is 75% of normal and is considered to be average stocking.

Although the assumptions used in Chapter 5 restrict results to pressure levels where Mach stem height is larger than tree height, it is not believed that serious errors are introduced in the region of regular shock reflection or in the region where Mach stem height does not exceed tree height. The isodamage curves above the "ideal limit of regular reflection" more or less follow the dynamic pressure lines presented in TM 23-200 (22) and are shown as dashed lines.

CONFIDENTIAL - FORMERLY RESTRICTED DATA.

Table 6.5--Stand table for a managed 60-year-old Douglas-fir plantation on a good site[1/]

Diameter Class (in.)	Diameter Midpoint (in.)	Average height (ft)	No. trees per acre[2/]
2	2.0		
4	4.0		
6	6.0		
8	8.0		
10	10.0		
12	12.0		
14	14.0	104	6
16	16.0	111	10
18	18.0	115	18
20	20.0	120	23
22	22.0	125	12
24	24.0	129	7

Total all trees	76
Total 6.0 in. or larger	76
Weighted average height	118.0 ft
Average d_{bh}	19.4 in.
Spacing	25 ft x 25 ft

1/ Stock table from: Management of Forests for Timber Production, Barr, P.M., Univ. of Calif., 1952.

2/ Based on average diameter for "normal" stands from Yield of Douglas-fir in the Pacific Northwest, McArdle, R.E., and W. H. Meyer, Tech. Bull. 201, U.S.D.A., 1930, Rev. Oct. 1949.

CONFIDENTIAL - FORMERLY RESTRICTED DATA

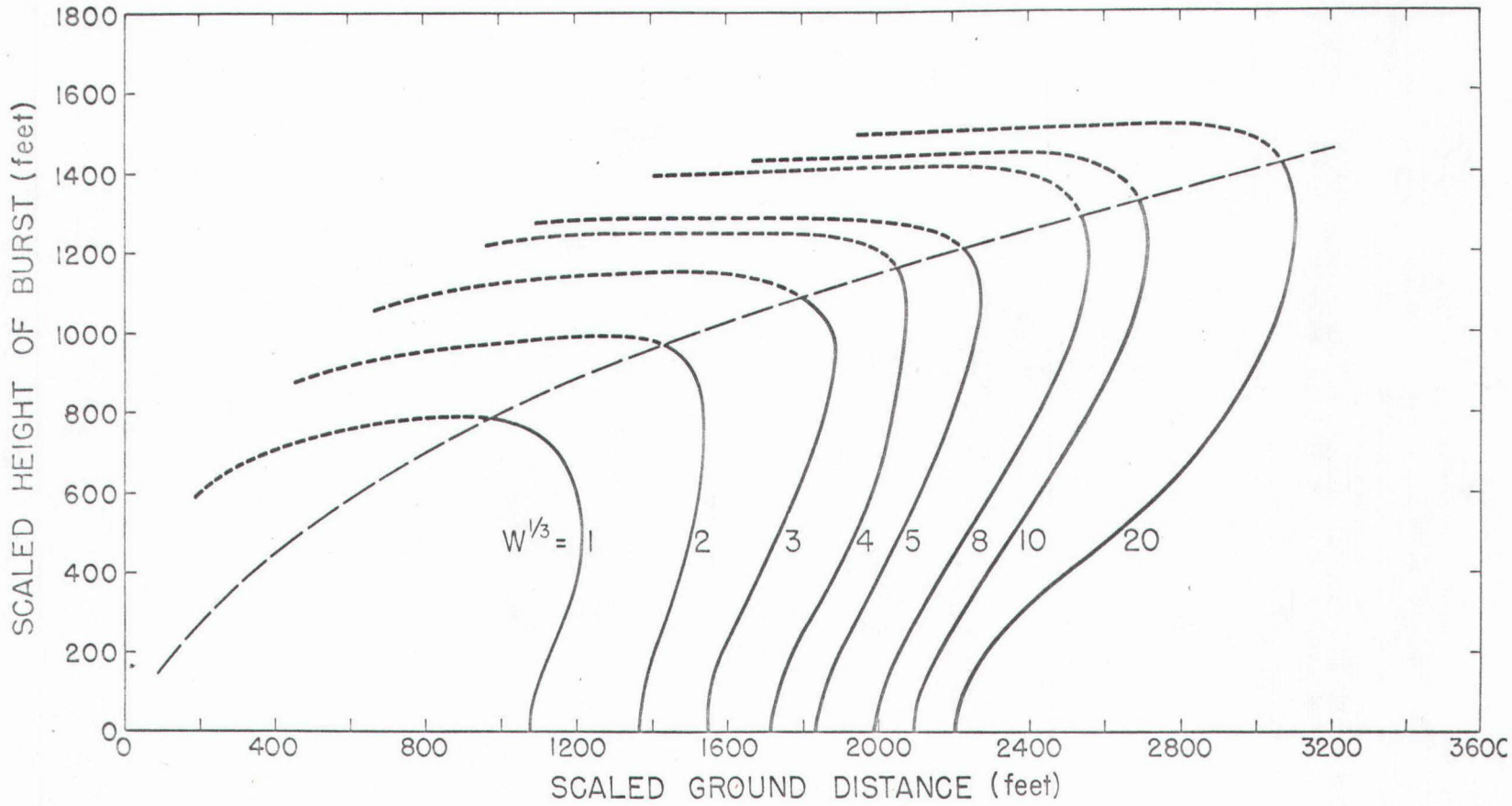

Figure 6.1--Light damage curves for Type I Forest Stand, by height of burst, ground distance and weapon size.

CONFIDENTIAL - FORMERLY RESTRICTED DATA

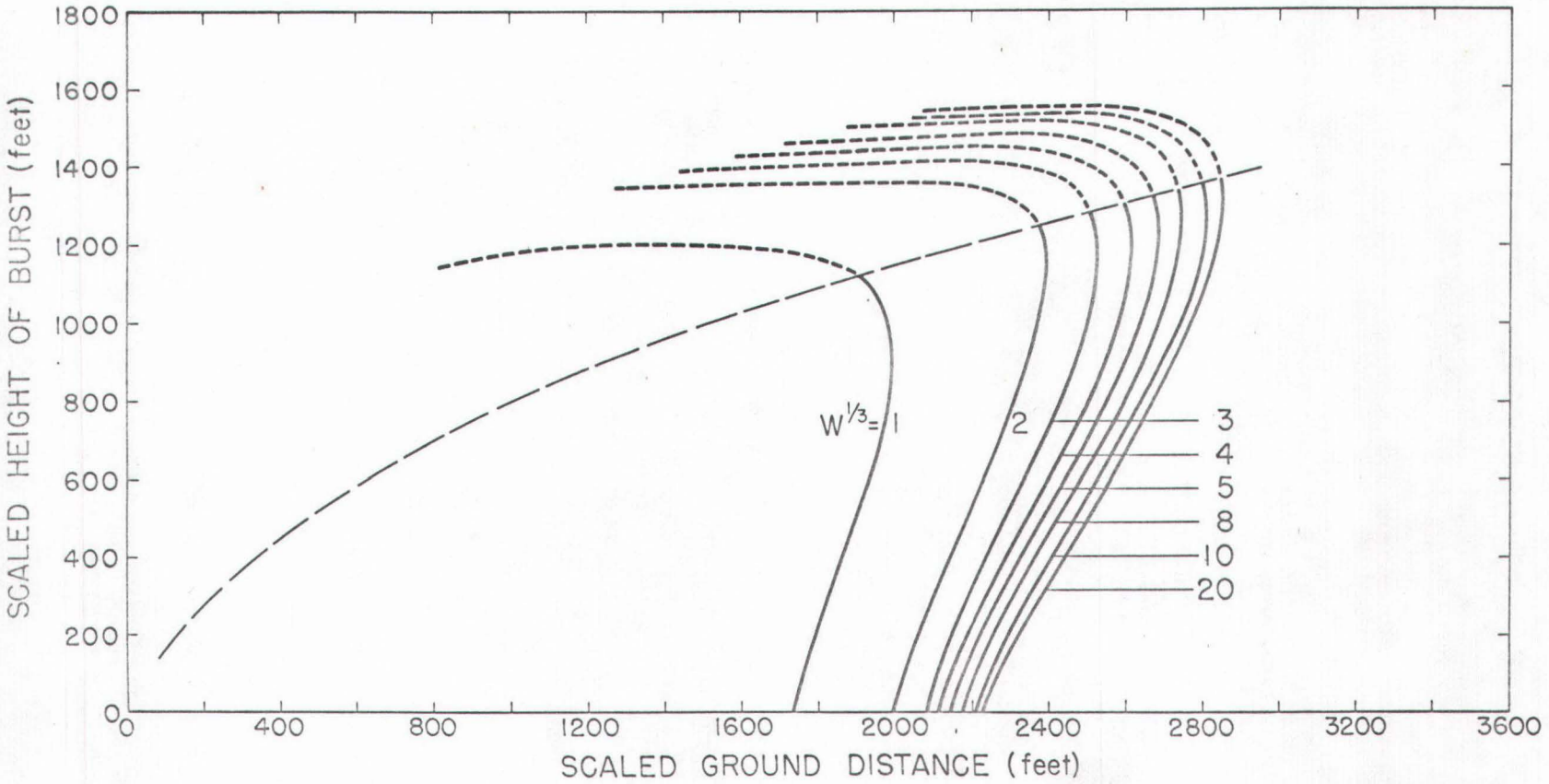

Figure 6.2--Light damage curves for Type II Forest Stand, by height of burst, ground distance and weapon size.

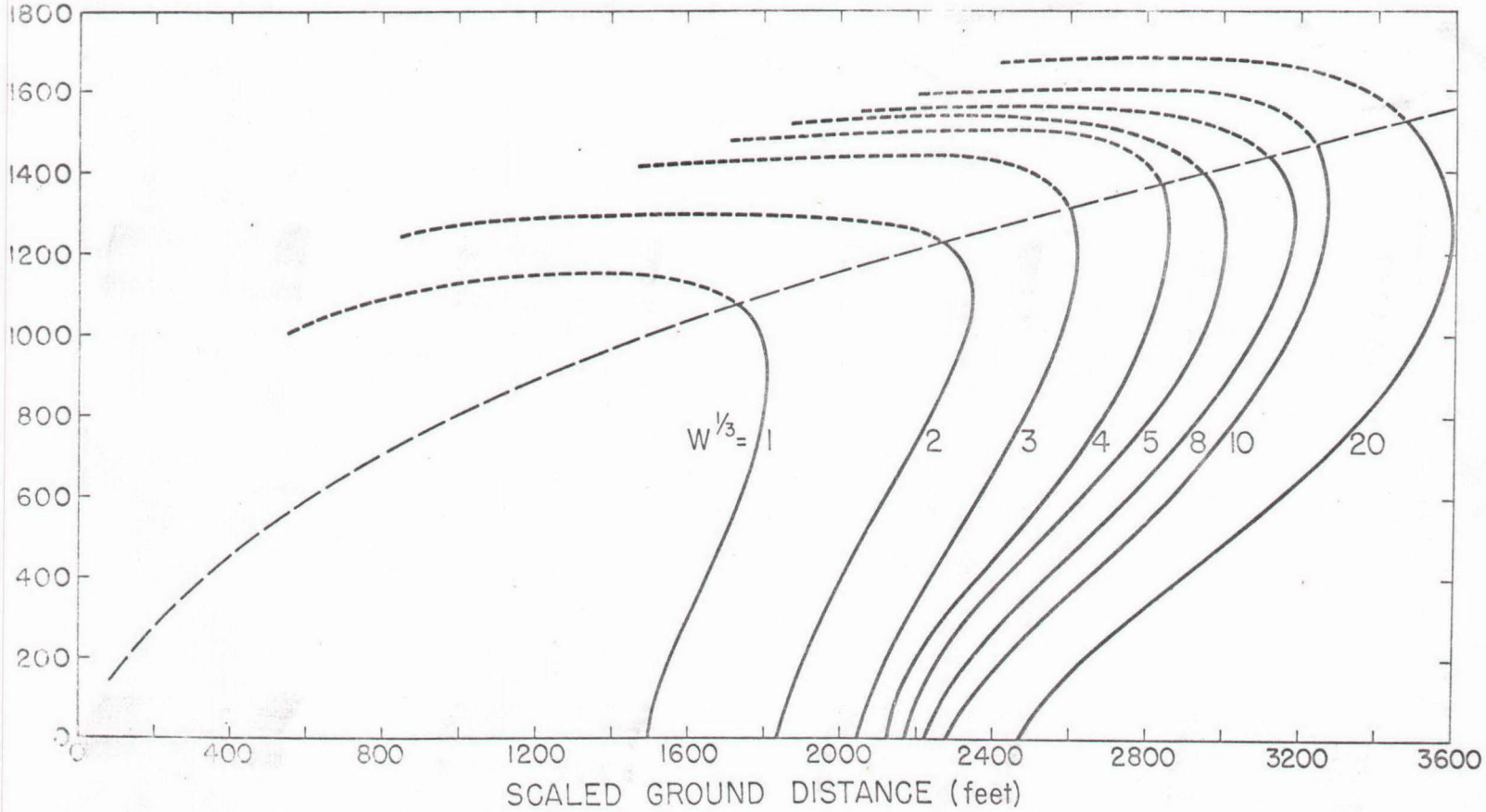

Figure 6.3--Light damage curves for Type III Forest Stand, by height of burst, ground distance and weapon size.

CONFIDENTIAL - FORMERLY RESTRICTED DATA

CONFIDENTIAL--FORMERLY RESTRICTED DATA

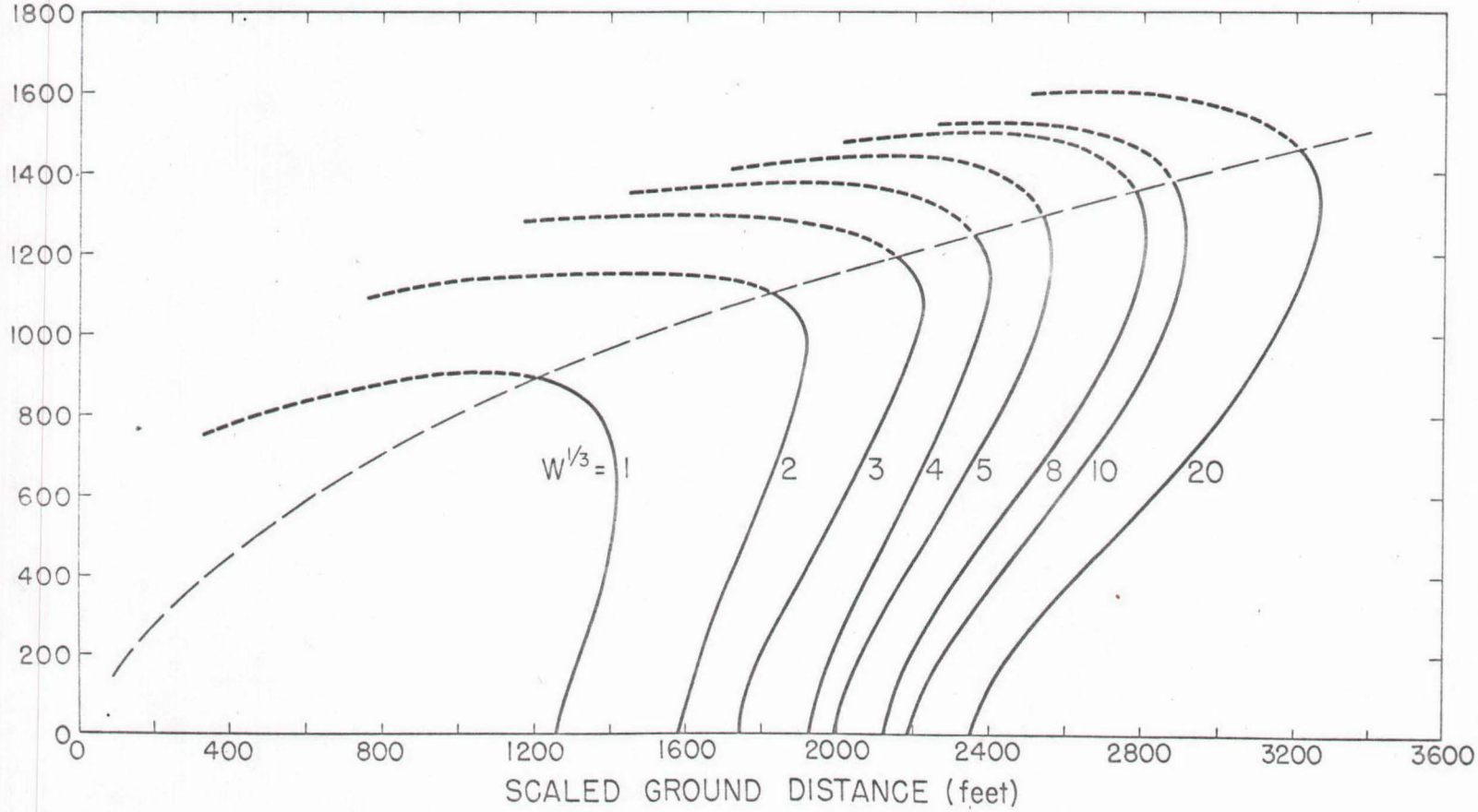

Figure 6.4--Light damage curves for Type IV Forest Stand, by height of burst, ground distance and weapon size.

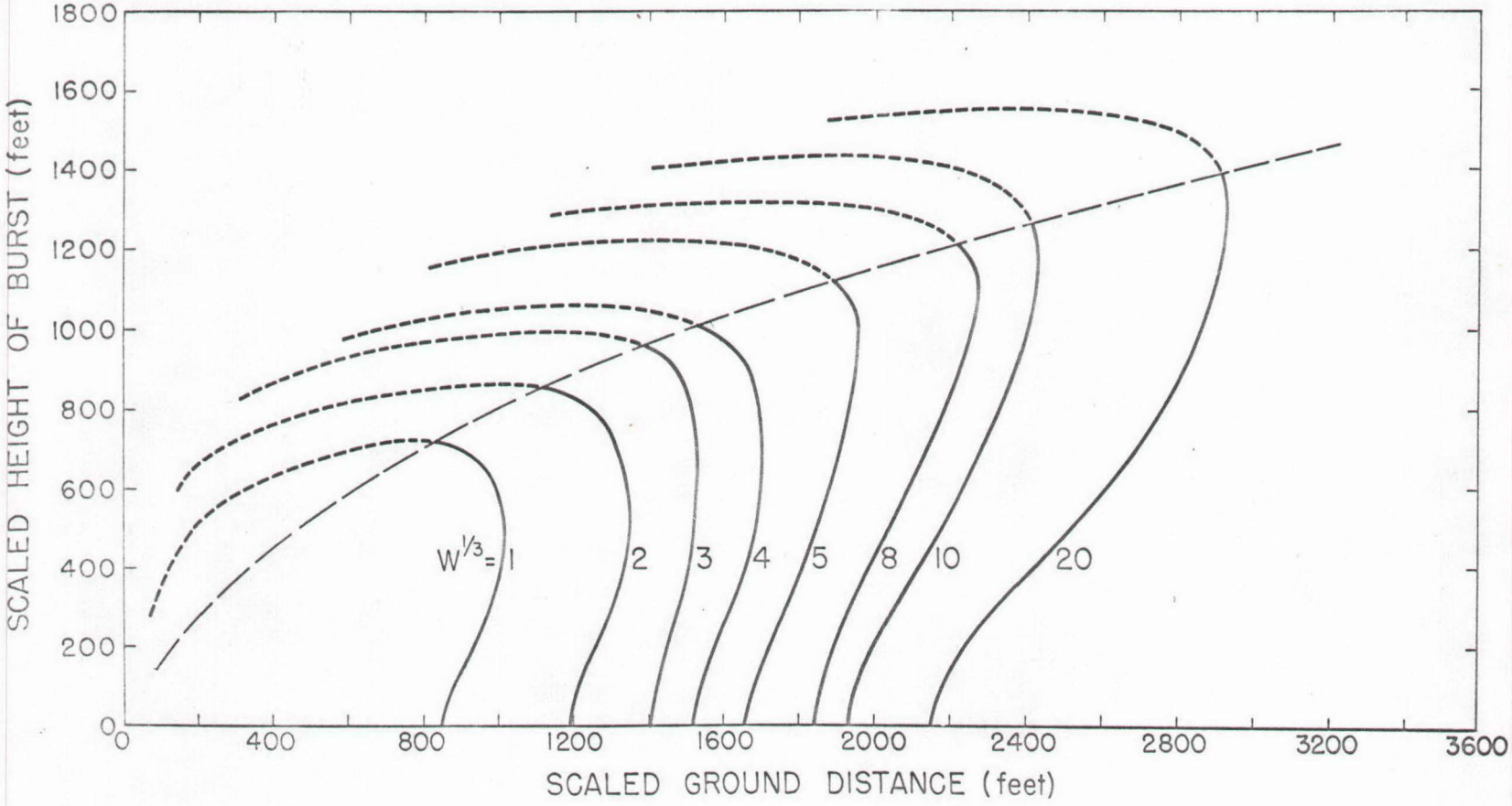

Figure 6.5--Light damage curves for Type V Forest Stand, by height of burst, ground distance and weapon size.

CONFIDENTIAL - FORMERLY RESTRICTED DATA

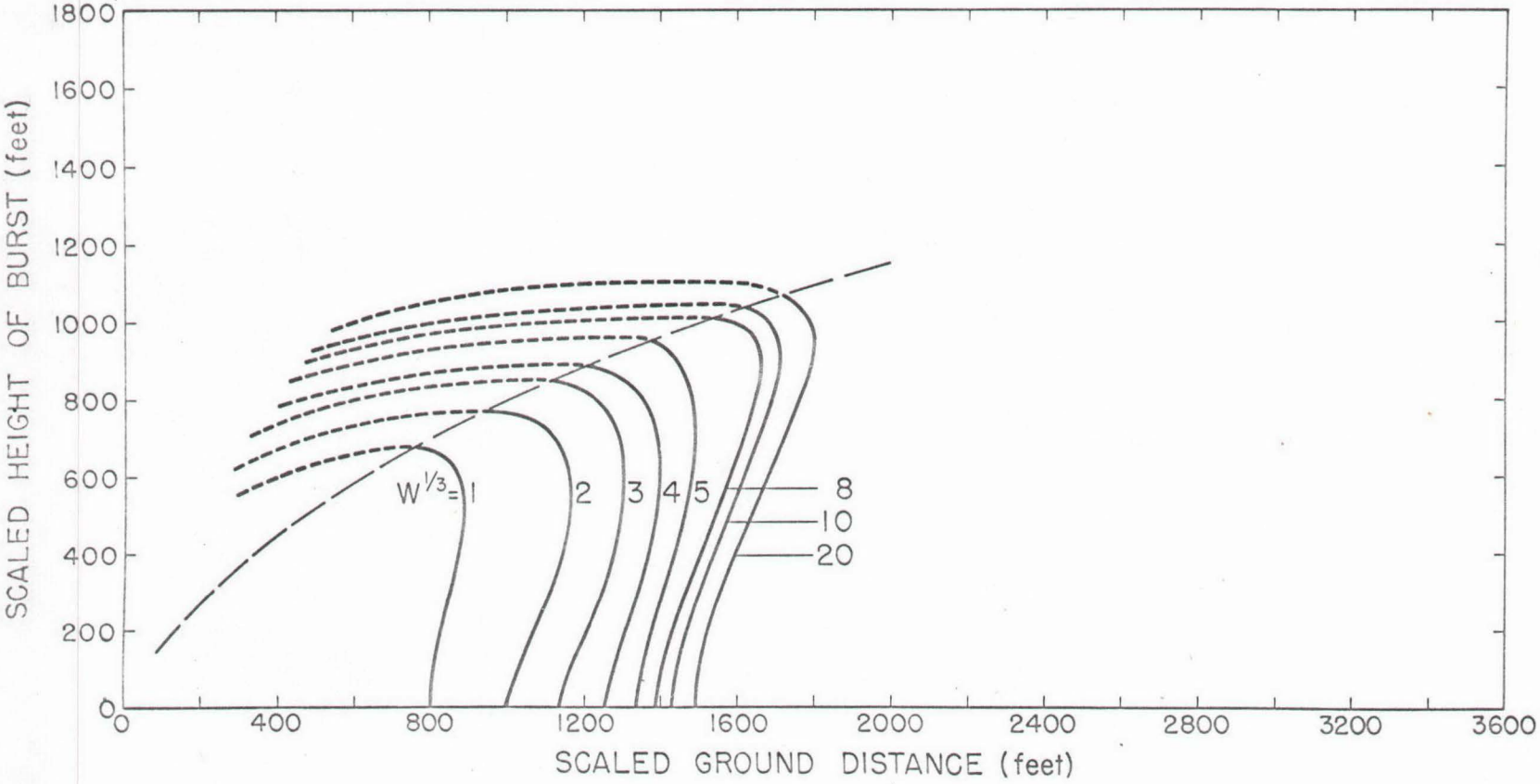

Figure 6.6--Severe damage curves for Type I Forest Stand, by height of burst, ground distance and weapon size.

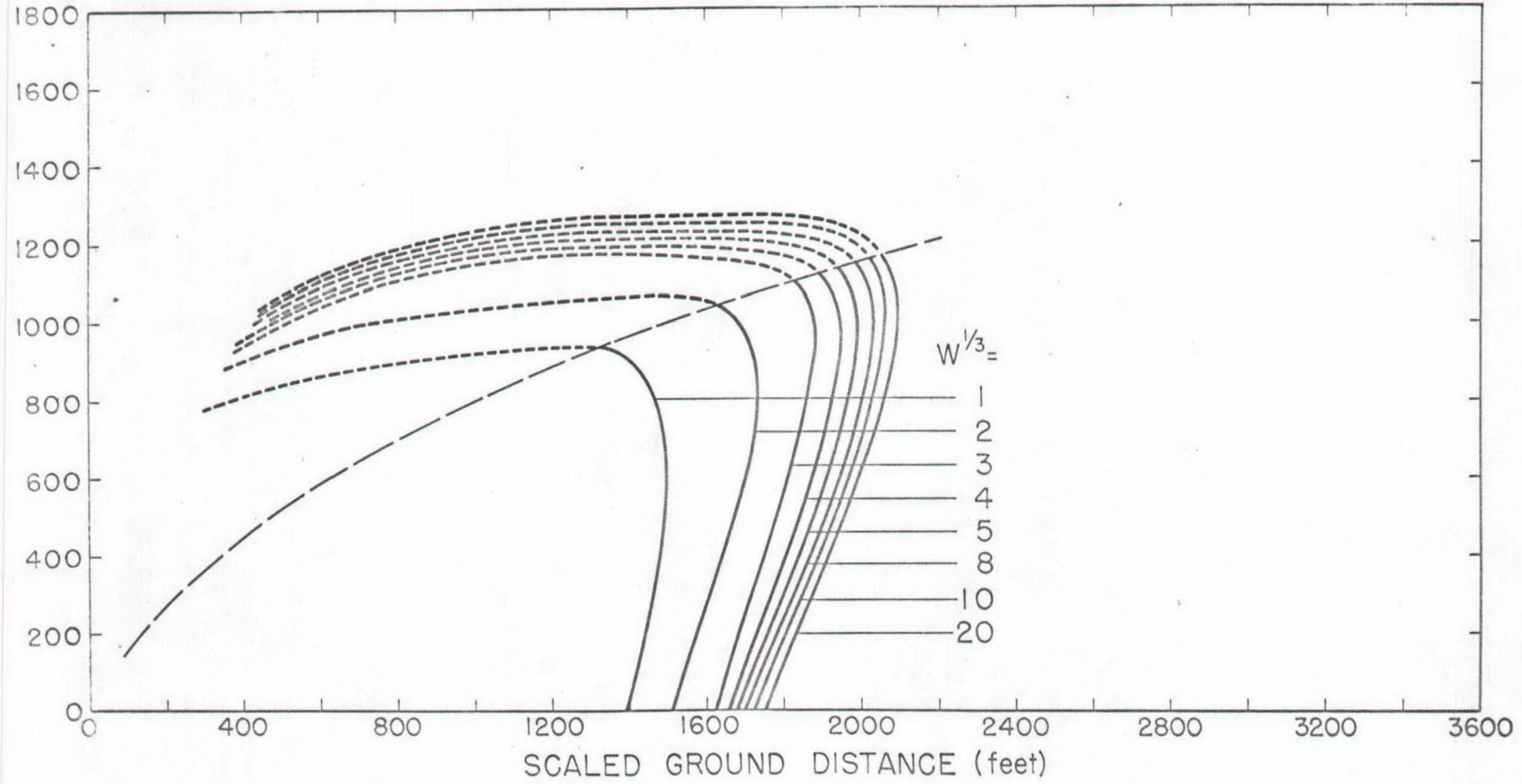

Figure 6.7--Severe damage curves for Type II Forest Stand, by height of burst, ground distance and weapon size.

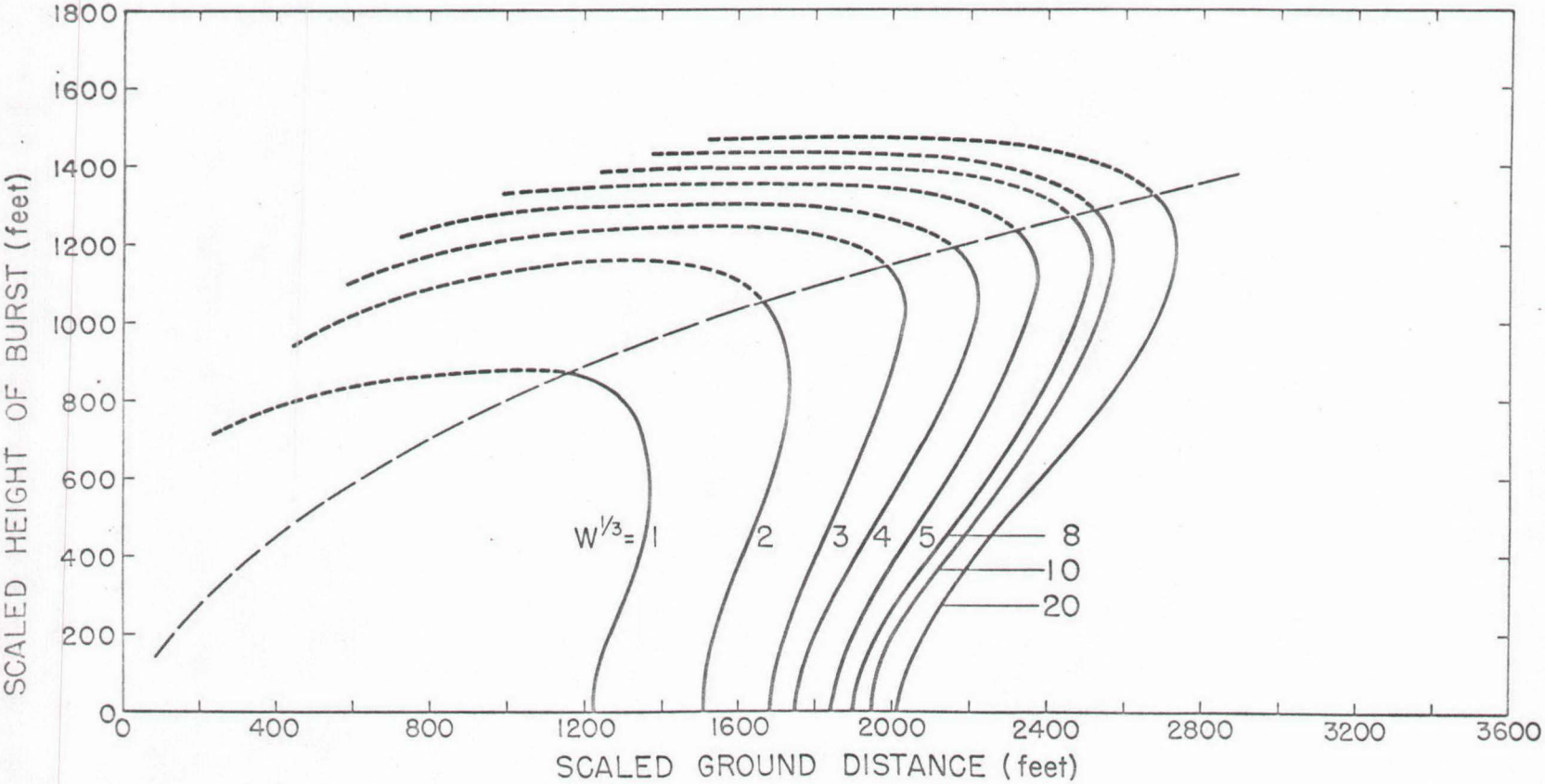

Figure 6.8--Severe damage curves for Type III Forest Stand, by height of burst, ground distance and weapon size.

CONFIDENTIAL - FORMERLY RESTRICTED DATA.

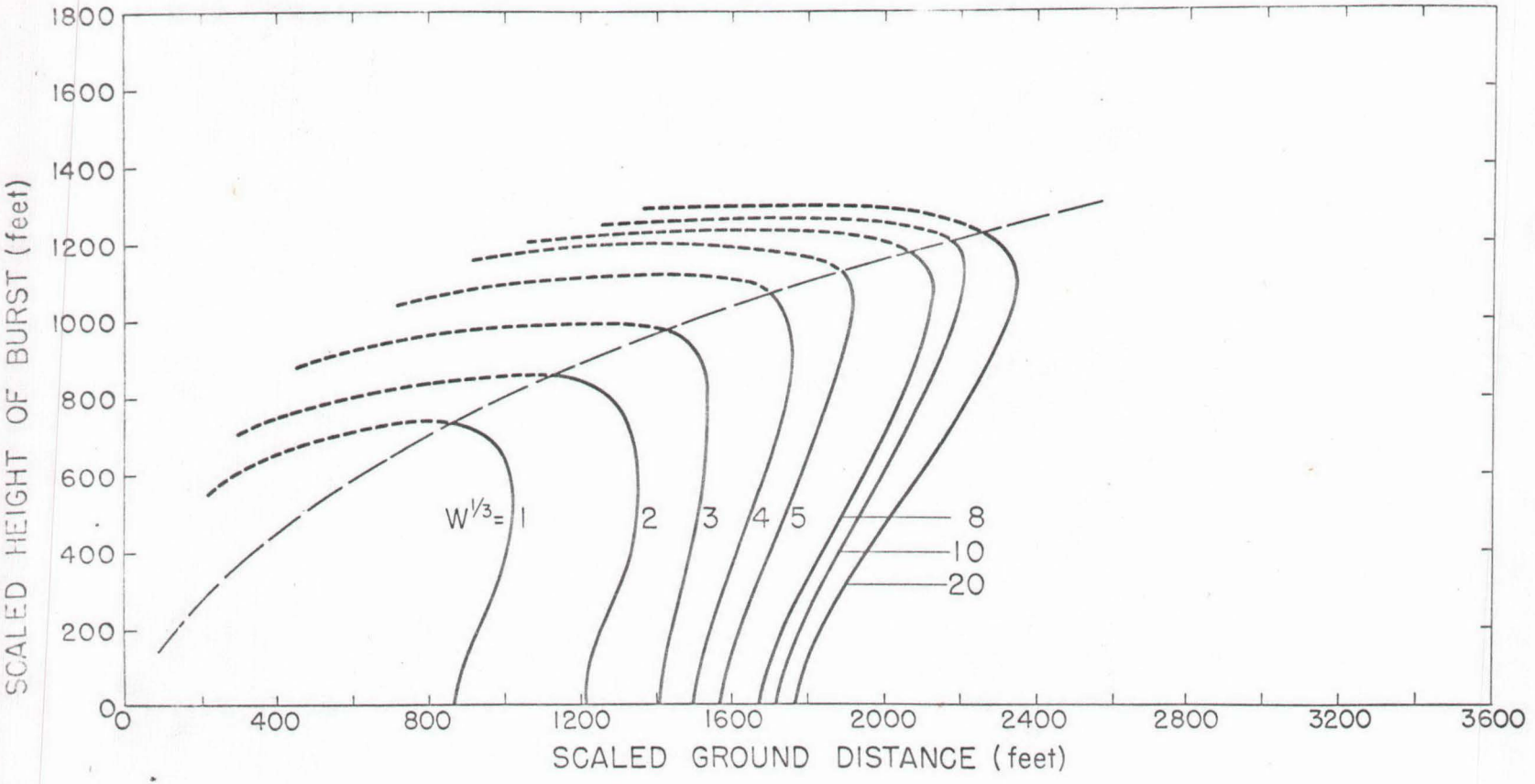

Figure 6.9--Severe damage curves for Type IV Forest Stand, by height of burst, ground distance and weapon size.

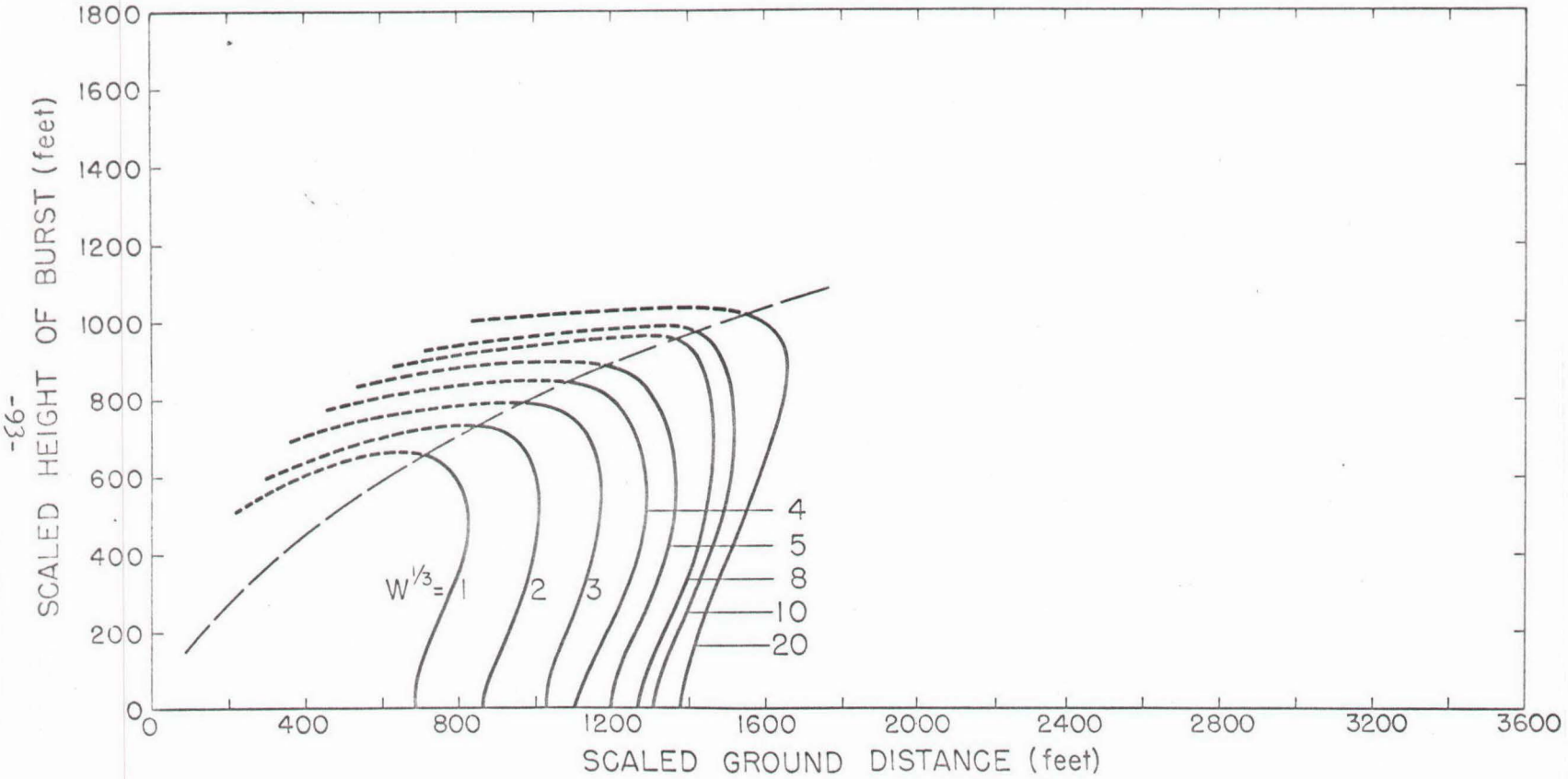

Figure 6.10--Severe damage curves for Type V Forest Stand, by height of burst, ground distance and weapon size.

APPENDIX

EXAMPLE OF CALCULATIONS OF STEM AND CROWN PARAMETERS; PONDEROSA PINE TREE, 24-40-I

CONFIDENTIAL - FORMERLY RESTRICTED DATA

EXAMPLE OF CALCULATIONS OF STEM AND CROWN PARAMETERS;
PONDEROSA PINE TREE, 24-40-I

Parameter	Source	Parameter value	Remarks
d_{bh}	Given	24.0 in.	
H_{bh}	Figure 2.1	101.5 ft	Good site
H	H_{bh} + 4.5	106.0 ft	
H_c	H x .40	42.4 ft	For 40 percent crown
B	Figure 2.2	4.3 in.	Average of poor and good site
d_i	24.0 - 4.3	19.7 in.	
f_c	H_c / H_{bh}	0.42	
a	Table 2.2	0.69	Good site
b	Table 2.2	0.52	Good site
c	b/a	0.76	Stem form factor
d_c	Equation (2.2)	12.5 in.	$f = f_c$
W_b	Equation (2.1)	400 lbs	Values of a and b from Table 2.1
W_f	Equation (2.1)	135 lbs	" " " "
W_b / W_f		2.96	
$\overline{H}_{cp}$	Figure 3.4	25.5 ft	
f_l	$\overline{H}_{cp} / H_{bh}$	0.25	
E	Table 3.1	0.97×10^6 lbs/in.^{2}	
I_i	$\frac{\pi d_i^4}{64}$	7380 in.^{4}	
k_r	Figure 3.7	196.8 lbs/ft	
τ_s	Equation (2.3)	2.69 sec	Values of a and b from Table 2.3
τ	Equation (2.3)	3.83 sec	" " " "
α/m_s	Figure 2.4	0.035 sec^{-1}	

CONFIDENTIAL - FORMERLY RESTRICTED DATA

Appendix (cont.)

Parameter	Source	Parameter value	Remarks
H_{cp}	$H_{bh} - \overline{H}_{cp}$	76.0 ft	
W_c	Equation (2.1)	535 lbs	Values of a and b from Table 2.1
h	$H_c - \overline{H}_{cp}$	16.9 ft	
$\overline{k}_a$	Equation (3.18)	136.0 lbs/ft	Using mean value for pine $\overline{E} = 0.69$ [1/]
m	Equation (4.13)	55.1 lbs sec^2/ft	
$\alpha/m\left(\frac{\tau_s}{\tau}\right)^2$	Equation (2.7)	0.0173 sec^{-1}	
f_m	Equation (3.8)	0.70	
S_m/S_{bh}	Equation (3.7)	1.00	$S = S_m$ and $f = f_m$
δ_r	Table 3.1	0.0051 in./in.	Ponderosa pine
y_r	Equation (3.14)	20.2 ft	$\delta_m = \delta_r$ and $y(f_1) = y_r$
R_r	Equation (3.10)	3,979 lbs	$y(f_1) = y_r$ and $R = R_r$
$(\rho U^2)_{RO}$	Equation (4.30)	29.7 lbs/$in.^2$	Rh = 0, Figure 4.3
$(\rho U^2)_R$	Equation (4.32)	168 lbs/$in.^2$	$D = R_r$, Figure 4.3
R_b	Equation (3.16)	4,616 lbs	$\overline{R} = 1.16$ [1/]
y_b	Equation (3.17)	59.2 ft	$\overline{Y}_b = 2.93$ [1/]

1/ Reference (6), Table 5.

CONFIDENTIAL - FORMERLY RESTRICTED DATA

NOMENCLATURE

a = constant

a_o = sound velocity in ambient air, ft/sec

b = constant

B = double bark thickness, in.

$c = \frac{b}{a}$, stem form factor

C = distance from outer fiber to neutral axis, in.

d = diameter along stem inside bark, in.

d_{bh} = stem diameter (outside bark) at breast height, in.

d_c = diameter of stem at base of crown inside bark, in.

d_i = stem diameter inside bark at breast height, in.

D = measured horizontal drag force of tree crowns, lbs

D_s = aerodynamic drag in direction of motion, lbs

e = base of natural logarithm (2.713 . . .)

E = modulus of elasticity of green wood, lbs/in.^{2}

E_b = static work for breakage, ft lbs

$\overline{E}_b$ = static work modulus for breakage

$\overline{E}_1$ = static work modulus for first maximum deflection

$\overline{E}_2$ = static work modulus for second maximum deflection

$f = H/H_{bh}$, fractional height of stem measured from top of stem downward

$f_1 = \overline{H}_{cp}/H_{bh}$, fractional position of loading

$f_c = H_c/H_{bh}$, fractional position of base of crown

$f_m = H_m/H_{bh}$, fractional position of maximum stress

h = distance from base of crown to center of pressure, ft

H = height of stem measured from top of stem downward, ft

CONFIDENTIAL - FORMERLY RESTRICTED DATA

H_{bh} = height of stem above breast height, ft

H_c = length of crown, ft

H_{cp} = distance to center of pressure from breast height, ft

$\overline{H}_{cp} = H_c - h$, distance to center of pressure, ft

H_m = height of stem above point of maximum stress, ft

I = moment of inertia inside bark, $in.^4$

I_+ = dynamic pressure impulse, lbs $sec/in.^2$

I_i = moment of inertia inside bark at breast height, $in.^4$

k = spring constant, lbs/ft

k_a = measured spring constant for tree stem, lbs/ft

$\overline{k}_a$ = average spring constant for particular species, lbs/ft

k_r = theoretical spring constant, lbs/ft

$\overline{K} = \frac{k_a}{k_r}$, spring constant modulus

L_n = total length of stem broken per acre in one tree diameter class, ft/acre

L_t = total length of stems broken per acre in all tree diameter classes, ft/acre

m = mass of tree with crown, lbs sec^2/ft

m_s = mass of stem without crown, lbs sec^2/ft

M = hD, drag bending moment about base of crown, ft lbs

n = 0, 1, 2 . . . . . increment division or the nth term

N_n = number of trees per acre in a diameter class

p_o = ambient pressure, $lbs/in.^2$

Δp = overpressure behind shock, $lbs/in.^2$

Δp_1 = peak overpressure, $lbs/in.^2$

P_1 = probability of stem breakage on first deflection

CONFIDENTIAL - FORMERLY RESTRICTED DATA

P_2 = probability of stem breakage on second deflection

P_t = total probability of stem breakage

q_1 = peak dynamic pressure, lbs/in.^{2}

Q = dynamic pressure wave form factor

R = horizontal applied force, or restoring force, lbs

R_b = horizontal force at breakage, lbs

$\overline{R}_b = \frac{R_b}{R_r}$, breakage force modulus

R_r = reference horizontal applied force, lbs

R_s = restoring force in direction of motion, lbs

s = stem displacement in direction of motion at point of loading, ft

$\dot{s}$ = stem velocity in direction of motion at point of loading, ft/sec

$\ddot{s}$ = stem acceleration in direction of motion at point of loading, ft/sec^2

s_m = maximum deflection amplitude, ft

S = extreme fiber stress, lbs/in.^{2}

S_{bh} = extreme fiber stress at breast height, lb/in.^{2}

S_m = maximum extreme fiber stress, lbs/in.^{2}

S_r = modulus of rupture of green wood, lbs/in.^{2}

t = time, sec

t_+ = positive phase duration time of shock, sec

Δt = 0.04, increment of time, sec

t_n = time scale, sec

u = particle velocity behind shock wave, ft/sec

u_1 = peak particle velocity behind shock, ft/sec

U = horizontal wind velocity, ft/sec

V = vector particle velocity, ft/sec

CONFIDENTIAL - FORMERLY RESTRICTED DATA

W = bomb yield, KT

W_b = weight of dry branchwood, lbs

W_c = weight of dry crown, lbs

W_f = weight of dry foliage, lbs

W_o = weight of dry crown, dry branchwood, or dry foliage, (as the case may be), lbs

y = stem deflection at loading point, ft

y_b = deflection at breakage, ft

y_n = amplitude of stem in free vibration after n oscillations

y_o = amplitude of stem in free vibration

y_r = reference stem deflection at point of loading, ft

y_1 = first maximum horizontal deflection, ft

y_2 = second maximum horizontal deflection, ft

$\bar{Y}$ = deflection modulus

$\bar{Y}_b = \frac{y_b}{y_r}$, breakage deflection modulus

$\bar{Y}_p$ = deflection modulus at proportional limit

$z = t/t_+$

$Z = d/d_{bh}$, ratio of diameter of stem to diameter of stem outside bark at breast height

$\frac{\rho U^2}{2}$ = dynamic pressure, lbs/in.^{2}

$(\rho U^2)_R$ = twice the dynamic pressure, defined by equation (4.32), lbs/in.^{2}

$(\rho U^2)_{RO}$ = twice the dynamic pressure, defined by equation (4.30), lbs/in.^{2}

α = internal damping factor

β = angle between horizontal particle velocity U , and vector velocity V , degrees

CONFIDENTIAL - FORMERLY RESTRICTED DATA

δ_m = maximum strain, in./in.

$\delta_r = \frac{S_r}{E}$, reference strain, in./in.

π = 3.1416

θ = angle of stem displacement, degrees

ρ = mass density of air, lbs sec^2/ft^4

ρ_o = ambient mass density of air, lbs sec^2/ft^4

ρ_1 = peak mass density of air, lbs sec^2/ft^4

τ = natural period of tree with crown, sec

τ_s = natural period of tree stem without crown, sec

ϕ = function

ψ = function

$\zeta = z/1.4$

$\lambda = \frac{\rho_1 - \rho_o}{\rho_1}$

CONFIDENTIAL - FORMERLY RESTRICTED DATA

LITERATURE CITED

1. Fons, W. L., and others
   1950. Preliminary study of the consequences of an atomic explosion over a forest, Tech. Memo. ORO-T-108, Confidential. Operations Res. Office, The Johns Hopkins University, 102 pp., illus.

2. Storey, T. G., and Fons, W. L.
   1956. Natural period characteristics of selected tree species, AFSWP-864. U. S. Forest Service, Div. of Fire Research, 36 pp., illus.

3. Lai, W.
   1955. Aerodynamic crown drag of several broadleaf tree species, AFSWP-863, U. S. Forest Service, Div. of Fire Research, 26 pp., illus.

4. Sauer, F. M., and others
   1951. Experimental investigation of aerodynamic drag in tree crowns exposed to steady wind--conifers, ORO Phase Report. U. S. Forest Service, Div. of Fire Research, 19 pp., illus.

5. Pong, W. Y.
   1956. Tree breakage characteristics under static loading of several hardwood species, AFSWP-970. U. S. Forest Service, Div. of Fire Research, 46 pp., illus.

6. Fons, W. L., and Pong, W. Y.
   1957. Tree breakage characteristics under static loading--ponderosa pine, AFSWP-867. U. S. Forest Service, Div. of Fire Research, 51 pp., illus.

7. Storey, T. G., and others
   1955. Crown characteristics of several coniferous tree species--relations between weight of crown, branchwood and foliage, and stem diameter, AFSWP-416. U. S. Forest Service, Div. of Fire Research, 95 pp., illus.

8. Storey, T. G., and Pong, W. Y.
   1957. Crown characteristics of several hardwood tree species--relations between weight of crown, branchwood and foliage, and stem diameter, AFSWP-968. U. S. Forest Service, Div. of Fire Research, 36 pp., illus.

9. Behre, C. E.
   1927. Form-class taper curves and volume tables and their application. Journal of Agricultural Research, XXXV, October 1927, pp. 673-744.

~~CONFIDENTIAL - FORMERLY RESTRICTED DATA~~

10. Clements, V. A., and others
1949. Form-class volume tables for ponderosa pine, Douglas-fir and white fir in California, Res. Note No. 60, California Forest and Range Experiment Station.

11. Brown, A. A., and others
1953. Blast damage to trees--isolated conifers, Proj. 3.3, Operation SNAPPER, WT-509, Confidential. U. S. Forest Service, Div. of Fire Research.

12. Sauer, F. M., and others
1954. Blast damage to coniferous tree stands by atomic explosions, Proj. 3.19, Operation UPSHOT-KNOTHOLE, WT-731, Confidential. U. S. Forest Service, Div. of Fire Research.

13. Fons, W. L., and Storey, T. G.
1955. Blast effects on tree stand, Proj. 3.3, Operation CASTLE, WT-921, Secret. U. S. Forest Service, Div. of Fire Research.

14.
1951. Forest Management Field Course. California Forest and Range Experiment Station, U. S. Forest Service.

15. Timoshenko, S., and Young, D. H.
1948. Advanced dynamics, pg. 37, first edition. McGraw-Hill Book Co., Inc., N. Y.

16. Tirén, L.
1926. Nagra Undersokningar Over Stamformen; (Some research on tree stem form) Skogsvardsforeningens Tidskrift, XXIV, pp. 23-88.

17. Laurson, P. G., and Cox, W.
1949. Mechanics of materials, pg. 157, second edition. John Wiley & Sons, Inc., N. Y.

18. Markwardt, L. J., and Wilson, T. R. C.
1935. Strength and related properties of woods grown in the United States. U. S. Dept. Agric. Tech. Bull. 479.

19. Sauer, F. M., and Lai, W.
1955. Dynamic pressure wave form-height of burst curves, AFSWP-419, Confidential. U. S. Forest Service, Div. of Fire Research.

20. Vortman, L. M., and Merritt, M. L.
1953. Methods for estimating blast loading on simple structures, AFSWP-226, Secret. Sandia Corp., Albuquerque, N. M.

CONFIDENTIAL - FORMERLY RESTRICTED DATA

21.

1953. Summary report of the Technical Director, Operation UPSHOT-KNOTHOLE, WT-782, Secret. Hdqtrs., Field Command, AFSWP, Sandia Base, Albuquerque, N. M.

22.

1955. Capabilities of atomic weapons, TM 23-200, Secret. AFSWP.

CONFIDENTIAL - FORMERLY RESTRICTED DATA

INITIAL
DISTRIBUTION LIST FOR
AFSWP-971

ADDRESSEE	ARMY	NO. OF CYS
Chief of Research and Development, D/A, Washington 25, D. C. ATTN: Atomics, Air Defense & Missile Division		1
Chief of Engineers, D/A, Washington 25, D. C.	ATTN: ENGNB	1
	ATTN: ENGEB	1
Commanding General, U.S. Continental Army Command, Ft. Monroe, Va.		1
President, Board #4, Headquarters, U.S. Continental Army Command, Ft. Bliss, Tex.		1
Commandant, Command & General Staff College, Ft. Leavenworth, Kans. ATTN: ALLLS (AS)		1
Secretary, The U.S. Army Air Defense School, Fort Bliss, Texas ATTN: Maj. George L. Alexander, Dept. of Tactics and Combined Arms		1
Director, Special Weapons Development Office, Headquarters, U.S. Continental Army Command, Ft. Bliss, Texas		1
Commanding General, Research & Engineering Command, Army Chemical Center, Md. ATTN: Deputy for RW & Non-Toxic Material		1
Commanding General, Aberdeen Proving Ground, Aberdeen, Md. ATTN: Director, Ballistics Research Lab.		1
Commanding General, The Engineer Center, Ft. Belvoir, Va. ATTN: Asst. Commandant, Eng. School		1
Commanding Officer, Engineer Research and Development Lab., Ft. Belvoir, Va. ATTN: Chief, Tech. Intelligence Branch		1
Commanding Officer, Picatinny Arsenal, Dover, N.J. ATTN: ORDBB-TK		1
Commanding Officer, Chemical and Radiological Lab., Army Chemical Center, Md. ATTN: Tech. Library		1
Commanding Officer, Transportation R&D Command, Ft. Eustis, Va. ATTN: Special Projects Division		1
Director, Technical Documents Center, Evans Signal Lab., Belmar, N.J.		1
Director, Waterways Experiment Station, P.O. Box 631, Vicksburg, Miss. ATTN: Library		1
Director, Operations Research Office, Johns Hopkins University, 7100 Connecticut Avenue, Chevy Chase, Md., Washington 15, D.C.		1
Chief of Ordnance, D/A, Washington 25, D.C. ATTN: ORDTX		1

INITIAL DISTRIBUTION LIST
FOR AFSWP-971

ADDRESSEE	NAVY	NO. OF CYS
Chief of Naval Operations, D/N, Washington 25, D.C.	ATTN: OP-36	2
Chief of Naval Operations, D/N, Washington 25, D.C.	ATTN: OP-03EG	1
Director of Naval Intelligence, D/N, Washington 25, D.C.	ATTN: OP-922V	1
Chief, Bureau of Ordnance, D/N, Washington 25, D.C.		1
Chief, Bureau of Aeronautics, D/N, Washington 25, D.C.		1
Chief, Bureau of Ships, D/N, Washington 25, D.C.	ATTN: Code 348	1
	ATTN: Code 423	1
Chief, Bureau of Yards and Docks, D/N, Washington 25, D.C.	ATTN: D-400	1
	ATTN: D-440	1
Chief of Naval Research, D/N, Washington 25, D.C.	ATTN: Code 811	1
Commander-in-Chief, U. S. Pacific Fleet, FPO, San Francisco, Calif.		1
Commander-in-Chief, U. S. Atlantic Fleet, U. S. Naval Base, Norfolk 11, Va.		1
Commandant of the Marine Corps, D/N, Washington 25, D.C.	ATTN: Code AO3H	4
President, U.S. Naval War College, Newport, R.I.		1
Superintendent, U.S. Naval Postgraduate School, Monterey, Calif.		1
Commanding Officer, U.S. Naval Schools Command, U.S. Naval Station, Treasure Island, San Francisco, Calif.		1
Commanding Officer, U.S. Fleet Training Center, Naval Base, Norfolk 11, Va.	ATTN: Special Weapons School	1
Commanding Officer, U.S. Fleet Training Center, Naval Station, San Diego, Calif.	ATTN: SPWP School	2
Commanding Officer, U.S. Naval Damage Control Training Center, Naval Base, Philadelphia, Pa.	ATTN: ABC Defense Course	1
Commanding Officer, U.S. Naval Unit, Chemical Corps School, Army Chemical Training Center, Ft. McClellan, Alabama		1
Commander, U.S. Naval Ordnance Laboratory, White Oak, Silver Spring 19, Maryland	ATTN: EE	1
	EH	1
	R	1
Commander, U.S. Naval Ordnance Test Station, Inyokern, China Lake, Calif.		1

ADDRESSEE	NO. OF CYS
NAVY (Cont'd.)	
Officer-in-Charge, U.S. Naval Civil Engineering Research and Evaluation Laboratory, U.S. Naval Construction Bn. Center, Fort Hueneme, Calif. ATTN: Code 753	1
Director, U.S. Naval Research Lab., Washington 25, D.C.	1
Commanding Officer and Director, U.S. Navy Electronics Lab., San Diego 52, Calif. ATTN: Code 4223	1
Commanding Officer, U.S. Naval Radiological Defense Laboratory, San Francisco, Calif. ATTN: Tech. Info. Division	1
Commanding Officer & Director, David W. Taylor Model Basin, Washington 7, D.C ATTN: Library	1
Commander, Norfolk Naval Shipyard, Portsmouth, Va. ATTN: Code 270	1
Commander-in-Chief Pacific, Pearl Harbor, T.H.	1
AIR FORCE	
Assistant for Atomic Energy, Headquarters, USAF, Washington 25, D.C.	1
Director of Plans, Headquarters, USAF, Washington 25, D.C. ATTN: War Plans Division	1
Director of Research & Development, Headquarters, USAF, Washington 25, D.C. ATTN: Combat Components Division	1
Director of Requirements, Headquarters, USAF, Washington 25, D.C. ATTN: AFDRQ-SA/M	1
Director of Intelligence, Headquarters, USAF, Washington 25, D.C. ATTN: AFOIN-1B2	1
Commander-in-Chief, Strategic Air Command, Offutt AFB, Nebraska ATTN: Special Wpns. Branch, Inspector Div., Inspector General	1
Commander, Tactical Air Command, Langley AFB, Va. ATTN: Document Security Branch	1
Commander, Air Material Command, Wright-Patterson AFB, Ohio	2
Commander, Air Research and Development Command, P.O. Box 1395, Baltimore 3, Md. ATTN: RDDN	1
Director, Air University Library, Maxwell AFB, Ala.	2
Commander, Wright Air Development Center, Wright-Patterson AFB, Ohio ATTN: WCOSI	1

ADDRESSEE	NO. OF CYS
AIR FORCE (Cont'd.)	
Commander, AF Cambridge Research Center, L.G. Hanscom Field, Bedford, Mass. ATTN: CRQST-2	1
Commander, AF Special Weapons Center, Kirtland AFB, N.M. ATTN: Library	1
Commandant, USAF Institute of Technology, Wright-Patterson AFB, Ohio ATTN: Resident College	1
Commander, Western Development Division, P.O. Box 262, Inglewood, California	1
The RAND Corporation, 1700 Main Street, Santa Monica, California (For Nuclear Energy Division)	1
Assistant Chief of Staff, Installations, Headquarters, USAF, Washington 25, D.C. ATTN: AFCIE-E	1
OTHER DOD AGENCIES	
Assistant Secretary of Defense, (Research and Development), Washington 25, D.C. ATTN: Tech. Library	1
U.S. Documents Officer, Office of the United States National Military Representative, SHAPE, APO 55, New York, N.Y.	1
Director, Weapons Systems Evaluation Group, OSD, Washington 25, D.C.	1
Commandant, Armed Forces Staff College, Norfolk 11, Va. ATTN: Secretary	1
Commander, Field Command, AFSWP, P.O. Box 5100, Albuquerque, N.M.	1
Commander, Field Command, AFSWP, P.O. Box 5100, Albuquerque, N.M. ATTN: Training Division	2
Chief, Armed Forces Special Weapons Project, Washington 25, D.C.	15
ASTIA, Document Service Center, UB Building, Dayton 2, Ohio ATTN: DCS-SA	10
OTHERS	
Los Alamos Scientific Laboratory, P.O. Box 1663, Los Alamos, N.M. ATTN: Report Librarian (For Dr. Alvin C. Graves, J-Division)	1
National Advisory Committee for Aeronautics, 1512 H Street, N.W., Washington 25, D.C. ATTN: Mr. Eugene B. Jackson, Chief, Div. of Research Information	1
Assistant Director of Research, Langley Aeronautical Lab., National Advisory Committee for Aeronautics, Langley Field, Va. ATTN: Mr. John Stack	1

ADDRESSEE	OTHERS (Cont'd.)	NO. OF CYS
Chief, Classified Technical Library, Technical Information Service, U.S. Atomic Energy Commission, 1901 Constitution Ave., N.W., Washington 25, D.C. ATTN: Mrs. Jean O'Leary (For Dr. Paul C. Fine)		1
Chief, Classified Technical Library, Technical Information Service, U.S. Atomic Energy Commission, 1901 Constitution Ave., N.W., Washington 25, D.C. ATTN: Mrs. Jean M. O'Leary		1
Forestal Research Center Library, Aeronautical Sciences Building, Princeton University, Princeton, New Jersey ATTN: Maurice H. Smith, Librarian (For Dr. Walker Bleakney)		1
Manager, Albuquerque Operations Office, U.S. Atomic Energy Commission, P.O. Box 5400, Albuquerque, New Mexico		1
Forest Service, U.S. Department of Agriculture, Washington 25, D.C. ATTN: Mr. A.A. Brown, Chief, Division of Forest Fire Research		5
Rensselaer Polytechnic Institute, Mason House, Troy, New York ATTN: Security Officer (For Dr. Clayton Oliver Dohrenwend)		1
Massachusetts Institute of Technology, Director, Division of Defense Laboratories, Lincoln Laboratory, Cambridge 19, Mass. (For Dr. Robert J. Hansen)		1
The University of Michigan, University Research Office, Lobby 1, East Engineering Building, Ann Arbor, Michigan (For Dr. B. Johnston)		1
Sandia Corporation, Sandia Base, Albuquerque, New Mexico ATTN: Classified Document Division (For Dr. Walter A. MacNair)		1
Superintendent, Eastern Experiment Station, U.S. Bureau of Mines, College Park, Md. ATTN: Dr. Leonard Obert		1
The University of Illinois, Civil Engineering, Rm. 207 Talbot Lab., Urbana, Illinois (For Dr. N. M. Newmark)		1

FS INFO - INTERMOUNTAIN
INTERMOUNTAIN RESEARCH
STATION
324-25th Street
Ogden, UT 84401

AD-33 Bookplate
(1—63)

NATIONAL

AGRICULTURAL

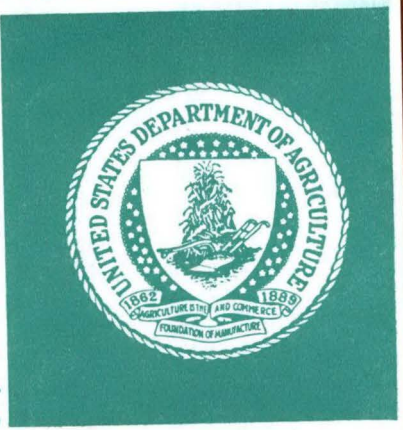

LIBRARY

RMRS Library - ~~Ogden~~

Property of
National FS Library
USDA Forest Service
240 W Prospect Rd
Fort Collins CO 80526